EPFL

Design and Development of Injectable, Tough and Intrinsically-Adhesive Hydrogels for Biomedical Applications

Peyman KARAMI

École
polytechnique
fédérale
de Lausanne

2021

To my family …

Acknowledgements

I would like to express my deep gratitude to my thesis director Prof. Dominique P. Pioletti for giving me the opportunity to work at the Laboratory of Biomechanical Orthopedics (LBO) of EPFL. I am grateful to his availability, involvement and support in the project throughout these years, which encouraged me to pursue my research career with confidence and joy, and gave me the freedom to carry on my research in my own way. I would also like to express my deep appreciation to my thesis co-director Prof. Christophe Moser, for all the great discussions, valuable comments and out-of-the-box solutions, especially concerning the photo-polymerization aspects of my thesis.

I would like to thank the jury committee members of my defense, Prof. Tatiana Segura, Prof. Luc Mongeau, Dr. John Christopher Plummer and Prof. Cécile Hébert for dedicating their precious time and expertise to review my work. Moreover, I am grateful for their precious comments to improve this work. I am also very grateful to Dr. Pierre-Etienne Bourban for the fruitful discussions and smart advices during my research.

Many thanks to Céline Samira Wyss, with whom I shared great collaboration during my research, for all our scientific discussions and our friendship. I also shared a couple of exciting years of research with Dr. Naser Nasrollahzadeh and Dr. Jens Antons who were very encouraging and constructive colleagues. It was indeed a pleasure working with them. Many thanks go to the SHAPER group members; Dr. Azadeh Khoushabi and Dr. Andreas Schmocker who helped me a lot during my first year, and for all the valuable discussions and their friendship. Moreover, I would like to thank Prof.

Abstract

Despite the development of hydrogels with a wide range of mechanical properties, insufficient adhesion between these materials and biological surfaces limits their use in the biomedical applications. Most recent advancements in highly adhesive hydrogel systems are focused on the preformed hydrogel patches and dry tapes. In the past proposed strategies for highly adhesive hydrogels, the developed materials are not intrinsically adhesive, but adhere to the targeted tissues thanks to specific developments such as chemically modifying the contacting surface. Therefore, hydrogels that exhibit both sufficient intrinsic adhesion to various biological surfaces and proper injectability, has yet to be demonstrated. The need for design, fabrication and characterization of adhesive hydrogel systems with broad physicochemical properties has remained a central challenge in the biomedical field.

In the first part, by controlling toughening processes, we design a composite double-network hydrogel with high water content, which creates a dissipative interface and robustly adheres to soft tissues. No tissue surface modification was needed to obtain high adhesion properties of the developed hydrogel. Instead, mechanistic principles were used to control interfacial cracks propagation. The integration of the dissipative polymeric network on the soft tissue surfaces allowed increasing significantly the adhesion strength. Our findings highlight the significant role of controlling hydrogel structure and dissipation processes for toughening the interface.

In the second part, we propose a universal framework for the design of injectable hydrogels that are intrinsically adhesive to various tissues. We fabricate a family of original polymeric backbones using a two-step functionalization process in order to make new hydrogels with available adhesive sites and the capability to form hybrid networks, as well as further enhancements through the fiber reinforcement for stronger synergetic effects. To achieve that, our approach (i) provides strong chemical bonds with nucleophiles at interface, immediately upon contact with tissues thanks to the designed available adhesive bonding sites, and (ii) forms a hybrid network by covalent and physical interactions between our engineered chains, so that the interfacial bonds and the hydrogel capability of dissipating energy produce a synergic effect for achieving high adhesion. In addition to high level of adhesion performance, the injectable hydrogel system presents a broad and tunable range of physicochemical properties. This is particularly important for biomedical applications which require superior material properties, such as for cartilage tissue engineering. Fast adhesion formation and one-pot polymerization are achieved while the biosafety concerns, which are crucial for many clinical applications, are satisfied.

Finally, with various in vitro, ex vivo, and preliminary in vivo studies, the biocompatibility and potential biomedical applications of our injectable adhesive hydrogels are demonstrated for cells scaffolding, soft tissues repair and tissue sealing. This is a design strategy which has potent implication in the way hydrogels are designed to reach high tissue adhesion, as it is not only a way towards synthesis of new biomaterials, but a general design approach based on an understanding of adhesion mechanism. Our approach can even further be used to fabricate more advanced adhesive systems with novel performances.

Keywords: Hydrogel, Adhesion, Photo-polymerization, Interface, Energy dissipation, Bioadhesive, Soft tissue, Fast curing, MeCHa-Gel, Injectability

Résumé

Malgré le développement des hydrogels ayant une large gamme de propriétés mécaniques, une adhésion insuffisante entre les matériaux et les surfaces biologiques limite considérablement leur utilisation dans le domaine biomédical. De plus, malgré les récents développements, une forte adhésion aux différentes surfaces biologiques n'a jamais été démontrée avec des matériaux injectables. Les avancées les plus récentes concernant les systèmes d'hydrogels adhésifs se sont focalisées sur des patches d'hydrogels préformés et des bandes d'hydrogels secs. Dans les stratégies d'adhésion proposées précédemment, les hydrogels développés ne sont pas adhésifs intrinsèquement, mais adhèrent aux tissus ciblés par des développements spécifiques telle que la modification chimique de la surface de contact par exemple. Par conséquent, les hydrogels présentant à la fois une adhésion intrinsèque suffisante et une injectabilité appropriée doivent encore être développés. En outre, la nécessité de concevoir et de fabriquer des systèmes d'hydrogels adhésifs reste un défi majeur dans le domaine biomédical.

Dans la première partie de ce travail, en contrôlant les processus de renforcement, nous avons conçu un hydrogel composite à double réseau avec une teneur en eau élevée, qui crée une interface dissipative et adhère fortement aux tissus mous. Aucune modification de la surface du tissu n'a été nécessaire pour obtenir des propriétés adhésives élevées de l'hydrogel développé. Des principes mécanistiques ont été utilisés pour contrôler la propagation de fissures interfaciales. L'intégration d'un réseau polymérique dissipatif sur les surfaces des tissus mous ont permis d'augmenter

considérablement l'adhésion. Nos résultats mettent en évidence l'importance du contrôle de la structure de l'hydrogel et des processus de dissipation pour renforcer l'interface.

Dans la deuxième partie de ce travail, nous avons proposé une approche universelle pour la conception d'hydrogels injectables qui sont intrinsèquement adhésifs aux surfaces de différents tissus. Nous avons fabriqué une famille de chaines polymériques originales en utilisant un processus de fonctionnalisation en deux étapes afin de fabriquer de nouveaux hydrogels avec des sites d'adhésion disponibles et la capacité de former des réseaux hybrides, ainsi que d'autres améliorations grâce au renforcement par des fibres pour des effets synergétiques plus élevés. Pour y parvenir, notre approche (i) fournit diverses liaisons chimiques fortes avec des nucléophiles à la surface, directement au contact des tissus grâce aux sites de liaisons adhésives disponibles, et (ii) forme un réseau hybride par interactions covalentes et physiques entre les chaines, de sorte que les liaisons interfaciales et la capacité de l'hydrogel à dissiper de l'énergie produise un effet synergétique pour atteindre une adhésion élevée. En plus de son haut niveau de performance d'adhésion, notre hydrogel injectable présente une large gamme de propriétés physicochimiques pouvant être ajustées. Ceci est particulièrement important pour des applications biomédicales nécessitant des propriétés mécaniques supérieures, telles que la réparation méniscale et l'ingénierie tissulaire du cartilage. Une adhésion rapide et une polymérisation en une seule étape sont obtenues tandis que les préoccupations relatives à la biosécurité, primordiales pour de nombreuses applications cliniques, sont adressées.

Table of contents

List of abbreviations

3D: Three-dimensional

2D: Two-dimensional

AFM: Atomic force microscopy

ACAN: Aggrecan

COL2a1:   Collagen type II

CPE4R: Reduced integration 4-node bilinear plane strain quadrilateral element

DN: Double network

Dopa: Dopamine

D-Water: Distilled water

E: Elastic modulus

EDC :   N-(3-Dimethylaminopropyl)-N′-ethylcarbodiimide hydrochloride

EWC: Equilibrium water content

FE: Finite Element

HA: Sodium hyaluronate

IPN: Interpenetrating polymer network

IWC: Initial water content

LAP: Lithium Phenyl(2,4,6-trimethylbenzoyl)phosphinate

NFC: Nano fibrillated cellulose

NIR: Near infrared

MeCHa:	Methacrylated Catechol-containing Hyaluronic acid
MePHa:	Methacrylated Phosphoserine-containing Hyaluronic acid
MePGa:	Methacrylated Phosphoserine-containing Gelatin
PAAm:	Poly(acrylamide)
PBS:	Phosphate buffered saline
PEG:	Poly(ethylene glycol)
PEGDM, PEGDMA:	Poly(ethylene glycol)dimethacrylate
PI:	Photoinitiator
SN:	Single network
SR:	Swelling ratio
UV:	Ultraviolet

List of Figures

List of Tables

Chapter 1- **Introduction**

1.1 Motivation

Advances in biomaterials have drawn much attention in biomedicine over the past decades. There are many clinical situations where it would be beneficial to propose solutions to bond ruptured tissues or to bond an artificial soft material to biological tissues. Water-containing adhesive biomaterials with a structural resemblance to biological soft tissues are attractive materials for various applications. Research in this interdisciplinary field is rapidly expanding and aims to restore, preserve, or enhance tissue functions.

A significant body of research has focused recently on the utilization of hydrogels for various clinical applications. In fact, the specific structures and the chemical behavior of hydrogels in biological environments, which should be nontoxic, extend their applications to the medical sciences. On the other hand, one of the advantages of using adhesive hydrogel systems is their ability to be formed by photo-polymerization as the liquid precursor can be injected by a minimally invasive method and cured in situ, while the gelation reaction is controllable through the ultraviolet irradiation and visible light.

The applications for the adhesive systems can be generally divided into two categories: a) the adherent is used to treat some portions of the tissue such as using hydrogels for tissue repair in articular cartilage defects [1] and b) the adherent acts like a glue to bond a ruptured tissue, to prevent leakage of fluid and/or gas from an incision, or provide adhesion between the attached materials, such as using the fibrin glue for colonic sealing [2] or hydrogels containing chondroitin sulfate used for meniscus repair [3]. However, the relatively low adhesion between the attached materials, as well as the usually observed low mechanical properties of the soft materials as well as the biological requirements, impose serious limitations on their functions.

In a bioadhesion system, both adhesive interactions between surfaces and cohesive bonding within the bulk materials must be considered, particularly for load bearing applications. Understanding of adhesion phenomenon and the effect of the governing parameters, design of a strong adhesive material for biomedical applications, adhesion characterization of hydrogel-tissue under different testing conditions, and performance evaluation of hydrogel in a real situation are the main challenges in bioadhesion studies. The present work aims to address these challenges.

1.2 Objectives

The goal of this project is to develop a biocompatible hydrogel system with tunable adhesion and physicochemical properties for biomedical applications. The developed integration method should tightly bond the surfaces in contact, provide enough adhesion, be easily applied clinically and promote tissue repair. To achieve this, the objectives are defined in the following:

- Understanding of the adhesion phenomenon and the contributing interface and bulk mechanisms for proposing a design strategy of highly adhesive hydrogel-tissue systems;
- Adhesion evaluation and interfacial characterization between the hydrogel and the tissue;
- Development of an intrinsically-adhesive design strategy for injectable hydrogels based on synergetic contribution of interfacial chemistry and bulk mechanics;
- Development and tailoring of injectable hydrogels with a wide window of physicochemical properties meeting the mechanical, biological and adhesive requirements for various applications;
- Optimization of the hydrogels processability, curing and mechanical/degradability/swelling properties.

- Evaluation of the bulk and adhesive properties and integration of hydrogel implant as well as long-term performance through in vitro and in vivo studies.

The present interdisciplinary project involves close collaborations with the Laboratory for Processing of Advanced Composites (LPAC), the Laboratory of Applied Photonics Devices (LAPD) and the Centre Hospitalier Universitaire Vaudois (CHUV).

1.3 Research Approach and Methodology

The following procedures are employed to achieve the abovementioned objectives:

Hydrogel-tissue adhesion phenomenon: The role of contributory factors on adhesion will be studied through different adhesive hydrogel-tissue systems, and the quality of interface and dissipation mechanisms of the adhesive materials will be investigated. To this end, the effect of various parameters such as covalent and ionic crosslinking density, network structure, polymerization, dimensional parameters and surface quality needs to be investigated.

Besides studying the adhesion through the mechanical tests in tensile and shear modes, in situ optical observation of fracture during deformation will also be performed. A polarizing optical system will be combined with the tensile tester and a set-up for crack propagation detection between the host tissue and the hydrogel will be developed. The crack growth velocity, crack initiation, crack advancing and stress distribution will be then thoroughly studied for different hydrogel-tissue interface systems.

Hydrogel design strategy: Based on the understanding of adhesion, the role of interfacial interactions and the toughness capability of the hydrogel on adhesion, a design strategy for highly adhesive hydrogel-tissue system will be proposed and evaluated. Accordingly, we will fabricate a family of original polymeric backbones in order to make new hydrogels with available adhesive sites and the capability to form hybrid networks, as well as further enhancements through fiber reinforcement for stronger synergetic effects. The robust adhesion could be therefore achieved using the resulting synergy between interfacial chemistry and bulk mechanical properties. Moreover, the synergy effect will be clearly demonstrated by varying the synthesis parameters and with no supplemental surface treatment.

The biological and mechanical requirements of the host soft tissues as well as the aforementioned design strategy will be then taken into account in order to achieve a platform for the adhesive material development. To this end, the surface chemistry and composition of surfaces in contact, as well as the mechanical specifications for the hydrogel bulk will be analyzed. All of the analysis procedures will be taken into account for the hydrogel development under a design platform for an adhesive hydrogel.
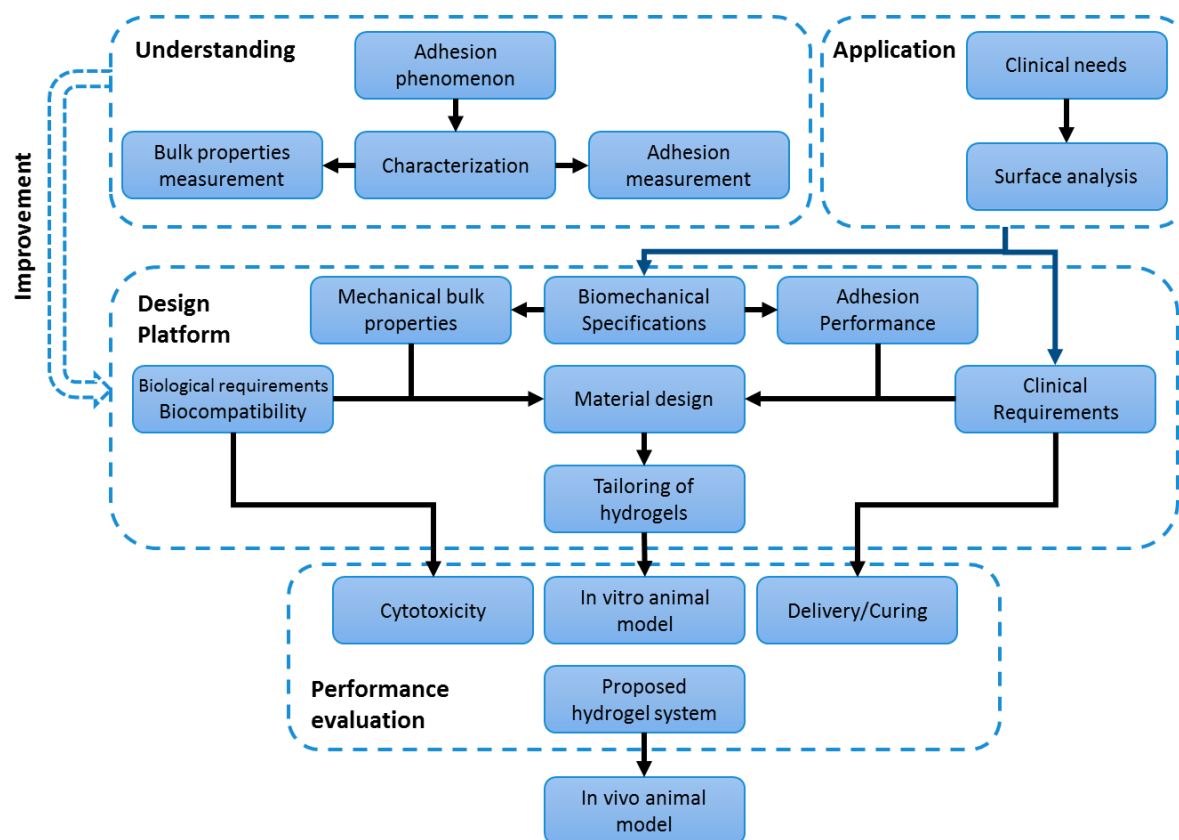
Figure 1.1. The adopted research approach.

Interfacial characterization and adhesion evaluation: Mechanical set-ups will be developed for adhesion evaluation under tensile and shear loading and the adhesive and cohesive behavior of the material will be studied. Adhesion evaluation methods should be developed for both soft-hard and soft-soft adhesion measurements. Moreover, the bulk properties of hydrogels, i.e. stiffness, toughness and strength, need to be evaluated through mechanical measurements. In particular for a load bearing tissue, the obtained properties for the hydrogel system should be compared to those of the host tissue.

As the integration of hydrogel into the tissues is in need of an intimate contact, an interface with a maximum of interfacial interactions between the tissues and the bioadhesive should be obtained. Work of adhesion will be characterized for a better understanding of the links between the hydrogel molecular structure and the tissue.

Tailoring of hydrogels: Strong adhesive hydrogels will be tailored to meet the adhesion targets in addition to the mechanical properties. In particular, for the composite hydrogels, matrices with the polymerization kinetics control and tough polymeric networks will be developed. Moreover, the effect of parameters like network structure, crosslinking and molecular composition on bonding and adhesive capability will be investigated. Based on the understanding of adhesion phenomenon and on the material design platform for injectable and intrinsically adhesive hydrogels, we will fabricate an original family of adhesive hydrogels.

Sample preparation: For *in vitro* and *ex vivo* adhesion and integration evaluations of hydrogel-tissue systems, tissue samples should be prepared for the different evaluation methods. Samples from bovine cartilage, bone and meniscus, as well as other soft tissues will be prepared for the preliminary study in the project. Special sample preparation techniques should be used based on mechanical properties of the selected tissues.

Biocompatibility and performances evaluation: The cytotoxicity of the hydrogel precursor and photo-polymerized hydrogel will be examined. Moreover, the bulk mechanical and adhesive properties for the hydrogels will be evaluated through various *in vitro* and *ex vivo* tests. The hydrogels will also be examined in *in vivo* animal model in order to study the mechanical and adhesive performance of the material as well as biomechanical performance with minimal alteration of physiological conditions.

The thesis is structured into six chapters including the present introduction. The employed materials and methods are presented in each corresponding chapter. The chapters are organized as follows:

Chapter 2 provides a brief review on the state of the art on hydrogel adhesion improvement approaches.

Chapter 3 presents the role of the mechanical dissipative processes on adhesive performance of hydrogels. To this end, composite double-network hydrogels are proposed to improve adhesion on biological surfaces and adhesion performance is analyzed.

Chapter 4 deals with the common adhesion measuring techniques and the developed custom-made adhesion setups in this work.

Chapter 5 presents the design strategy for intrinsically adhesive and injectable single network hydrogels. Accordingly, a family of original hydrogels is fabricated based on a synergetic design, which is demonstrated clearly for the injectable hydrogels. Furthermore, a wide and tunable window of physicochemical performances of the hydrogels is analyzed and reported.

Chapter 5 is also dedicated to the performance evaluation of the proposed adhesive hydrogels for various applications including tissue scaffolding, sealants, and tissue adhesives. The *in vitro*, *ex vivo* and *in vivo* characterizations are performed to further study the performance the hydrogels.

Chapter 6 summarizes the concluding remarks and provides perspectives for future work.

The flowchart shown in Figure 1.2 summarizes the adopted research approach in this thesis.

Adhesion understanding and characterization

Adhesion phenomenon | Role of mechanical dissipation processes for toughening the interface

Dissipative hydrogels | Design of composite double-network hydrogels (covalently cross-lined PEGDMA, ionically cross-linked alginate network and NFC reinforcement), non-degradable — **Chapter 3**

Characterization | Adhesion characterizations: AFM, Tensile, Shear, etc. Development of custom-made adhesion setups. Bulk and interfacial fracture tests — **Chapter 4**

Design strategy for injectable and intrinsically-adhesive hydrogels

A bioinspired design platform with wide window of properties | Design and development of a family of biodegradable cross-linkable polymers (MeCHa, MePHa and MePGa) and fabrication single-network intrinsically-adhesive hydrogels

Synergetic adhesion mechanism | Direct demonstration of the synergetic contribution of hydrogel bulk mechanics and interface energy on the obtained high adhesion performance using the hydrogel synthesis parameters

Fiber-reinforcement | Fabrication of composite version of the developed hydrogel family (Collagen and NFC reinforcement) — **Chapter 5**

Performance evaluation

Potential applications | Study of hydrogels potential in tissue scaffolding, tissue sealing, and soft tissue gluing

Characterization | Mechanical characterization, swelling behaviour, biodegradation kinetics (window of tunable properties). Biocompatibility analysis. *In vitro*, *ex vivo* and *in vivo* evaluations — **Chapter 5**

Figure 1.2. Flowchart of the adopted research sections.

Chapter 2- **State of the art**

2.1 Background and Challenges

Strong integration of biological surfaces and hydrogel materials, is required for successful performance of many biological systems made out of the soft materials [1, 2]. There is also a broad range of applications for the materials with sufficient adhesion to biological tissues in biomedicine; from drug delivery [3] to biomedical devices [4]. There are a number of tissue adhesives that are commercially available, however they suffer from poor biocompatibility or insufficient bonding strength [5]. Tissue adhesives such as the fibrin glue and COSEAL present weak adhesion to tissues [6], and cyanoacrylate adhesives may induce a cytotoxic reaction and have lack of analogy with tissues dynamics due to their rigidity [7]. Despite the development of numerous adhesives hydrogels [8-11], high adhesion performance has not been achieved, in particular for load bearing tissues such as cartilage [12] or meniscus [13].
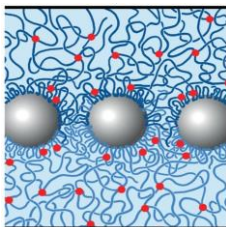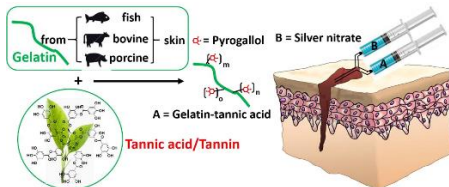
Previous studies have proposed different strategies for adhesion increase mainly by the improvement of interfacial interactions [14-21]. However, the energy required to break these interactions is often very low [22]. Nanoparticles, such as silica nanoparticles, surface modified carbon nanotubes and
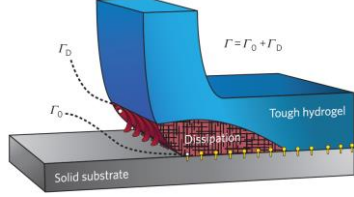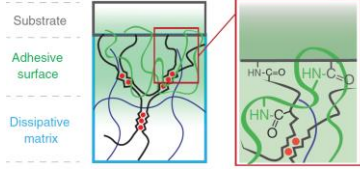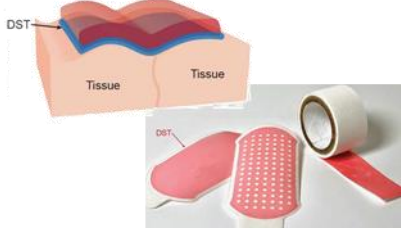
cellulose nanocrystals, have been used for adhesion improvement but through weak physical interactions. They adhere weakly to biological surfaces and present adhesion energies in the range of 1-10 J m^{-2} [8]. Bioinspired adhesives, such mussel inspired adhesives, which are based on creating interfacial bond strength of the catechol moieties, exhibit weak adhesion [23]. Although robust bonding of hydrogels to some inorganic solid surfaces such as metal or ceramic has been obtained, it requires time-consuming surface modification of solids [24] or porous surfaces structure [25], which is not suitable to biological tissues. Similarly, the developed strategies to achieve an adhesive contact between dry elastomers to solid materials, such as glass or metals are not applicable to water containing hydrogels [26]. Recently, biocompatible adhesive hydrogel systems have been developed but they still necessitated a treatment of the tissue surface such as example for cartilage [27] or they are based on higher polymer content impairing therefore their injectability.

Furthermore, a reliable hydrogel design would require high water content, quick implantation, and biocompatibility. The high water content is key to insure the injectability of the hydrogels. These constraints impose limitations on adhesion performance.

Table 2.1 summarizes the various proposed solutions for adhesion improvement in the hydrogel systems.

Table 2.1. Some recently proposed mechanisms for improving hydrogel adhesion

Current adhesive systems for adhesion improvement

Adhesive system	Adhesion Energy / Description	Example	References
Tissue adhesives	1 to 10 J.m^{-2} - Covalent bonds with tissues - Possibility for cytotoxicity - Low matrix toughness - Rigidity	Fibrin Glue Cyanoacrylate (super glue) Polyethylene glycol–based adhesives 	[6], [28], [29], [30], etc.
Chemical treatment of tissue	1 to 100 J.m^{-2} - Strong interfacial chemical bonds - Low adhesion	Functionalized chondroitin sulphate to chemically bridge gel and tissue (2007) 	[31], etc.
Nanoparticle-hydrogel adhesion	~ 10 J.m^{-2} - Weak physical interactions - Hydrogen bonding - Very low adhesion with tissues	Silica nanoparticles & hydrogel (PDMA, Polyacrylamide and Gelatin) (2014) 	[8], etc.
Natural/Biologically inspired adhesives	1 to 50 J.m^{-2} - Weak physical interactions	Tannin-inspired antimicrobial bioadhesive (2018) 	[32], [19], [1], [24], etc.
DN hydrogel + silanation	~ 1000 J.m^{-2} - Not applicable to biological surfaces - Hydrogel water content: 74-80% - Long surface modification	Surface silanation & a DN gel (2017)	[24], etc.

DN hydrogel patch + surface treatment	~ 1000 J.m^{-2} - Hydrogel water content: 67-85% - Surface treatment needed	Bridging adhesive & a DN gel (2017) 	[27], [24].
Dry double-sided tape	~ 1000 J.m^{-2} - Not injectable - Surface treatment needed	Dry DST DN hydrogel (2020) 	[33].

2.2 Clinical needs

Hydrogels have drawn great attention in the biomedical areas owing to their resemblance to living tissues and exceptional properties such as high water content, softness, flexibility, biocompatibility [34-37]. Therefore, they have remarkable potential for tissue engineering applications, drug delivery, wound dressing and other biomedical applications [34, 38]. However, there are serious challenges associated with their poor mechanical and in particular adhesive properties. The weak and brittle adhesion of hydrogels to biological surfaces considerably hampers their integration and function in biomedical applications. On the other hand, obtaining sufficient adhesion is not the only matter of importance; as for many applications, the developed adhesive material should also present specific range of mechanical properties and meet other biological requirements. This could represent a serious challenge since meeting all these requirements is rare and difficult to achieve [39]. This is even more challenging in the field of orthopedics where there is almost no developed hydrogel presenting all these properties especially for load bearing applications like cartilage repair and meniscus tear

treatment. Thus, the need for a general strategy for the design and fabrication of adhesive hydrogel systems has remained a central challenge in the field.

Cardiovascular surgeries: Minimally invasive reconstructive cardiovascular surgery is being pursued to avoid complications from invasive open-heart procedures; however, one of the main challenges is the inability to reconnect tissue or attach prosthetic materials in a dynamic environment, such as continuous tissue contractions and blood flow, and in the presence of blood. Within a minimally invasive procedure, sutures can cause local tissue damage and do not provide an immediate liquid proof seal. On the other hand, current available tissue adhesives such as medical grade cyanoacrylate or fibrin sealant, can be easily washed out under in vivo dynamic conditions and either are toxic or exhibit poor adhesion strength properties. Therefore, they cannot withstand the forces inside the heart chambers and major blood vessels [40, 41] and usually become ineffective in the presence of blood [42]. Very recently, a blood-resistant glue for repair of vessels has been proposed using a hydrophobic light-activated adhesive (HLAA); however, in spite of obtaining stronger adhesion than standard sealants such as fibrin, the adhesion is not sufficient (about 35 kPa) [43].
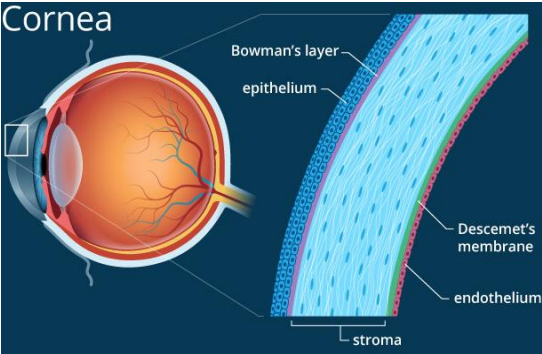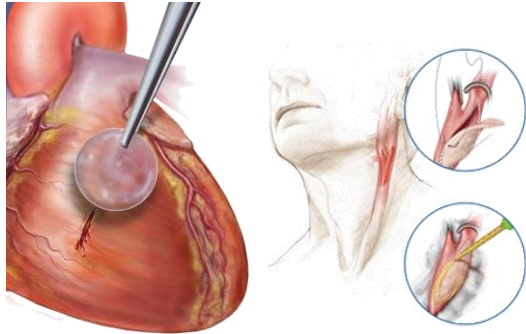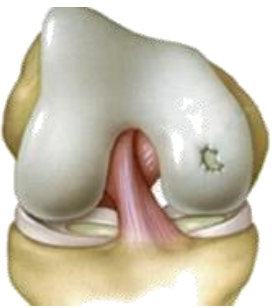
Cartilage repair: Cartilage repair is a highly challenging application where there is a significant need for a tissue integration method. Cartilage is made of a thick matrix of proteoglycans and collagen and this dense lubricating tissue is particularly challenging for adhesives and bonding strategies [44, 45]. Currently, there are limited surgical methods and no highly strong adhesive that is capable of bonding or integrating cartilage tissue. For example, a novel bioadhesive using chondroitin sulphate, as one of the strongest cartilage adhesives proposed in the literature, has been developed to bond hydrogels to articular cartilage defects but it presents not more than 45 kPa adhesion strength [31]. On the other hand, the low mechanical properties are other major limitations of this material [17]. Moreover, there is the same challenge to integrate a hydrogel used to fill a cartilage defect on a subchondral bone. For cartilage damages with the subchondral bone involved, osteochondral plugs transplantation surgeries represents a possible solution for creating hyaline-like repair [46]; however, robust tissue integration and stability during the healing process is still problematic. Another proposed method is using the fibrin-based glues to bond a cartilage scaffold to the subchondral bone, however, one of the major drawback is the intrinsic low resultant adhesion force obtained between the attached materials [47]. Thus, developing materials with the capability to create high adhesion in cartilage repair surgeries is highly needed.

Meniscus tear treatment: The treatment to restore the integrity and function of injured meniscus is another challenging clinical situation. Meniscus has a weak and location dependent healing response due to low cell density, limited vascular network constrained to the peripheral region, the dearth of healing factors and the presence of a thick hypoxic extracellular matrix [48]. Meniscus tears are often repaired using sutures, staples, stingers and screws [49, 50]; however gap formation occurs between the anchors resulting in contact healing limited to the point of fixation [51]. Failure to restore functional meniscus tissue ultimately results in total or partial removal of the tissue [52]. Tissue adhesives could be attractive biomaterials to be used for treating meniscus tears [53]. Only few tissue adhesives, such as Cyanoacrylate, Dermabond® and fibrin glue, are already used in clinical practice, but they are not suitable for the repair of meniscal tears due to their insufficient mechanical and adhesive properties or toxicity [53, 54]. Therefore, the development of materials, which are strong, non-toxic, and with high adhesive properties could be used in this clinical situation.

Corneal lacerations: The cornea is the transparent and dome-shaped front part of the eye. The most current treatments for corneal injuries include suturing and gluing. However, sutures can cause infection, inflammation, neovascularization, and induce astigmatism. Current tissue adhesives, such as Cyanoacrylate and fibrin glue, have limitations and can cause foreign-body sensation, local inflammatory reaction, toxicity and conjunctival hyperemia [5, 55, 56]. Thus, a new biocompatible adhesive, such as an adhesive transparent hydrogel with reduced side effect, could be used for the treatment of corneal incisions.

Table 2.2 shows some potential applications, as example, in which development of adhesive hydrogels can be used for new clinical translations.

Table 2.2.   Some potential applications for adhesive and biocompatible hydrogels.

Adhesive Function	Example / some requirements	Ref.
Temporary sealing with subsequent implant removal	**Corneal laceration/ Stroma damage** - High mechanical stiffness - Very high transparency - Fast curing - Low swelling - Injectability - Integration with stroma, etc.	[57]
Temporary sealing	**Glaucoma Surgery** - Proper sealing under wet condition - Fast curing - Injectability, etc.	[58]
Long-term sealing with implant degradation	**Wound healing Repair of cardiac tissue** - Sufficient stretchability and toughness - Fast curing - Low swelling - Perfect sealing, etc.	[59]
Long-term stability and high mechanical performance	**Meniscus repair** - High mechanical toughness under high loads - Low or negative swelling - Sufficient deformability - Fatigue performance, etc.	[53]
Long-term mechanical performance with/out degradability	**Cartilage repair/replacement** - High mechanical stiffness - Toughness but under high loads - Fast curing - Low swelling - If degradable: controllable compatible with tissue growth - Fatigue performance, etc.	[60]

2.3 Adhesion mechanisms

Looking at a variety of different researches on adhesive materials in biomedical field, it could be easily noticed that the obtained adhesion in the hydrogel-tissue systems is often lower than the adhesion needed. The factors that determine biological adhesion, or enhance the bioadhesion between two surfaces in contact, are generally classified into the effects of surface morphology, chemical interactions, physiological factors and physical-mechanical interactions [61, 62].

Although adhesion can be improved by better surface interactions (bonding) leading to a strong interface [8, 20, 31, 43, 63], and for many experts of adhesion surface energy is of the highest importance [64], there are a lot of attempts in biomedical areas based on increasing the surface interactions but without any considerable resulting adhesion.

For a high adhesive system, the surface interfacial interactions are not necessarily sufficient [24]. Fracture mechanics offers a powerful tool to be particularly useful at predicting the path followed by cracks propagating in both monolithic and bonded systems [65]. Hence, it can provide a framework for a better understanding of bioadhesion mechanism. According to the studies on crack propagation mechanisms as well as the properties of soft materials with viscoelastic behavior, the mechanical dissipation capability of the adhesive is also required for high adhesion systems, not only as a contributory factor for making high adhesion, but as the main parameter [22]. However, in the biomedical researches, this parameter has not been systematically taken into account for the material design. On the other hand, in spite of few recent studies on the effect of dissipation in adhesion community, the correlation between the dissipation capability and other adhesion parameters has not been thoroughly studied.

2.3.1 Mechanical dissipation and surface interactions

The energy required to break the interactions at interface is often very low. For example, breaking the attractive forces between the atoms of the adhesive and the substrates gives rise to small energies, known as the thermodynamic work of adhesion [66]. For debonding at an interface between two

materials, the thermodynamic work of adhesion is in the order of tens of mJ/m^2 [66] that is often measured by contact angle or JKR method [67]. Although it is taken for granted that chemical bonds provide strong adhesion, the total energy needed to break all the bonds at the interface is not high. For a pure interface made of just strong chemical bonds it is only possible to get about 1 J/m^2 [68]. There are similar limitations for physisorption interactions; although Van der Waals bond lengths are longer than those of other molecular forces, they are still short in absolute terms so that these forces only act over very small distances [62]. Even employing other mechanisms, such as roughening the surface for improving the interactions at the interface, do not necessarily and noticeably improve adhesion. In particular for biological applications, the viscosity of the adhesive might be too high to fill all the surface features created by roughness and it can even reduce adhesion. This is because failure to fill the features does not just mean a slight reduction in surface area; it means that there is a crack built into the bond [22], and the stress needed to initiate an adhesive failure decreases sharply in the presence of any pre-crack in the system. Entanglement of polymer chains across the interface is another mechanism which can considerably improve adhesion. However, without dissipation, it cannot give a very strong adhesion [22]. Thus, obtaining high adhesion only through making good interactions at interface is not a reliable approach.

On the other hand, there could be a great dependence on mechanical toughness and dissipation for high adhesion. It implies that significant energy can be dissipated in the system, particularly through viscoelastic deformation of the material. In other words, the material's dissipative capability allows keeping the interface and results in substantial dissipation of mechanical energy in regions around the cracks as there is a crack growth stage from the crack initiation to the final steady state. For the materials without (or with low) energy dissipation, the interfacial cracks reach the steady state immediately after their initiation. They propagate easily along the interface because of the brittle nature of the interfacial interactions. It could be stated that, for an adhesion system with enough interactions energy, high adhesion can be obtained as much as the energy that can be dissipated. Therefore, if a material is not dissipative, it seems it cannot provide high adhesion. However, it should be noted that the effective dissipation and a reliable measurement is of high importance, and controversial.

Table 2.3 presents a summary of the two sets of interfacial and dissipation mechanisms for the design of adhesive systems.

Table 2.3. Mechanisms for improving interactions and dissipation energy

Intrinsic and Dissipation/Toughening Mechanisms

Interfacial Interactions Mechanisms				Mechanical Dissipation Mechanisms			
Mechanism	**Description**	**Example**	**References**	**Mechanism**	**Description**	**Example**	**References**
Chemical interactions	The ionic and covalent bonds result in a chemical interaction at the interface. An order of magnitude weaker bond is formed when there is hydrogen bonding. Due to short bonds lengths, surfaces must be brought very close together and remain in this proximity for the bond to be stable.	Providing chemical bonding between the carboxylate molecule of the cement and hydroxyapatite mineral in the tooth, using zinc polycarboxylates for dental cements	[14-20, 31, 53, 63, 69-71], etc.	**Polymer chains fracture**	Dissipation of mechanical energy stored in the chain and possibility of irreversible damage in polymer networks	Interpolymer reinforcement between PEG and PAA yielding high fracture strength	[72], [73], [74], [75], [76], [77], [78], [79], [80], etc.
Intermingling and entanglement effect	Some materials may intermingle or entangle at the bonding interface, which typically is the case with polymer chains where one end of a molecule can diffuse into the other material. Polymer/polymer entanglement requires many nm of intermingling.	Processing a resilient denture liner onto an acrylic resin denture base	[8], [81], [82], [83], etc.	**Reversible/ physical crosslinking**	Chains detachment from physical crosslinkers under mechanical loads relaxes stretched polymer chains and therefore dissipates energy in the network. The physical crosslinkers can usually be recovered.	Stress relaxation through breaking and reforming of the ionic crosslinks in chitosan-based gels	[84], [85], [86], [87], [88], [89], [90], [91], [92], [93], [94], [95] [111], etc.
Physisorption/ dispersive interactions	The surfaces of two materials are held together by van der Waals forces; the attractive forces between two molecules, each of which has a region of small positive and negative charge.	Artificial fibrillar adhesives Inspired by the climbing ability of gecko lizards	[96], [97], [98], etc.	**Transformation of domains**	Polymer chains and crosslinkers may contain certain domains that transform between different configurations under mechanical loads and dissipate energy.	Folded proteins and polysaccharides in biological polymers and mechanophores	[99], [100], etc.
Mechanical processes	Surface modification through mechanical texturing is a method to create anchor points, when the adhesives attach to surface by mechanical interlocking.	Abrasive particles (such as silicon carbide or alumina) impinge on the biomaterial, and the resulting impact increases its surface roughness [28,54].	[25], [101], [102], etc.	**Fibers fracture and pullout**	Fracture and pullout of fibers embedded in a hydrogel matrix in the bridging zone of the crack can dissipate mechanical energy in the hydrogel.	Polyglycolic acid fiber reinforced agarose	[103], [104], [105], [106], [107], etc.
Physical processes	Various methods could be used to modify surfaces, such as exposure to plasma, corona discharge, ions and ultraviolet (UV). Plasma processing produces reactive species such as ions and free radicals.	Surface plasma processing for fibroblast cells adhesion in which molecules can be grafted onto the activated surface	[108], [109], [110], [111], [112], etc.				

2.3.2 Bio-adhesion design

Although surface interactions at the interface and bulk mechanical toughness generally provide better adhesion, this adhesion and its contributory parameters are not well understood. It seems that designing a balance between the contributory factors is required leading to an ideal adhesion system. These two determinants should work in concert with one another in order to achieve desirable adhesion between the surfaces of interest. Despite the fact that surface interactions energy at the interface is relatively low for high adhesion, it is still of high importance. The mechanical dissipation capability of the material cannot be used when there are weak interactions at the interface. In fact, this is the interactions energy, albeit probably very low, that defines how much of the available dissipation capability could contribute to adhesion. In brief, it seems that making a high adhesion system begins with enough surface interactions but dramatically rises with the mechanical capability of the bulk material.
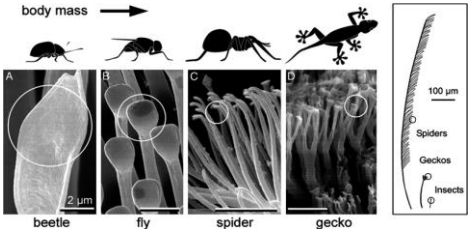
In the absence of almost no general adhesion improvement platform in biomedical field, it is intended to propose and take advantage of a reliable strategy for material design applicable in many applications. Combined with various surface treatments, several tough hydrogels have been developed, such as composite hydrogels, interpenetrating network and double network hydrogels, that can effectively dissipate energy. However, for an adhesive hydrogel system in biomedical area, not only the range of adhesion should be improved but it should be maintained while satisfying the range for other mechanical and biological parameter. More reliable toughening mechanisms should be introduced for long term performance of the adhesive hydrogels.

2.4 Nature inspiration

Nature can be a valuable source of inspiration for highly adhesive materials. Wet adhesion of hydrogels on different substrates can be found in nature for various loading conditions, such as tough adhesion of mussel's on rock under the sea-shore environment [63]. However, the nature-inspired researches for design of adhesive hydrogels often presents very low adhesion. For example, it is widely discussed in literature that mussel inspired adhesives adhere weakly to tissues [27]. This could be mainly due to ignoring the fact that achieving high adhesion energy requires the synergy of interfacial and material parameters as well as a comprehensive design inspiration. Table 2.4 presents several natural adhesives systems and attachment strategies found in animals and plants.

Table 2.4. Nature adhesive systems.

Bio-adhesives and attachment strategies found in animals and plants

Natural system	Description	Adhesive mechanism	References
Frog tongue	- The tongue is highly damped like a shock absorber, absorbing energy and so preventing separation from the insect. - Coated with a thin layer of saliva with non-Newtonian properties - 50 times greater work of adhesion than known synthetic polymers such as the sticky-hand toy.	A combination of a soft, viscoelastic tongue coupled with non-Newtonian saliva 	[113], [114], etc.
Crucifix Toad skin	- A sticky substance over their skin to protect themselves from biting insects. - The glue jams up the insects' jaws, causes them to stick to the skin, and the frogs can later eat the stuck insects. - It hardens within seconds and sticks well, even in moist environments. - Stronger than available non-toxic medical adhesives.	Exudation of a tacky and elastic glue onto dorsal skin when provoked 	[115], [116], [117], etc.
Sandcastle worms	- Able to harness underwater adhesive proteins for their own benefits. - Building tubular shells by gluing together sand grains and mineral particles, with a multipart, rapid-set, self-initiating adhesive. - The adhesive is composed of oppositely charged polyelectrolytic components, containing significant amount of Dopa residues.	Chemical wet adhesion 	[118], etc.
Caddisfly larva	- Coacervates are likely associated with the underwater adhesion of the silk-like fibers secreted by caddisfly larvae. - Their glue has a balanced ratio of positive to negative charges, similar to that of sandcastle worms, but the oppositely charged residues are distributed in alternating patches on one macromolecule rather segregated into different proteins.	Coacervate structures for underwater adhesion 	[118], [119], etc.

Natural system	Description	Adhesive mechanism	References
Mussels	- Strong attachment to different surfaces in wet environments. - It is widely discussed that the presence of an amino acid (Dopa) in the byssal plaque of the mussel is responsible for the mussel's ability to stick.	Chemical moisture-resistant adhesion 	[120], [69], etc.
Clingfish	- Clingfishes adhere equally well to a diversity of surfaces that differ greatly in roughness with an adhesive disc on their abdomens that is unhindered by rough, slippery or wet surfaces. - The adhesive force is 80 to 230 times the body weight of the fish. - Adhesion and friction forces work together to keep the fish's grip discs in place. - A ring of hairlike structures surrounding the disc, increases the surface area of the disc, which in turn increases friction.	hierarchically structured microvilli on the ventral surface of the adhesive disc 	[121], [122], etc.
Gecko	- A complex hierarchical structure of lamellae (1-2 mm), setae (5-10 μm), branches (1-2 μm) and spatula (100-200 nm) to generate the contact area necessary for dry adhesion. - The setae, composed of β-keratin and α-keratin, exhibit an adhesive shear force of 194 μN and an adhesive normal force of approximately 20 μN.	Dry nano-scale reversible adhesion 	[123], [124].
Insects	- Smooth pads (ants, bees, cockroaches, and grasshoppers) consist of a dense fibrous material that is soft in compression, strong in tension, and possesses functional material properties including adaptability, viscoelasticity, and pressure sensitivity. - Hairy pads (beetles, flies, and spiders) are composed of a diverse density of setae which range in length from few micrometers to several millimeters.	Smooth or hairy pads, wet adhesion 	[125], [123].
Natural system	**Description**	**Adhesive mechanism**	**References**

		Physical contact and chemical adhesion	
Plants	- English ivy: bio-adhesion to climb vertical surfaces, the attachment process through physical contact, chemical adhesion, and shape changes of the root hairs. - Sundew: bio-adhesion for capturing insects. The adhesive secreted has unique physical properties including high viscosity and elasticity. When dried, the adhesive formed an intricate network of nanofibers and nanoparticles. - Algae: remarkable ability to rapidly and permanently attach to surfaces underwater due to the secretion of extracellular polymeric substances (EPS).		[123], [126], [127], [128], [129], [130], etc.

2.5 Photo-polymerizable hydrogels

Hydrogels are often classified based on their composition, synthetic or natural origins and type of cross-linking. Natural hydrogels often presents higher biocompatibility and lower stability than the synthetic hydrogels, and are formed with natural materials such as gelatin, alginate, proteins, collagen, etc. [131, 132]. Chemical hydrogels are cross-linked with covalent bond formation mechanism, resulting in irreversible network formation. Physical hydrogels cross-linking mechanism is based on physical interactions between polymeric chains (ionic interactions, hydrogen bonding, entanglements, etc.), leading to reversible cross-linking mechanism [133]. Among various types of polymerization mechanisms (e.g. chemical, thermal etc.), photo-polymerization exhibits significant advantages such as *in situ* curing, polymerization at ambient temperature, and spatial and temporal control over the hydrogel gelation [134]. In photo-polymerization, the hydrogel network is cross-linked triggered by visible or ultraviolet light, which initiates and propagates the reaction, and irreversibly transforms the liquid precursor into a solid hydrogel. The fine control over polymerization kinetics is particularly useful for the fabrication of many biomaterials in various physiological conditions. Photo-polymerization technique has a wide variety of biomedical applications such as in bio-adhesive technology, tissue engineering and drug delivery [135].

Figure 2.1 demonstrates the radical polymerization process. The photo-polymerization starts with an initiation process where a radical is generated by exposing a photo-initiator to the light stimulus. The radical adds across the carbon-carbon double bond, generating a carbon-centered radical. The resulting radical reacts with another monomer. The propagation reactions occur and the chain grows quickly. Polymerization stops through one of several termination reactions, including combination and disproportionation which eliminate the radical [136, 137].

Initiation: $I \xrightarrow{stimulus} I\bullet$

$I\bullet + M \longrightarrow IM\bullet$

Propagation: $M_i\bullet + M \longrightarrow M_{i+1}\bullet$

Chain Transfer: $M_i\bullet + RH \longrightarrow M_iH + R\bullet$

Termination: $M_i\bullet + M_j\bullet \longrightarrow M_{i+j}$

$M_i\bullet + M_j\bullet \longrightarrow M_i + M_j$
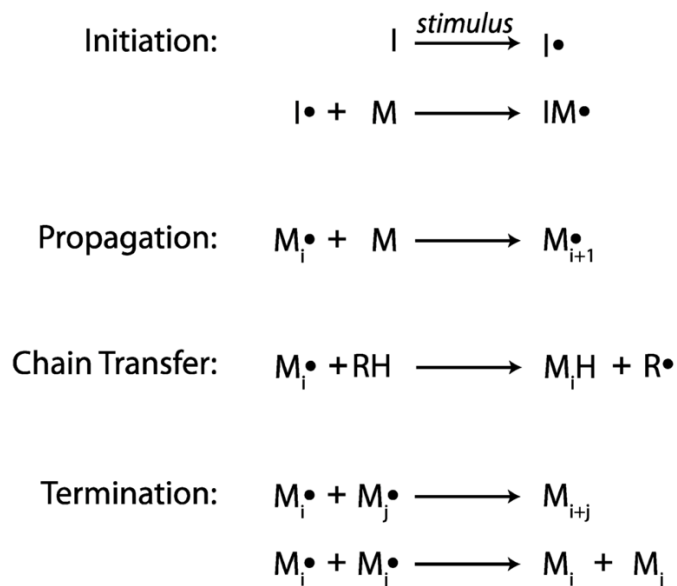
Figure 2.1. The radical polymerization process. I = an initiator, M = vinyl monomer, M_i or M_j = polymer with, i or j repeat units, respectively, H = hydrogen, RH = a compound with a readily abstractable hydrogen [137].

There are also some challenging issues when using the photo-polymerization methods. The biocompatibility and biosafety concerns limit the type of initiator and light parameters (e.g. wavelength and intensity) [138]. Furthermore, the light penetration energy could either limit the polymerization depth or full polymerization of hydrogels [139].

Chapter 3- **Composite Double-Network hydrogels to improve adhesion on biological surfaces** [1]

3.1 Background and Challenges

Despite the development of hydrogels with high mechanical properties, insufficient adhesion between these materials and biological surfaces significantly limits their use in the biomedical field. By controlling toughening processes, we designed a composite double-network hydrogel with high water content, which creates a dissipative interface and robustly adheres to soft tissues. No tissue surface modification was needed to obtain high adhesion properties of the developed hydrogel. Instead, mechanistic principles were used to control interfacial cracks propagation. The integration of the dissipative polymeric network on the soft tissue surfaces allowed increasing significantly the adhesion strength. Our findings highlight the significant role of controlling hydrogel structure and dissipation

[1] Karami, P., et al., Composite double-network hydrogels to improve adhesion on biological surfaces. ACS applied materials & interfaces, 2018. 10(45): p. 38692-38699.
The DIC method in this chapter was developed in collaboration with Céline Samira Wyss.

processes for toughening the interface. This research provides a promising path to the development of highly adhesive hydrogels for tissues repair.

Strong integration of hydrogels and biological surfaces is needed for successful tissue repair in biomedicine [1, 2]. Tissue adhesives such as the fibrin glue and COSEAL present weak adhesion to tissues [6], and cyanoacrylate adhesives may induce a cytotoxic reaction [4]. Despite the development of numerous adhesives hydrogels [8-11], high adhesion performance has not been achieved, in particular for load bearing tissues such as cartilage [12] or meniscus [13]. Furthermore, a reliable hydrogel design would require high water content, quick implantation, and biocompatibility. The high water content is key to insure the injectability of the hydrogels. These constraints impose limitations on adhesion performance. Previous studies have proposed different strategies for adhesion increase mainly by the improvement of interfacial interactions [14-21]. However, the energy required to break these interactions is often very low [22]. Although robust bonding of hydrogels to some inorganic solid surfaces such as metal or ceramic has been obtained, it requires time-consuming surface modification of solids [24] or porous surfaces structure [25], which is not suitable to biological tissues. Recently, biocompatible adhesive hydrogel systems have been developed but they still necessitated a treatment of the tissue surface such as example for cartilage [27] or they are based on higher polymer content impairing therefore their injectability.

Focusing on mechanical aspects for adhesion, various toughening mechanisms have been implemented into hydrogels to enhance the fracture energy [140], but the potential of using highly tough hydrogels as adhesive implants is not well explored. Recent developments show that toughness could be improved by employing composite hydrogels [141], homogeneous network structure [142], interpenetrating polymer network [143] or double network structure [144]. Here, we have developed a hydrogel design which provides robust adhesion on soft tissues including articular cartilage and meniscus. The composite double-network hydrogel presents not only high cohesive toughness but also high resistance to interfacial crack propagation, which is of key importance for adhesion [24, 145]. The low dissipation of a chemically crosslinked polymer is significantly enhanced by the combination of fiber reinforcement and a second physically crosslinked network. Thus, the hydrogel can dissipate a considerable amount of energy and protect the interactions at the interface during detachment from the tissue. The proposed dissipative hydrogel can also form sufficient interfacial interactions so that the energy can be dissipated. We propose that the combination of nano-fibrillated cellulose (NFC) reinforcement and physical crosslinking of alginate in PEGDMA network can highly

increase the hydrogel-tissue adhesion due to the balance between the interfacial interactions and bulk properties.

In addition, the adhesion performance of the material is obtained while it has high water content (~90% of water). The liquid precursor can be injected directly onto the tissue surface and be crosslinked through photo-polymerization. The biocompatible photo-crosslinked PEGDMA can present controllable mechanical properties and be used in wide range of biomedical applications [103, 146], in particular for the tissues subjected to high loadings [147]. Hydrophilic and stiff NFC fibers form a network through hydrogen bonds and physical entanglement [148]. They have demonstrated potential as a biocompatible reinforcement phase to enhance the mechanical properties of the hydrogel and curing time reduction through light scattering during polymerization [147, 149]. The physical interactions and the ease of gelation of alginate as a natural biomaterial are also advantageous to tailor the favorable properties of hydrogel in tissue engineering applications [150].

Our approach for the development of the proposed composite hydrogel is to create a network of rigid fibers into a dissipative matrix in order to maximize the protection of the contact points. Indeed, enhanced intimate contact can be obtained by interfacial reactions promoting local load transfers. As shown in Figure 3.1, the hydrogel matrix can form interfacial interactions with the large surface of the NFC fibers due to their high aspect ratio [148]. In addition, interfacial adhesion might be enhanced due to mechanical interlocking of fibres with the tissue [151].
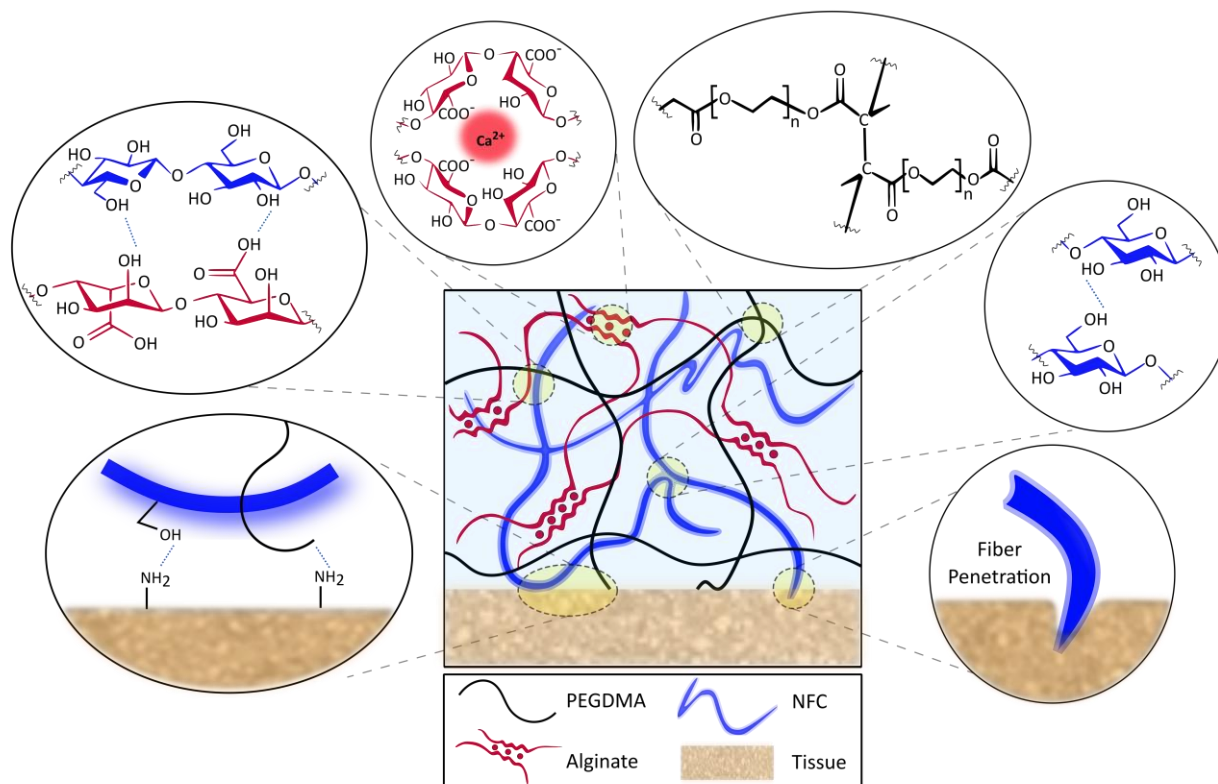
Figure 3.1. Schematic illustration of adhesive design of the hydrogel. The dissipative matrix consists of a deformable synthetic polymer (PEGDMA) interpenetrated with a ionically crosslinked natural polymer (alginate), reinforced by cellulose fibers (NFC). The various possible toughening mechanisms of the hydrogel contribute to high protection of interfacial bonding on the tissue. Mobility of PEGDMA network, physical crosslinking of alginate chains, pullout of NFC entanglements, interfacial hydrogel bonds, and fiber-fiber and fiber-matrix interface interactions improve the interfacial and hydrogel bulk toughness required for a dissipative interface.

3.2 Materials and Methods

3.2.1 Materials

The PEGDMA was synthesized using Poly(ethylene glycol) (Sigma-Aldrich) with a molecular weight of 20 kDa, as previously reported [103, 152]. Dried poly(ethylene glycol) (20 g) was dissolved in 60 ml of dichloromethane (99.8%, Acros) and mixed with methacrylic anhydride (94%, Sigma-Aldrich) and triethanolamine (99%, Sigma-Aldrich) under dry argon flow for five days. The solution was precipitated in diethyl ether (99.5%, Acros), filtered and dried overnight. For radical polymerization

of PEGDMA network, Irgacure 2959 (BASF) was used as photoinitiator. The NFC was provided by EMPA (Swiss Federal Laboratories for Materials Science and Technology, Dübendorf, Switzerland). The slurry of bleached softwood cellulose pulp (Zellstoff Stendal) was fibrillated with high-shear homogenization and long NFC fibers were used with a diameter of 10-200 nm [153]. Sodium alginate (Sigma-Aldrich) was crosslinked with calcium sulphate (Sigma-Aldrich) as ionic crosslinker.

3.2.2 Hydrogels synthesis

The NFC-reinforced hydrogel precursor was synthesized by dissolving PEGDMA (10 wt%) in phosphate buffered saline (PBS, pH 7.4) and mixing with NFC (0.5 vol. %) and Irgacure 2959 (0.1 $g.ml^{-1}$%). The hydrogel precursor was homogenized using an Ultra-Turrax at 12000 rpm for 20 min. The degassed mixture was then poured into the specific molds made of Teflon and covered with microscope slides (see Figure 3.2). The double network PEGDMA-alginate hydrogel was synthesized by mixing PEGDMA (10 wt%), calcium sulphate (0.1 wt%), sodium alginate (1.2 wt%) and Irgacure 2959 (0.1 $g.ml^{-1}$%) in distilled water. The dissipative NFC-PEGDMA-alginate hydrogel was synthesized by mixing PEGDMA, calcium sulphate, NFC (0.5 vol%), and Irgacure 2959 in distilled water. The mixture was then homogenized at 12000 rpm for 20 min and sodium alginate was added. The PEGDMA molecules were crosslinked by ultraviolet irradiation with a light intensity of 5 $mW.cm^{-2}$ for 30 minutes.

3.2.3 Tissue sample preparation

For the adhesion test, tissue samples were prepared in cylindrical shape with a diameter of 6.6 mm and a height of 10 mm for different bovine tissues including cartilage, meniscus, and bone (see Figure 3.2). The cartilage pieces were prepared from the superficial, middle and deep zones of articular cartilage obtained from the femoro-patellar groove. The meniscus samples were cut from the central region of the lateral meniscus in the circumferential direction and the bone pieces were prepared from the subchondral region below the calcified cartilage of the femoro-patellar groove.

After placing the tissue samples into the two-piece mold, the hydrogel precursors were poured onto the prepared samples in the mold and photopolymerized on the top of the tissue surface. The obtained hydrogel has a diameter of 15 mm and a height of 4.5 mm. The two-piece mold was removed after polymerization and the attached tissue was quickly gripped for the adhesion test.

3.2.4 Adhesion, fracture, and dissipation measurements

A custom-made adhesion setup was designed for measuring the adhesion strength of hydrogel on a tissue surface in tensile mode. The load is applied on the plane along the interface to minimize the bulk deformation of the hydrogel, and thus provide a reliable measure of adhesion between the deformable hydrogel and the tissue surface. The adhesion setup has also a simple gripping system for the deformable hydrogel and a quick and reproducible performance for adhesion measurement. The mechanical set-up used for the adhesion test is reported in Figure 3.2. The adhesion measurement was performed using an Instron E3000 linear mechanical testing machine (Norwood, MA, USA) with a 250 N load cell and a constant speed of 0.1 mm.s^{-1}. The adhesion strength was determined by dividing the maximum adhesion force by the surface area of the hydrogel-tissue contact. The work of adhesion was also calculated from the integrated area under the load-displacement curve divided by the contact area. The maximum force in the load-displacement curve corresponds to the work of adhesion for crack initiation while the work of adhesion for crack propagation corresponds to the area from the maximum adhesion force to the complete detachment.

We compared the adhesion performance of the gel with a commercial fibrin sealant (Tisseel™, 2 ml) from Baxter International Inc. The control glue was used according to the manufacturers' instructions. Briefly, separate vials of thrombin and fibrinogen components were thawed at 37 °C, and then injected simultaneously on the tissue surface with a double-syringe applicator to glue the hydrogels to the tissue. The glue was allowed to cure at RT for 10 min. The mechanical test was subsequently performed at a rate of 0.1 mm.s^{-1} and the adhesion strength was measured.
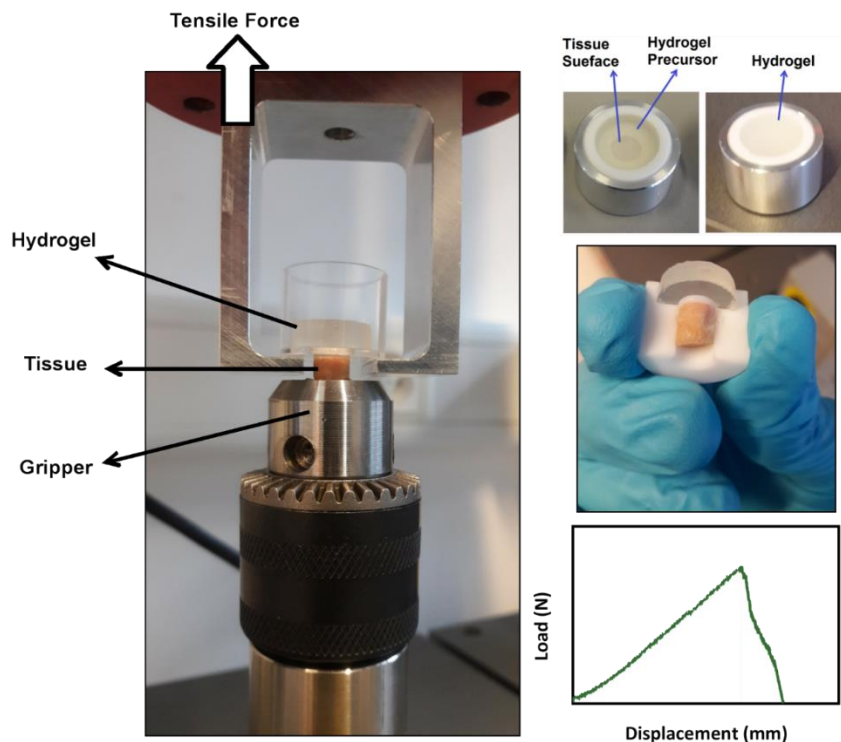
Figure 3.2. The custom-made adhesion setup for evaluation of hydrogel-tissue attachment in traction mode. The tissue samples were placed into a two-piece mold, then the hydrogel precursors were photo-polymerized on the top of the tissue surface. The tissue was gripped after UV illumination and the load was applied along the interface using an Instron E3000 linear mechanical testing machine. The adhesion strength was calculated by dividing the maximum adhesion force by the surface area of the interface. The work of adhesion was obtained from the integrated area under the load-displacement curve divided by the interface area.

The fracture tests were performed on the hydrogels strips (30 mm $\times$ 20 mm $\times$ 2 mm) with a 5 mm edge crack in the middle of the hydrogel. The hydrogel grippers were pulled with a constant stretch rate of 0.1 mm.s^{-1} and the force-displacement was recorded (the setup developed by Céline Wyss).

For measuring the energy dissipation, tensile test was performed on hydrogel samples with 5 mm x 2 mm cross-section. The hydrogels were stretched to 40 % strain and then unloaded with the same rate of 0.1 mm.s^{-1} and the hysteresis loop of the real stress-strain curve was measured.

3.2.5 Interfacial crack propagation and Digital Image Correlation (DIC)

To evaluate the interfacial crack propagation on the tissue, a hydrogel-tissue fracture test was performed on articular cartilage attached to various hydrogels. The rectangular tissue samples were cut from the femoro-patellar groove with a thickness of 2 mm and a width of 15 mm. The hydrogels strips (20 mm × 15 mm × 2 mm) were polymerized on the flat and thin cartilage surface in a Teflon mold and then a sharp interfacial notch 3 mm length was created. The tissue samples were gripped via the bone part below the cartilage layer, while the distance between the hydrogel-cartilage interface and the hydrogel gripper is 15 mm. The hydrogels were pulled to complete detachment and the interfacial crack propagation was detected. Digital Image Correlation (DIC) was also performed using VIC-3D system (Correlated Solutions, Inc., Irmo, SC, USA) to measure the deformation field around the interfacial crack tip. A speckle pattern was randomly applied to the hydrogel surface with graphite (GRAPHIT 33, Kontakt Chemie) to make a grey level distribution and obtain sufficient contrast for imaging.

3.2.6 Swelling ratio and water content

The swelling ratios of the hydrogels were evaluated in PBS at room temperature. The hydrogel precursors were injected into moulds with a diameter of 8 mm and height of 4.5 mm. The cured hydrogels were then detached from the mould and immersed into PBS solution. The swelling ratio was measured by $SR\,(\%) = (W_s - W_0) / W_0 \times 100$. The equilibrium water content (EWC) of hydrogels was also measured by $EWC\,(\%) = (W_s - W_d) / W_d \times 100$, where W_s and W_d are the weight of the hydrogel after 3 days of swelling and after drying, respectively. The samples were also weighted immediately after synthesis (W_0) in order to measure the water content of hydrogel after synthesis.

3.2.7 Cytocompatibility

Cytocompatibility of the developed hydrogel, with 88% of water content, was evaluated in a direct contact testing as well as cells proliferation study.

Direct contact test. Sterilized cylindrical hydrogels were placed and fixed separately in the middle of cell culture vessels with a diameter of 35 mm. Bovine chondrocyte cells were then seeded around the samples (10000 cell/cm^2). 2.5 mL of cell culture medium, supplemented with 10 vol% Fetal Bovine Serum (FBS), 1 vol% Penicillin Streptomycin (PS) and 1 vol% L-Glutamine, was added to each vessel. After samples were incubated at 37 °C in 5% CO2 for one week, cells were stained with 1 mL methanol for 30 s followed by 1 mL diluted Giemsa solution in order to color the cells.

Proliferation study. The cytocompatibility of the composite double-network hydrogel was investigated by proliferation study as well. The bovine chondrocyte cells were cultured on a 6-well plate with 100'000 cells/well and 6 ml of culture medium in each well. 70 µm cell strainers were placed on the top of the wells, then the sterilized hydrogel samples, with 2.5 mm thickness, were placed in the strainers. The culture medium was changed every 2 days. To evaluate cells proliferation at different time points, the medium was aspirated and each well was filled with 1 ml of medium with 10 vol% PrestoBlue[TM] assay (A13261, Life Technologies) according to manufacturer's instructions. After incubation for 30 min, the solution was distributed in a black 96-well plate. The proliferation was then evaluated using a microplate reader (Wallac 1420 Victor2, PerkinElmer) and the fluorescence at 595 nm was measured. Each test was performed in triplicate. For each time point, three wells without the presence of hydrogel were considered as the positive control.

3.2.8   Statistical analysis

All data were expressed as mean ± standard deviation. Statistical analysis was conducted with ordinary one-way or two-way analysis of variance (ANOVA) followed by Tukey's multiple comparisons test to determine statistical significance (*$p < 0.05$, **$p < 0.005$, ***$p < 0.001$, ****$p < 0.0001$).

3.3 Results and discussion

To evaluate the adhesion performance of the developed hydrogels on soft tissues, we tested various hydrogels presenting different dissipative networks. Figure 3.3A shows the adhesion strength on the middle zone of articular cartilage of hydrogels with different dissipative mechanisms. The wide range of the measured adhesive performance is observed on the tissue for single-network PEGDMA (21.9 ± 4.82 kPa), composite NFC-PEGDMA (52.7 ± 13.15 kPa), double-network PEGDMA-alginate (71.3 ± 4.76 kPa), and composite double-network NFC-PEGDMA-alginate (139.5 ± 6.94 kPa) hydrogels. The results indicate a promising improvement in the integration between the hydrogel and the tissue. The composite hydrogel with the dissipative matrix is significantly more adhesive to articular cartilage than hydrogels presented in previous works [31, 70, 71, 154] or existing tissue adhesives such as fibrin glue (2-20 kPa) [154, 155]. The dissipative hydrogel presents significantly higher

adhesive strength than that of the control Tisseel™ (14.3 ± 2.6 kPa) while no surface modification is carried out.

It is observed that both the adhesion and the dissipation potential conspicuously increase for the proposed hydrogel structure (see Figure 3.3B). For the NFC-reinforced hydrogel, the pullout mechanism of fiber entangles and the presence of hydrogen bonds between the fibers and the polymeric matrix contribute to higher energy dissipation. The toughening mechanism improves the resistance to crack initiation and consequently the adhesion strength is higher than the PEGDMA hydrogel. As previously reported [84, 156], thanks to the reversible ionic crosslinking of alginate chains in the PEGDMA-alginate hydrogel, a larger region around the interface is subjected to energy transfer and the hydrogel exhibits a pronounced hysteresis. The adhesion response is relatively high as substantial amount of energy can be transferred by unzipping alginate chains around the hydrogel-tissue interface. However, NFC-PEGDMA-alginate can dissipate much higher energy, even more than the summation of the dissipation potential in composite and double-network hydrogels (1.6 kJ/m^3), which indicates a synergetic effect between ionic crosslinking and fiber reinforcement. The high adhesion of this hydrogel is mainly due to the ability of the hydrogel networks to stress transfer from the interface, which leads to substantial amount of energy required for crack propagation (see Figure 3.4).

The composite hydrogel can dissipate more energy through the sacrificial bonds at the matrix-fiber interface [157] while the rigid cellulose fibers improves the stiffness of the hydrogel as well [103]. When the hydrogel network is under large deformation, the polymeric matrix forms microcracks, which begin to propagate. The NFC reinforcement can deflect the crack path through the interfacial bonds with the matrix and consequently increase the ability of the hydrogel to transfer energy [158]. It can also be enhanced by the pullout of NFC entangles [140, 159]. However, as the crack propagation can occur in the polymeric matrix, we develop the NFC reinforced composite with a dissipative double-network matrix. Moreover, the degree of bonding energy and density of contact points between the tissue surface and the hydrogel improve the interface quality [2, 160]. With sufficient hydrogel-tissue interfacial bonding, the combination of ionic and covalent crosslinking in the double-network matrix, reinforced with cellulose fibers, gives the composite hydrogel a high fracture resistance.
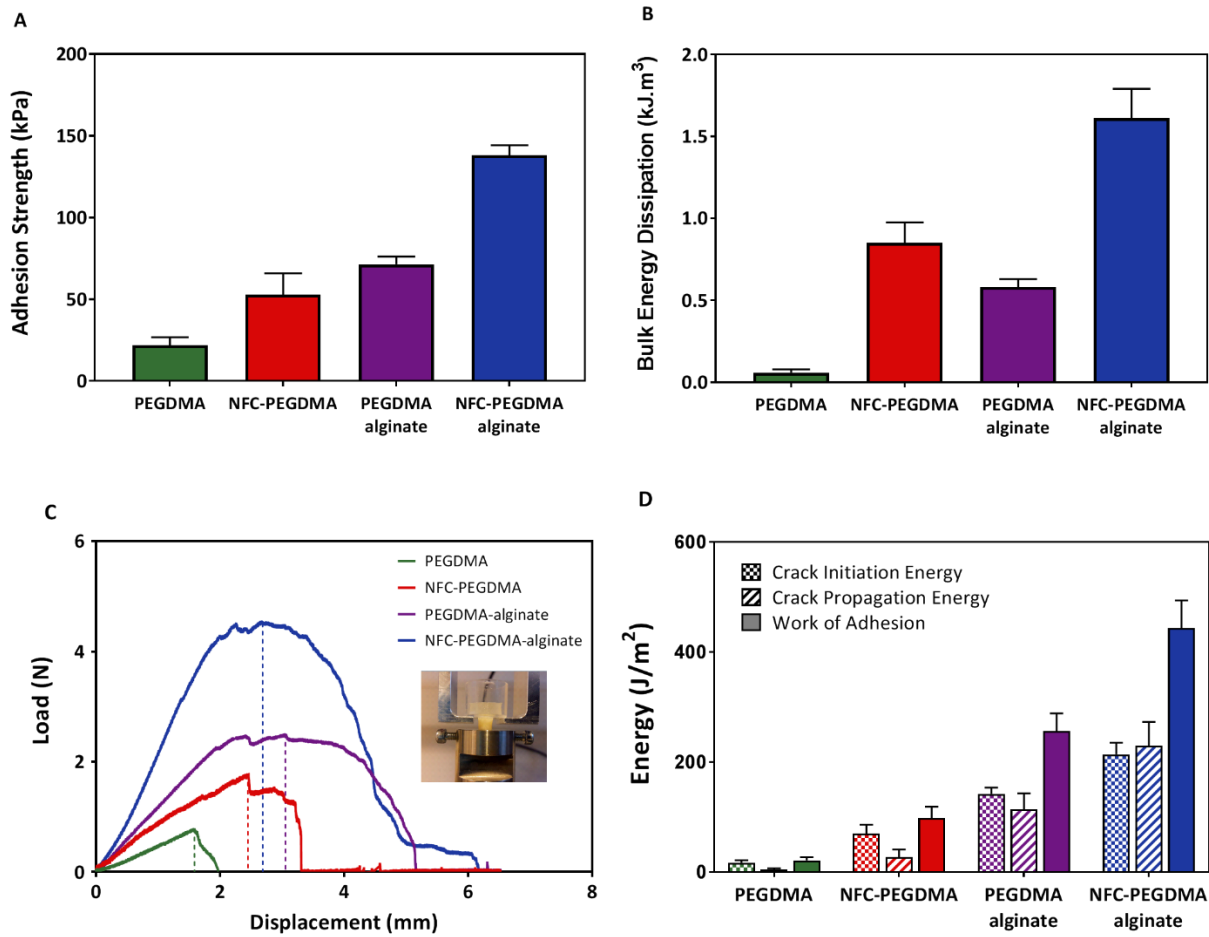
Figure 3.3. Adhesion performance of different hydrogels on cartilage. (A) Adhesion strength, (B) Hydrogel ability for energy dissipation at 40% of tensile strain, (C) Load-displacement curves and (D) Crack initiation and propagation energy, and work of adhesion (n=3).

It is also important that the proposed hydrogel network gives a high work of adhesion, compared with that of a network with low dissipation. As shown in Figures 3.3C and D, the adhesion presents a sudden drop after the peak force for the single-network PEGDMA, indicating that the required energy for crack propagation is relatively low. In contrast, the tough hydrogel shows high energy for both crack initiation and crack propagation and thus an intimate contact between the hydrogel and tissue surface (see Figure 3.4). The high work of adhesion as well as the high adhesion strength demonstrates the reliable material performance of the composite hydrogel with the dissipative matrix. Comparing the detachment of the proposed hydrogel with high crack propagation energy in comparison with

PEGDMA hydrogel, the failure occurs slowly and requires large deformation for the composite double-network hydrogel while the interfacial cracks move rapidly after initiation between PEGDMA hydrogel and cartilage.

A

B
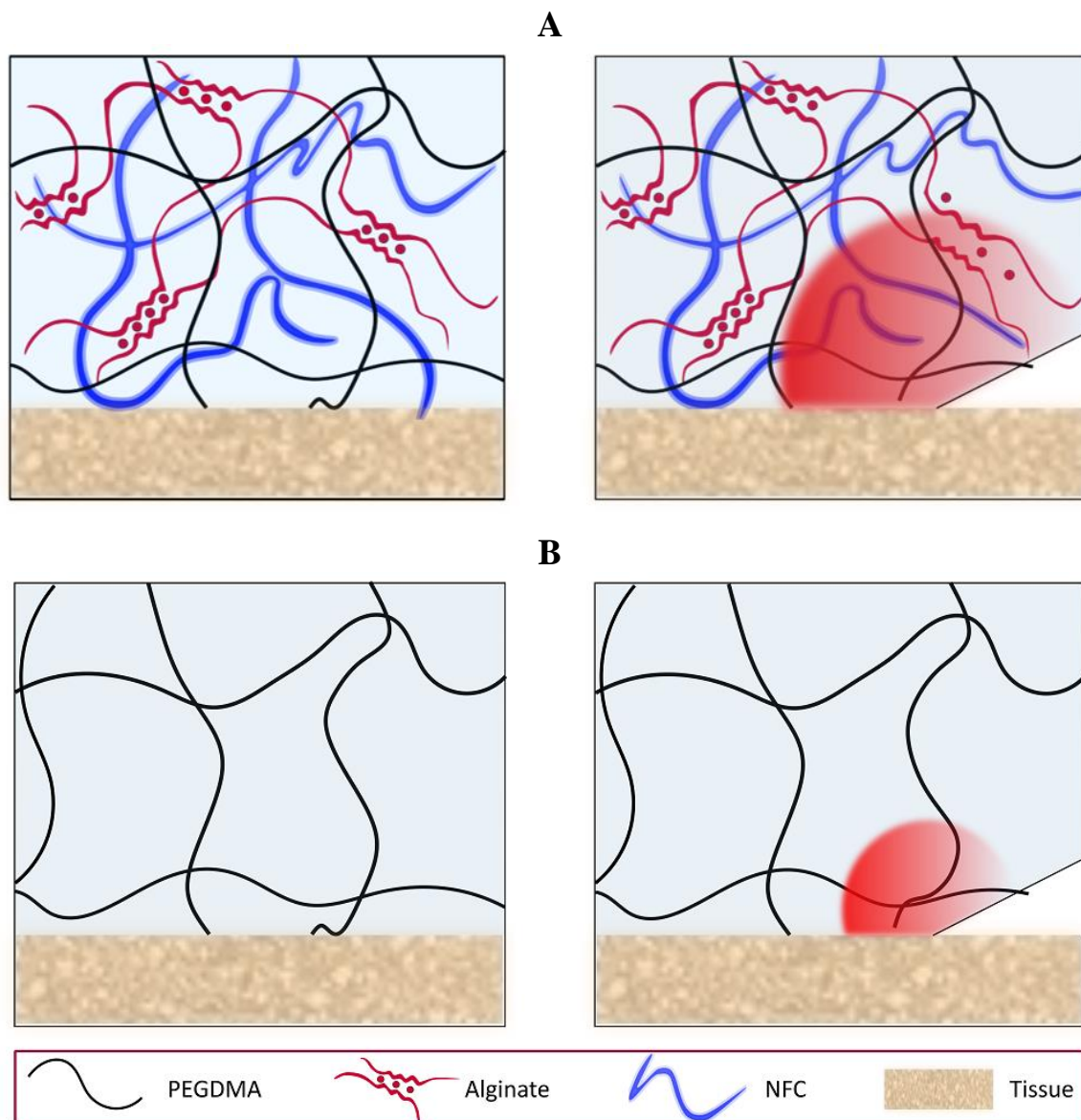
Figure 3.4. Adhesion mechanisms of the composite double-network hydrogel on tissue. (A) The various dissipation mechanisms of the hydrogel allows energy transfer over a large region around the crack tip before the propagation. (B) The hydrogel with a weak dissipative mechanism has a low crack initiation energy and a small affected zone, while the dissipative hydrogel absorbs much energy before crack propagation.

To assess the crack propagation in the hydrogel-tissue interface, we designed a hydrogel-tissue fracture test on thin hydrogel strips with a pre-existing crack at the tissue interface, as demonstrated in Figure 3.5 A and B. To compare the results with the fracture resistance of the bulk hydrogel, we performed a single edge notch test on rectangular hydrogel sample as well. The fracture strength is reported for evaluating the cartilage-tissue interface. This value is compared to its corresponding value for the bulk hydrogel. Since the fracture strength depends on the crack length, we used the same geometry, i.e. same thickness, crack length and grip to grip distance, for the interfacial and bulk fracture tests. Figure 3.5 D allows us to compare the fracture strength of bulk hydrogel and the hydrogel-tissue interface for various networks. The presence of NFC fibers in the single or double network hydrogel matrix considerably improves the fracture strength of the bulk hydrogel. However, the interfacial fracture strength is much lower. As shown in Supplementary Figure S3.1, the roughness of the crack surface in the bulk material and at the hydrogel-tissue interface are different, which may be attributed to fiber bridging effect. The crack advance in bulk composite hydrogel is constantly kinked or stopped (presence of microcracks), which creates the rough crack surface. On the other hand, higher interfacial fracture strength of PEGDMA-alginate than for NFC-PEGDMA might be due to better affinity of alginate with the tissue, which lead to better interfacial interaction. Bulk energy dissipation in Figure 3.3B and bulk fracture strength in Figure 3.5D follow the same variations for the different studied materials. The adhesion strengths and the interface strengths obtained by the two different tests are as well correlated for each material. DIC analysis was also performed to analyze the local strain field distribution. As shown in Figure 3.5C, E and Supplementary Figure S3.2, the energy transfer occurs over a localized region around the crack tip before the crack propagation. The strain field of the hydrogel attached to the tissue is markedly lower than in the notched bulk hydrogel. However, the strain concentration is deviated at around 45° in the hydrogel attached to the cartilage, indicating that the interfacial adhesion is sufficient to transfer energy to the bulk material. Promoting interfacial interactions such as interfacial bridging with fiber penetration (see Figure 3.1) enhance the energy transfer to the bulk material and provide further protection of the interface. Further numerical analysis as well as AFM measurement are presented in Appendix 1 and 2.
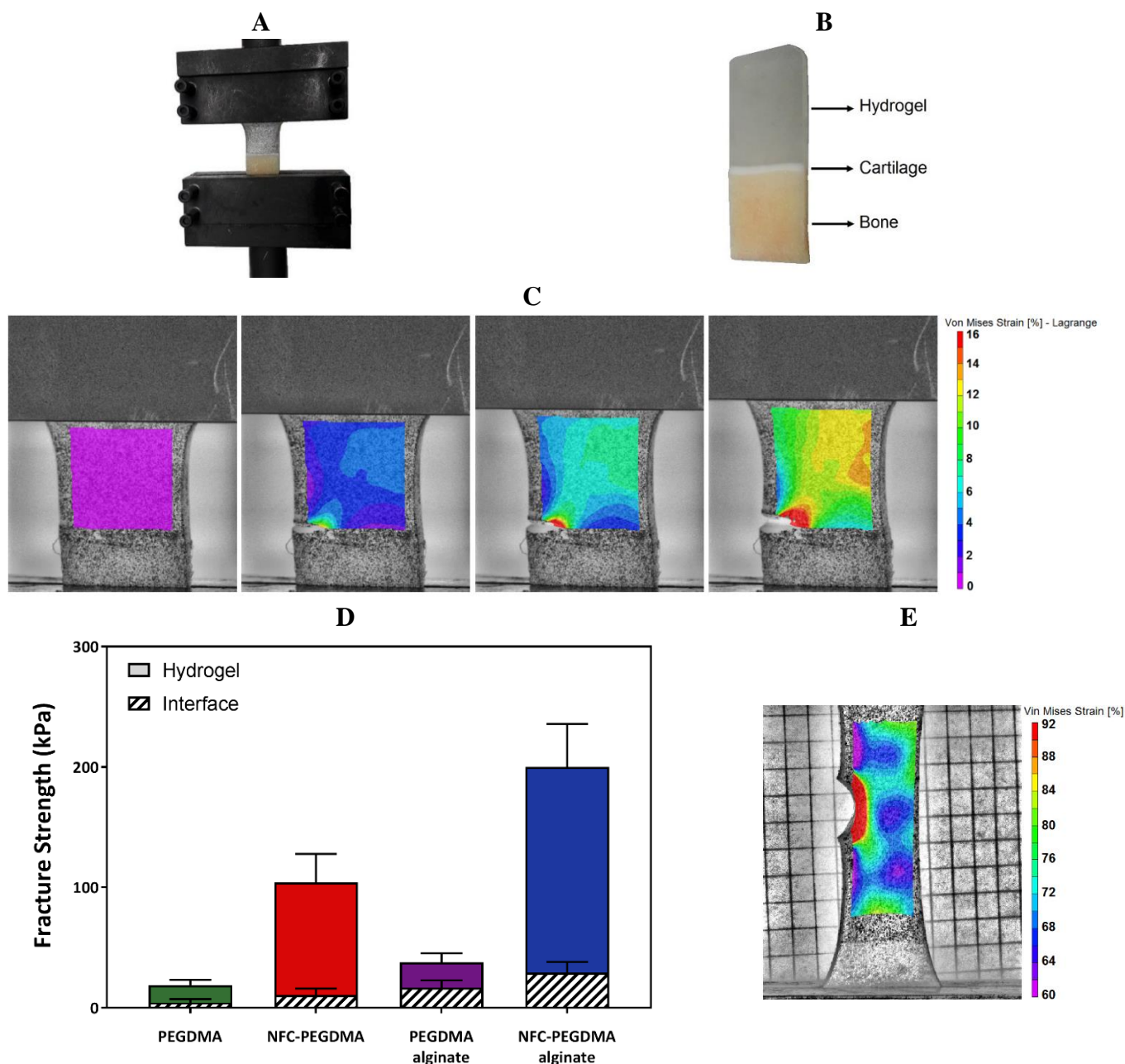
Figure 3.5. Comparison of interfacial and bulk fracture for different hydrogel networks. (A) The fracture setup. **(B)** The rectangular tissue samples (cartilage layer on bone) are cut from the femoro-patellar groove with a thickness of 2 mm and a width of 15 mm. After curing hydrogel strip on the cartilage surface, an interfacial notch is cut with a 3 mm length between the hydrogel and tissue. **(C)** DIC imaging from progressive formation of the affected zone around the interfacial notch between the NFC-reinforced hydrogel and the tissue before propagation. **(D)** Fracture strength of hydrogel and hydrogel-tissue interface for different hydrogels. **(E)** DIC imaging around the notch in hydrogel bulk before crack propagation.

To further evaluate the adhesive potential of the composite double-network hydrogel, we polymerized and bonded the hydrogel to different load bearing musculo-skeletal tissues. Figure 3.6 demonstrates the adhesion strength of hydrogels with different networks on subchondral bone, articular cartilage, and lateral meniscus. The adhesion values show an overall increase for all hydrogels on the meniscus. The highest measured adhesion is for NFC-PEGDMA-alginate and the variation of adhesion values is similar to that of cartilage. As the bulk property of each hydrogel is the same for different tissues, the enhanced adhesion on meniscus indicates a higher intrinsic strength of the hydrogel-meniscus interface. On the other hand, stronger interactions allow more dissipation of energy around the interface. The higher adhesion is not only due to the contribution of bonding energy, but much more to the energy transfer in the bulk material. In contrast, despite an overall improvement in the adhesion of the tough hydrogels (NFC-PEGDMA, PEGDMA-alginate and NFC-PEGDMA-alginate) on bone, there is no significant difference between them. It suggests that this behavior is mainly due to a lower quality of the hydrogel-tissue interface, which correspondingly reduces the energy required to advance an interfacial crack. Moreover, the higher difference of mechanical stiffness between the hydrogel and bone may be attributed to stress concentration at the interface under large deformation.

We also applied a hydrogel precursor to different zones of articular cartilage to examine the effect of structural and compositional variations of cartilage on the adhesion response. As shown in Figure 3.7, the adhesion strength varies at the superficial, middle and deep zones of cartilage. The attachment of hydrogel gives the highest adhesion on the superficial zone and the lowest value on the deep zone. This may be due to the higher water concentration as well as the higher collagen content but with small size at the superficial zone [154], which can raise the possibility of hydrogen bond formation and intermingling effect at the interface. Therefore, the higher surface energy can lead to an effective combination of hydrogel bulk properties and interfacial bonding.
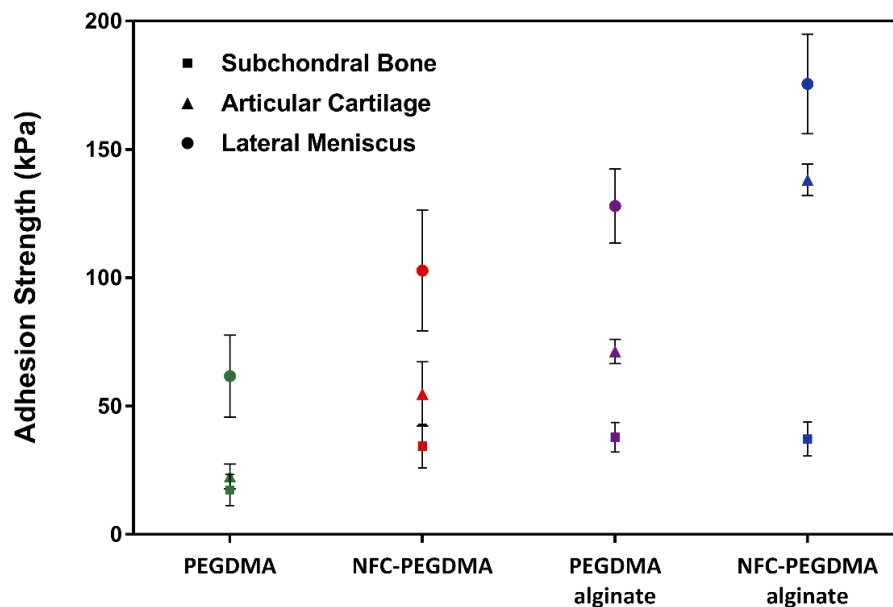
Figure 3.6 Adhesion strength for bone, articular cartilage and lateral meniscus (n=3).
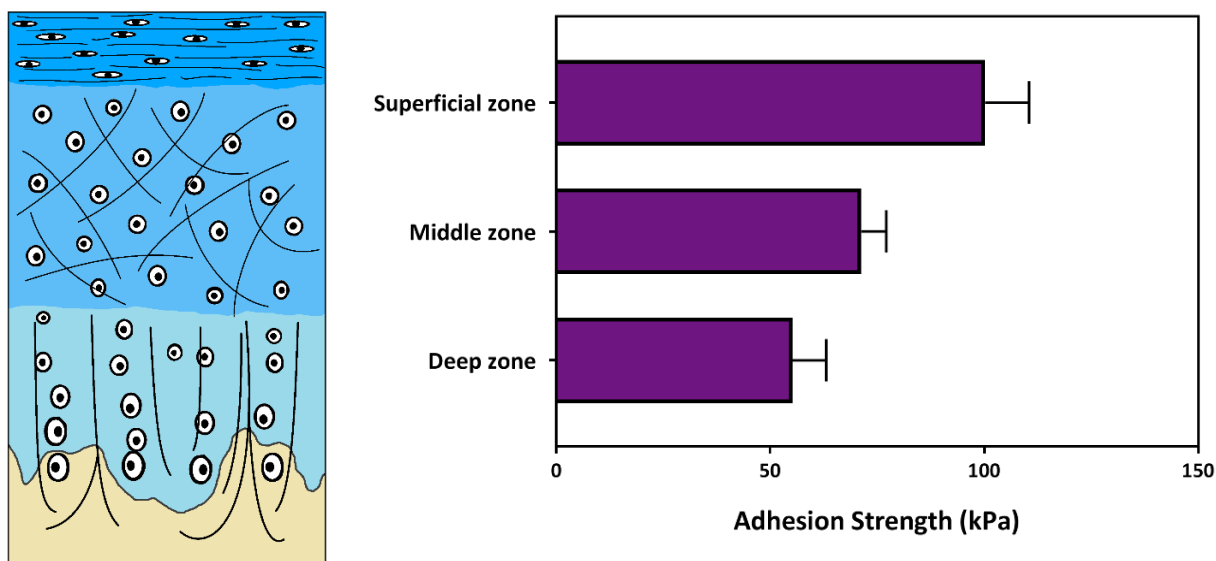
Figure 3.7. Adhesion strength for different zones of articular cartilage. The highest adhesion is observed on the superficial zone and the lowest value on the deep zone. The superficial region has the highest water concentration. The collagen fibers of this zone are packed tightly and oriented parallel to the articular surface and with small diameter. The middle zone has thicker collagen fibers and randomly oriented. The deep zone has largest collagen fibers perpendicular to the surface. It contains the highest proteoglycan content and the lowest water concentration.

The swelling ratio as well as the EWC of the hydrogels is shown in Supplementary Figure S3.4. The addition of NFC decreases the swelling ratio of both neat and double-network hydrogels, implying that the swelling ratio of the fiber-reinforced hydrogels can be tuned by the finer concentration at high water contents. Moreover, the cytocompatibility of the hydrogel was assessed and shown by the direct contact test and proliferation study using chondrocyte cells (see Supplementary Figures S3.5 and S5.6).

3.4 Conclusions

By implementing various toughening mechanisms in hydrogel design, cracks propagation can be controlled which as a result significantly increase the adhesive and cohesive fracture resistance. This approach allowed us to develop biocompatible hydrogel structure containing a high water content, which opens a promising pathway towards the development of injectable adhesive hydrogels for biomedical applications. In particular, the developed composite double-network hydrogel demonstrates high adhesion strength on load-bearing tissues such as cartilage and meniscus, while no pre-treatment is required on the surface of these tissues.

Summary: Considering the mechanistic origins of fracture energy, the knowledge and principles for crack propagation control, as well as the physical and chemical behavior of polymeric networks of hydrogels, could be employed in order to propose a design strategy for highly adhesive hydrogel systems. As a result, the designed hydrogel should be able to dissipate a substantial amount of mechanical energy in the process zone or the bridging zone upon crack propagation. To demonstrate this, a multiple dissipation mechanisms was implemented into the hydrogel and the influence of dissipation capability on adhesion was investigated. The role of low but critical interfacial interactions was also shown on adhesion.

Dividing the crack regions into crack surface, process zone and bridging zone, hydrogels were synthesized to be able to dissipate energy in each one of these regions. Three main components were selected based on three different mechanisms for energy dissipation; reversible crosslinking, chain fracture and fiber pullout. To test the proposed design, the synthetic polymer network of polyethylene glycol dimethacrylate (PEGDM) was covalently crosslinked. To dissipate substantial amount of energy in the process zone, a reversibly crosslinked network of natural alginate was then used to

synthesize a double network (DN) hydrogel, in which the physical crosslinking and chain scission dissipate mechanical energy. Moreover, the hydrogel was reinforced using nanofibrillated cellulose (NFC) in order to dissipate more energy in the bridging zones. In fact, it is expected that the combination of these mechanisms -or maybe other mechanisms- can provide promising strategies to dissipate much more energy and enhance fracture toughness, and consequently, interfacial toughness.

As shown in Supplementary Table S3.1, four hydrogels were synthesized with different levels of mechanical dissipation capability obtained by different mechanisms.

Supporting Information for Chapter 3
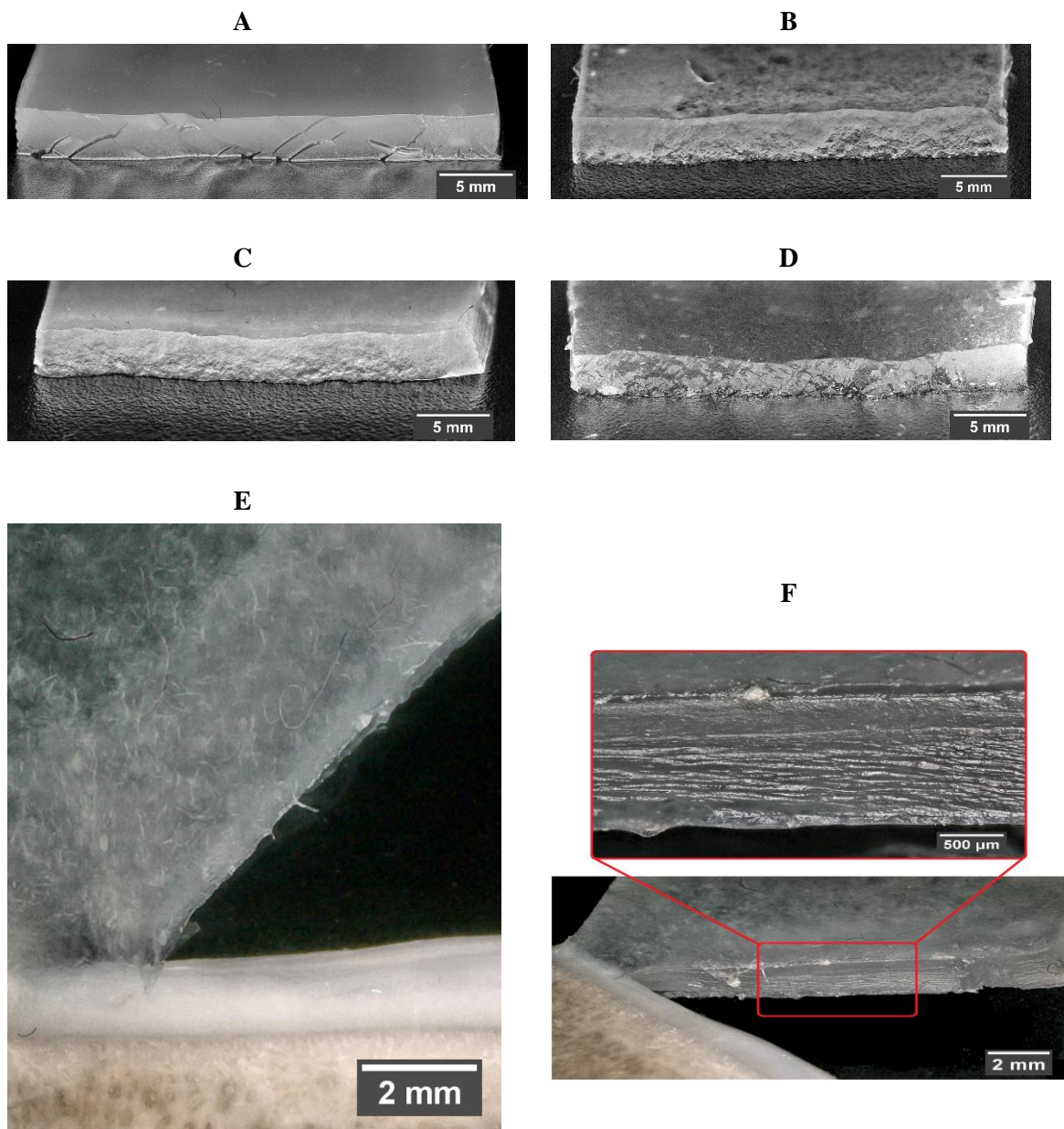
Supplementary Figure S3.1. Surface of the crack in the bulk hydrogel for: (A) PEGDMA, (B) double-network PEGDMA-alginate, (C) composite NFC-PEGDMA, and (D) composite NFC-PEGDMA-alginate hydrogels. (E) Crack opening between the composite hydrogel and cartilage: (F) Surface of the crack at the tissue-hydrogel interface.
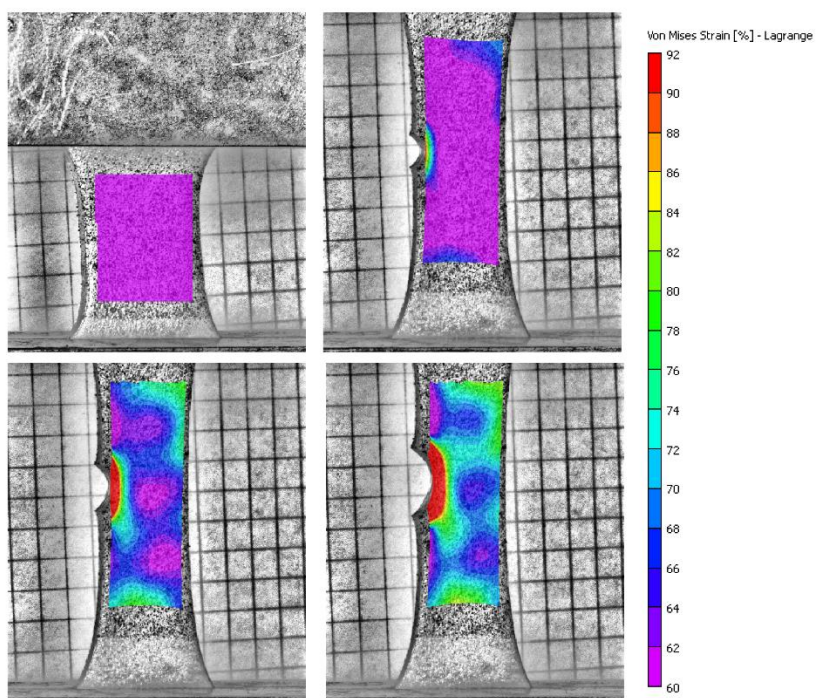
Supplementary Figure S3.2. DIC imaging from progressive formation of the affected zone around the notch in the NFC-reinforced hydrogel bulk. The hydrogel transfers energy around the interface through the dissipation mechanisms before the crack starts to propagate.
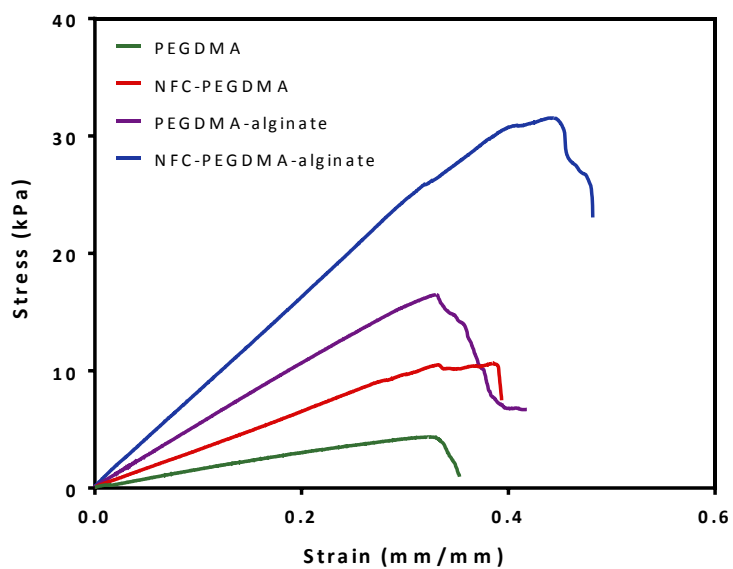
Supplementary Figure S3.3 Interfacial fracture test: representative stress-strain curves for different hydrogels.

A

B   **C**
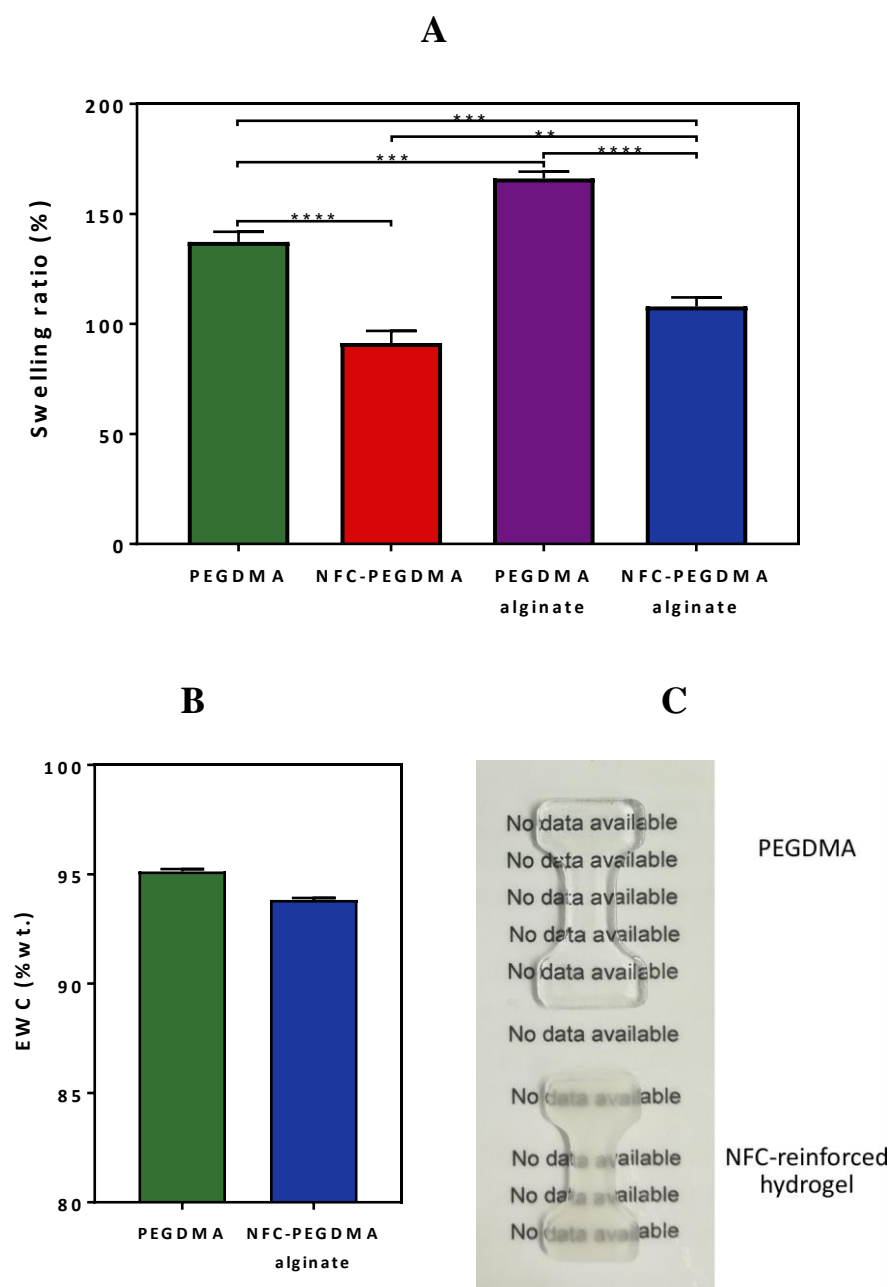
Supplementary Figure S3.4. (A) Swelling ratio of the hydrogels and (B) the equilibrium water content (EWC) of the composite double-network hydrogel in comparison to PEGDMA hydrogel (n=3). The initial water content after synthesis is ~88% for NFC-PEGDMA-alginate. Fiber entanglements with each other and with the polymeric network contribute to an increase of physical interactions in the network and decrease the hydrogel mesh size and slightly the EWC. (C) Comparison of the transparency between PEGDMA and the composite hydrogel.
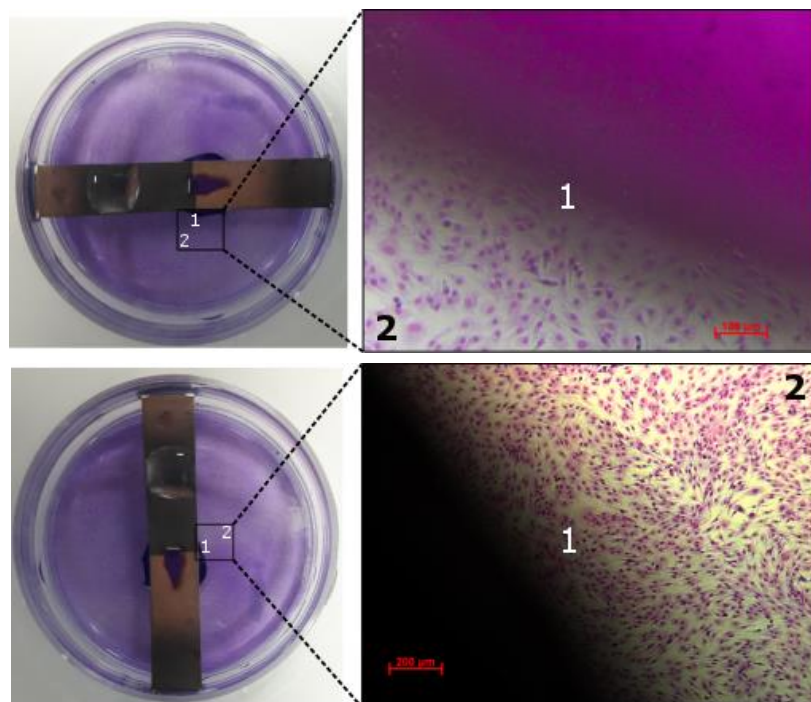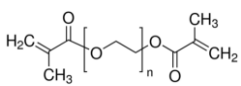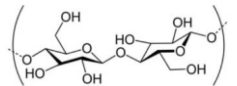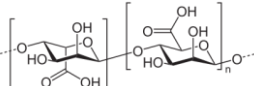
Supplementary Figure S3.5. Direct contact test to visualize the distribution of cells around the hydrogel: Giemsa staining for the fixed hydrogel (left) and microscopy of the colored cells (right). The morphology of the cells in contact with the hydrogel samples demonstrates were similar to areas far from the hydrogel.
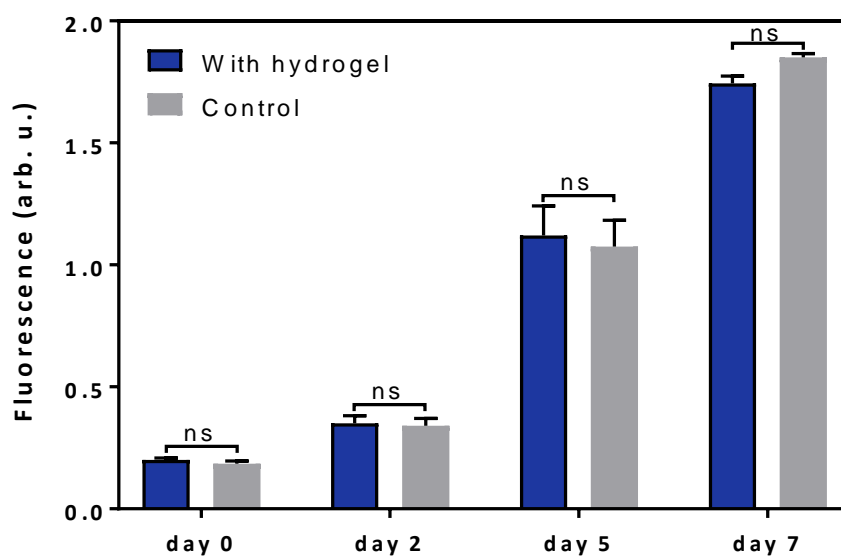
Supplementary Figure S3.6. Cells proliferation with/out presence of the composite double-network hydrogel. There was no significant difference between the samples with hydrogel and control group over seven days, confirming that the hydrogel does not affect the cells proliferation. We observed the maximum fluorescence in day 7 corresponding to maximum proliferation possible in the used wells.

Supplementary Table S3.1. Hydrogel networks according to dissipation mechanisms

Hydrogel	Hydrogel Network	Dissipation Mechanism			Dissipation Capability
		Polymer chain fracture	**Fibers fracture and pullout**	**Reversible/physical crosslinking**	
		Polyethylene Glycol Dimethacrylate	Nanofibrillated Cellulose	Alginate Network	
1	Neat PEGDM (20kDa)	✓			Low dissipation
2	Composite PEGDM + NFC	✓	✓		High dissipation in bridging zone
3	Double Network PEGDM+Alginate	✓		✓	Substantial dissipation in process zone
4	Composite PEGDM+Alginate	✓	✓	✓	Significant dissipation in process & bridging zones

Chapter 4-   **Adhesion Measurement**

In the present chapter, the developed custom-made adhesion measuring methods are introduced and compared for hydrogel-tissue adhesion. Moreover, the common standard techniques are presented in order to provide an overall insight into adhesion characterization of hydrogels and biological surfaces. The importance of using the developed measurements are discussed and their performance are analyzed.

4.1 Challenges and background

Evaluation of the adhesion system and the selection of the proper adhesion measurement method for a given application are of high importance [161]. The mechanical techniques employed for adhesion evaluations are generally divided into peel, lap and butt methods. Although each one of these methods gives useful information on the adhesion system, it is sometimes needed to employ different measuring methods to provide a proper adhesion evaluation. This is especially true for many biomedical applications where the material integration is one of the major considerations. It is common to observe very different results with the same materials tested by the three ways [22], as the adhesion response under each loading condition could be different. On the other hand, a reliable

measuring of the adhesion between a very deformable material and a solid surface is rather difficult, since the interface boundary conditions and the bulk deformation of the layer are closely and very nonlinearly coupled [162]. Moreover, there are some limitations with the common measuring methods such as the large deformation of the material which could influence on the obtained results, suitable gripping system of the deformable material, accurate and controllable process for attaching the material and the substrate, sample preparation of tissues with complex geometries, reproducibility, etc. Designing new adhesion setups is therefore needed for a better adhesion evaluation.

4.2 Direct adhesion measurement

Qualitative or quantitative adhesion characterization of tissue adhesives could be carried out using various direct (mechanical tests) or indirect (e.g., XPS and contact angle analysis) measuring techniques. Direct adhesion characterization is widely used and includes: pull out, tension, lap shear and peeling tests. Pull-out testing is a tensile test that is performed to measure the adhesive strength. A standard test may require a constant pull speed or pull at a constant hold force. Tension testing is the application of a uniaxial force to measure the performance of a test sample up to the point of yield or breaking. Tensile test results provide a profile of the force, extension and time. For adhesive testing, the data curve of the force vs extension is largely used to determine ultimate tensile strength. The peel test is a more common quantitative measurement for the resistance of bonded joints to peeling forces. They are mainly used for the comparative evaluation of adhesives and surface treatment methods because they are very sensitive at discerning differences in the adhesion and cohesion behavior in the adhesive film. Standard test methods tend to prescribe the speed and angle of separation to be repeatable. The lap shear test is the most commonly used standard test for testing adhesion by pulling bonded layers apart along the plane of adhesion. The result can be a breakaway of the adhesive layer from the substrate, or more likely a breakdown in the cohesion of either the substrate or the adhesive layer, or both. Following the standard, the overlap corresponds to a width of 25 mm and a length of 12.5 mm. Each end of the sample is held by grips and pulled apart at a controlled rate, and the force applied is expressed proportionately to the total adhesive surface area or shear area.

4.3 Atomic Force Microscopy for adhesion measuring of hydrogel and tissue contact

The main objective for development of this measuring technique is to evaluate and analyze the quality of interface interactions between tissue and hydrogel substrate under very low deformation. In addition, the new method should be used for adhesion measurement of hydrogels from very soft to stiff hydrogels. A reliable evaluation of interfacial interactions is another objective in the current analysis.

4.3.1   Atomic Force Microscopy

Unlike other microscopic techniques, Atomic Force Microscopy (AFM) is a near-field approach, in which the sample surface is directly probed by a tip. Thus, the interaction forces between atoms within the sample surface and the AFM tip can measured. The forces are derived from the degree of deflection of a cantilever. There is an optical system for detection of a laser beam, reflected from the back of the cantilever to a position-sensitive photodetector. As the cantilever deflects, there is a positional change of the reflected laser beam, and this change is translated into height information and finally into force. If no interaction occurs no forces are exerted on the cantilever, but with development of the bonds between molecules during the time of contact, a force is exerted during retraction. This force increases until at a critical force, the rupture or adhesion force, the breakage occurs [163]. Figure 4.1 shows a schematic of AFM measurements.
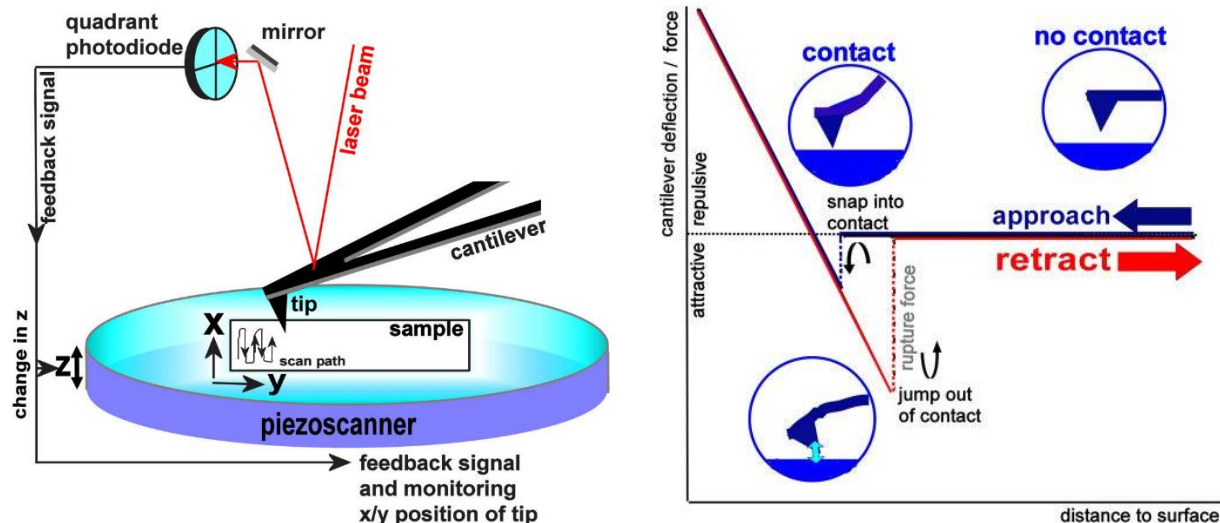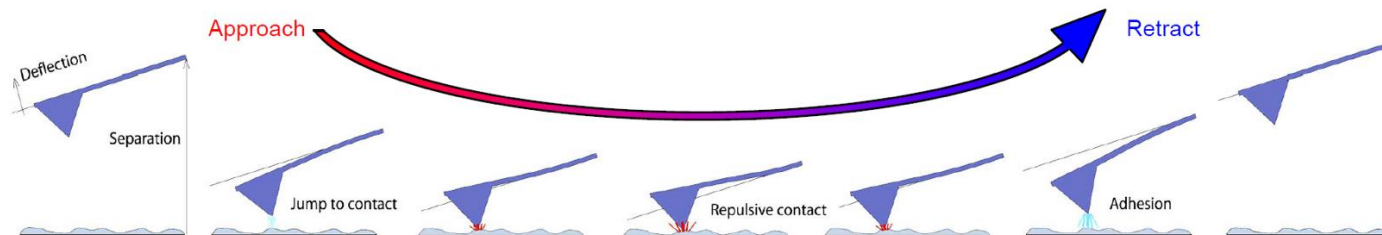
Figure 4.1 Atomic force microscopy technique and schematic AFM force-distance curve **(top)**. Schematic of the tip movement during approach and retract in force spectroscopy **(bottom)** [163].

4.3.2   The developed technique

In order to measure the adhesion of a tissue piece to a hydrogel with AFM, the tissue plays the role of a cantilever tip. A tiny piece of cartilage is glued on a tip-less cantilever. The hydrogel samples are deposited on a substrate surface. The measurements are performed in water. A drop of water was placed on the top of the hydrogel sheet. Therefore, it covers the hydrogel surface while it does not touch the bottom substrate. Consequently, the hydrogel won't be floating during the measurements and stays quite stable. Moreover, there is no need for using glue in order to fix the hydrogel sheet.

The cantilever with the piece of cartilage, as its tip, approaches the surface in liquid and the measurements can be performed. Figure 4.2 illustrates the schematic of the AFM test for adhesion measurement using a piece of tissue attached to a tip-less cantilever.
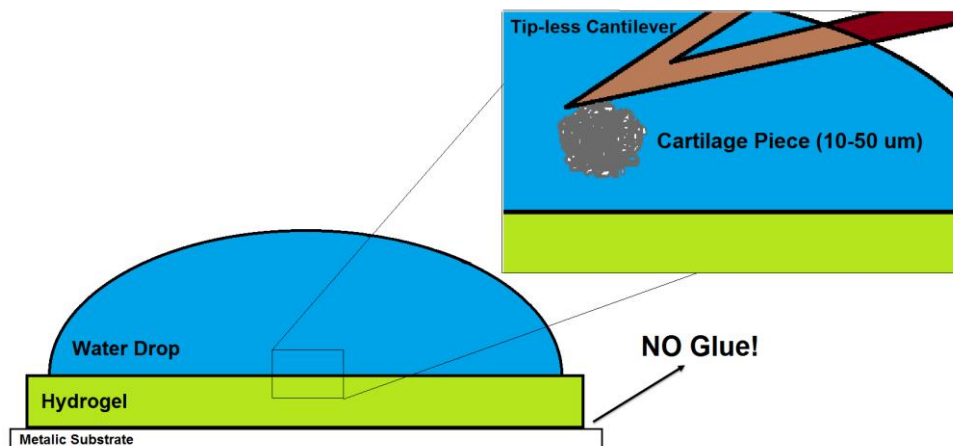
Figure 4.2. Test mechanism: schematic of the designed technique for adhesion measurement between cartilage piece and the hydrogel sheets.

4.3.3 Test procedure

Hydrogel synthesis: The cartilage pieces were tested on four hydrogel sheets: single-network PEGDMA hydrogel, NFC-reinforced PEGDMA, DN PEGDMA-alginate hydrogel and NFC-reinforced PEGDMA-alginate (see the details for hydrogels synthesis in section 3.2).

Tissue preparation: Tiny tissue pieces should be prepared for gluing to AFM cantilever. To this end, cryogenic grinding has been performed on the bovine articular cartilage at -196 °C. The range of tissue particle size was obtained between 10 to 50 µm in diameter. Then the tissue particles were lyophilized. We received the cartilage particles for this experiment from ETH, Zurich (Prof Marcy Zenobi-Wang Lab).

Thin hydrogel sheets: All hydrogel sheets have to be used in swollen state. This is because the samples dimension should not vary during the test, particularly for a thin layer of hydrogel.

Measuring map: As the AFM measurement presents high variations, it is very important to perform the measurements with a large number of replicates and on the different measuring points in order to obtain a reliable statistical approach. Thus, we performed the tests using a measuring map on the surface of the hydrogel sheets, with a distance of 100 µm between the measuring points.

The designed procedure for depositing the hydrogel samples, gluing the cartilage particles using an eyelash to the tip-less cantilever and the measuring map are shown in Figure 4.3. AFM microscope Stuart was used to perform the measurements (figure 4.4).

A

| Swollen hydrogel disks (0.5 mm thickness) | Clean glass cover slip attached to metal disc | Water drop on the hydrogel sheet | Cartilage piece glued to cantilever tip |

B
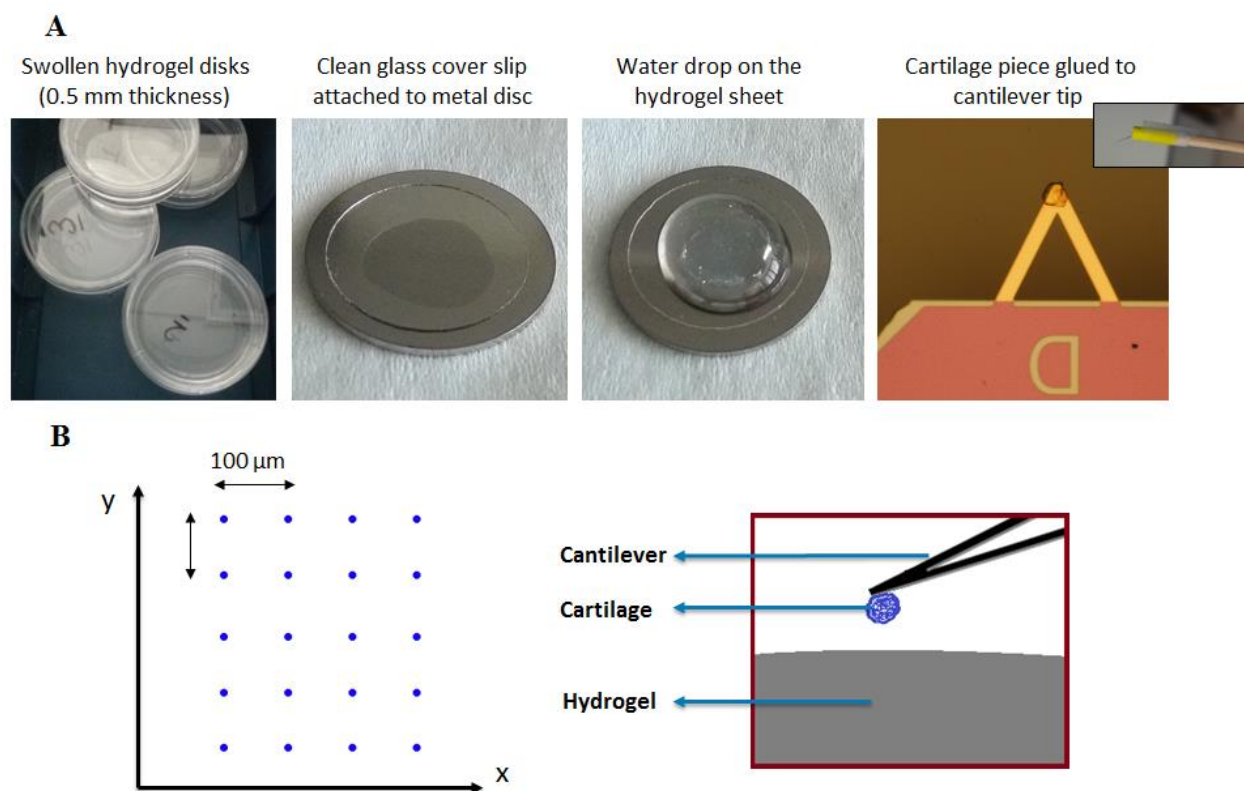
Figure 4.3. (A) Preparation of the designed technique for adhesion measurement between cartilage piece and the hydrogel sheets and (B) measuring map on the hydrogel sheet measurement for the pull-off force and energy between cartilage and hydrogel in water.
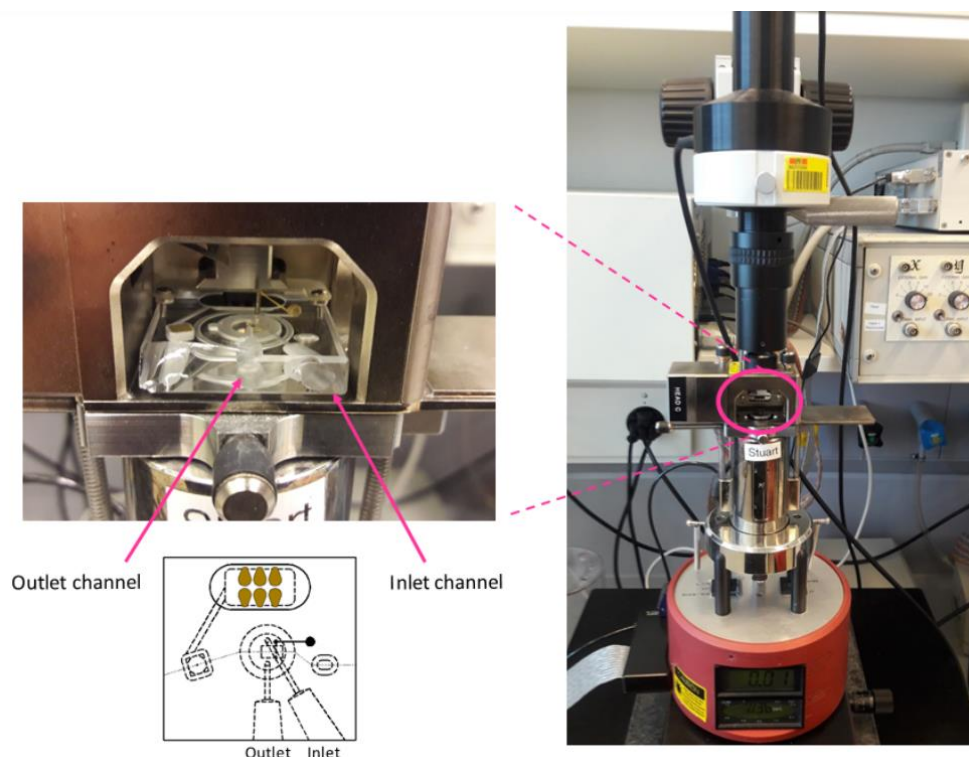
Figure 4.4. Right: AFM microscope Stuart, Left: the liquid cell.

General description of the measurement: To have a reliable measurement, three rounds of experiments were performed in three different days. In each round, all hydrogel samples were tested two times and in random order, as shown in Figure 4.5:

- all measurements were performed with 10 seconds of touching on the hydrogel surface with 10 nN force;
- every set of experiments consists of 60 - 70 measurements;
- the prepared cantilever with cartilage piece was kept in water during the time between circles and measurements;
- pieces of hydrogel were also kept in the distilled water.
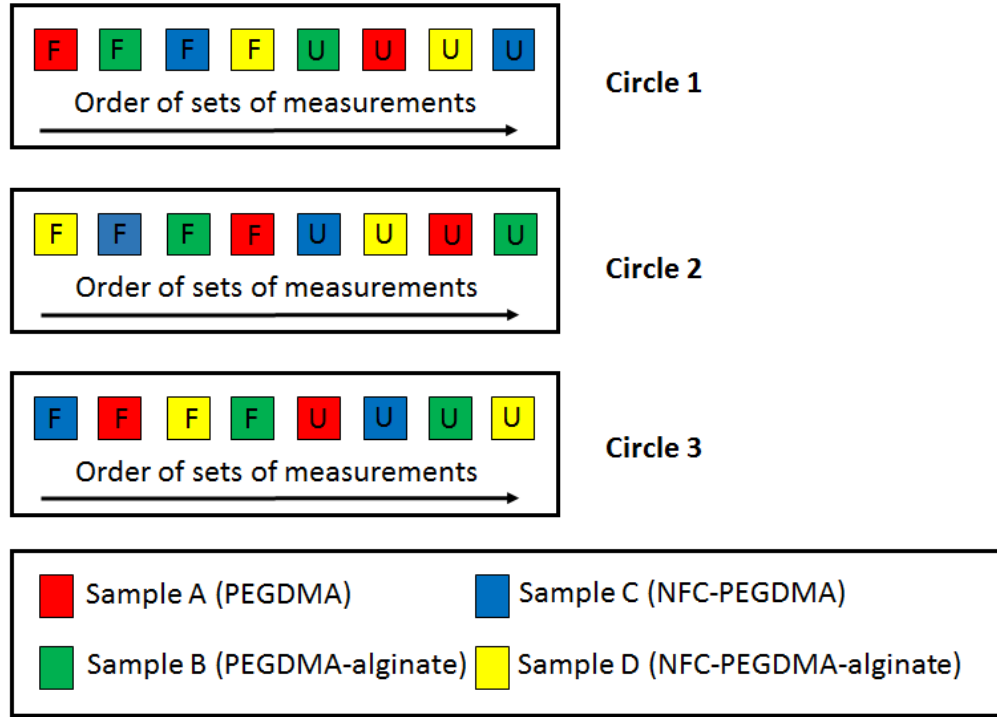
Figure 4.5. The test procedures for different hydrogels: three rounds in three days and two measurements for each sample. The tests were performed randomly.

F: measurement with a fresh hydrogel piece, **U:** measurement with a used hydrogel piece.
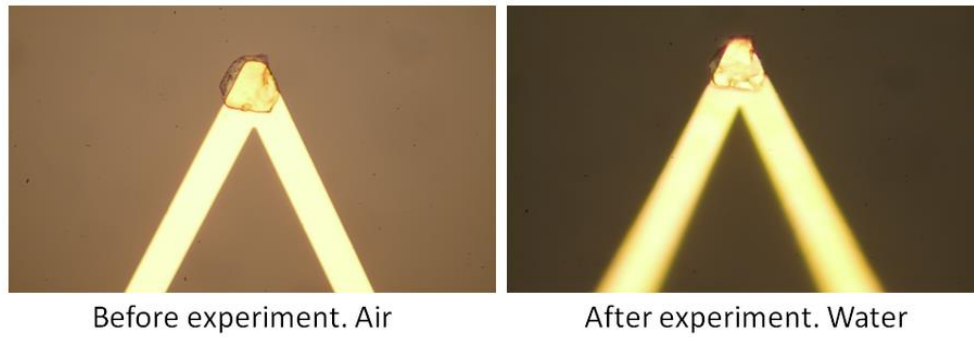
Figure 4.6. The cantilever before and after the experiment.

4.4 Adhesion measurement in traction mode

A new adhesion setup was designed and successfully used for measuring adhesion strength of a soft viscoelastic layer on a solid surface in traction mode. It has been tried to address the recurrent

problems in the common adhesion tests for the soft materials but with a quick and reliable test. The idea is to apply the load on the plane along the interface and there is therefore no large deformation in the bulk, unlike a common traction test. A specific experimental geometry has been used minimizing the bulk deformation of the layer. The gripping system is very simple and in fact the setup geometry by itself provides the material gripping. It was found that the test process is relatively simple to be implemented and widely applicable for soft layers of arbitrary viscoelastic properties. Schematic illustration of the concept of loading condition in the setup is shown in Figure 4.7.

4.4.1 Sample preparation and test procedure

Samples are prepared in cylindrical shape through a controllable process for different tissues like cartilage and bone. The cylindrical samples are made using hole saw which is a specific tool for cutting. The internal diameter of the tool was used for cutting tissues. Figure 4.8 shows sample preparation method for the bovine articular cartilage. Hydrogels are photopolymerized on the top of the tissue surface in specific molds designed for this purpose, then the molds are removed, the tissue is quickly gripped and the test is performed.
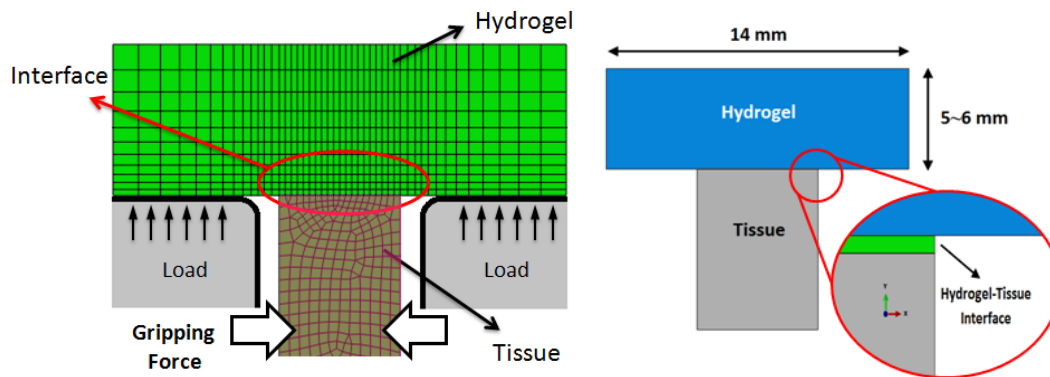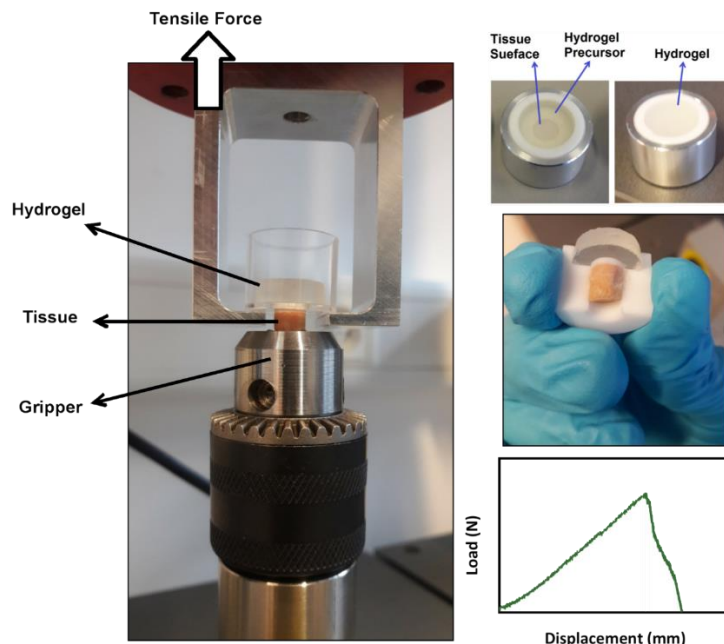
Figure 4.7. The custom-made adhesion setup for evaluation of hydrogel-tissue attachment in traction mode: schematic illustration of the test **(top)** and adhesion setup **(bottom).** The tissue samples were placed into a two-piece mold, then the hydrogel precursors were photo-polymerized on the top of the tissue surface. The tissue was gripped after UV illumination and the load was applied along the interface using an Instron E3000 linear mechanical testing machine. The adhesion strength was calculated by dividing the maximum adhesion force by the surface area of the interface. The work of adhesion was obtained from the integrated area under the load-displacement curve divided by the interface area.
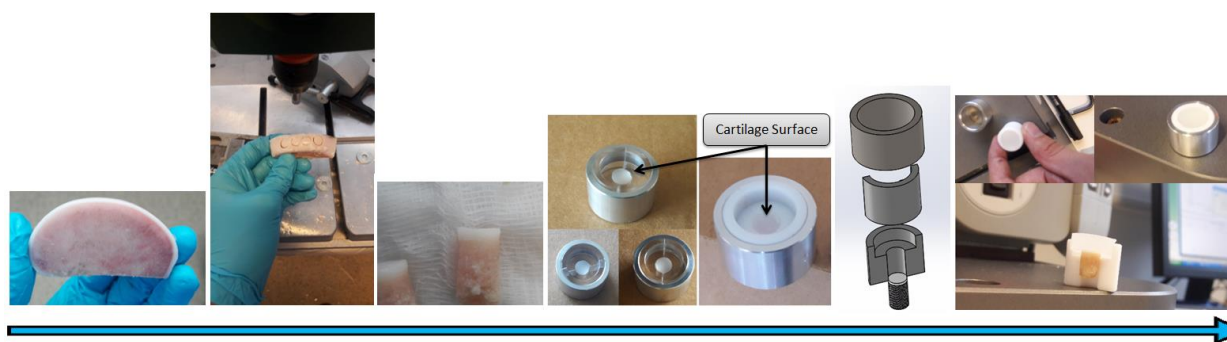
Figure 4.8. Sample preparation from bovine articular cartilage: the cylindrical cartilage-on-bone samples are made using a hole saw. Hydrogel precursor is cured on the top of the tissue surface in Teflon molds and then the molds are removed.

Observations: The details were presented in the Chapter 3.

4.5 Lap shear adhesion measurement

The shear adhesive strength of our bioadhesives to soft tissues was evaluated on various types of tissues. The measurements were performed using a shear test setup based on ASTM F2255 standard for strength properties of tissue adhesives in lap shear [164]. Briefly, tissue samples were prepared with 25 mm width and a thickness of less than 5 mm. A thin layer of bioadhesive (25 µl) was applied to the overlap area between the wet tissue sample and the coated glass substrate (10 mm × 25 mm). The tissue surface of the prepared meniscus samples (cut from the central region of the lateral meniscus) was smaller due to the native tissue dimensions. While applying 1 N load to the bond area, the bioadhesive was photo-cured between the substrates for 60 seconds. The tests were conducted using an Instron E3000 mechanical testing machine equipped with a 50 N load cell. A constant loading rate of 1 mm.s^{-1} was applied and adhesion strength was determined by dividing the maximum load by the overlap area.

Figure 4.9. In vitro lap shear adhesion setup and schematic of the test procedure. The bioadhesives are applied to the overlap area between the tissue substrate and coated slide and subsequently photo-cured.

Observations: The details are presented in the Chapter 5.

Chapter 5 - **An intrinsically-adhesive family of injectable hydrogels with functional physicochemical performance for regenerative medicine**

5.1 Motivation

Attaching hydrogels to soft internal tissues is crucial for the development of various biomedical devices. Tough sticky hydrogel patches present high adhesion, yet with lack of injectability and the need for treatment of contacting surface. On the contrary, injectable hydrogels are highly attractive owing to their ease of use, shape flexibility and their minimally invasive character, compared to their conventional preformed counterparts. Despite recent advances in material developments, a hydrogel that exhibits both proper injectability and sufficient intrinsic adhesion, has yet to be demonstrated. Herein, we propose a paradigm shift towards the design of intrinsically adhesive networks for injectable hydrogels. The bioinspired design strategy not only provides strong adhesive contact, but also results in a wide window of physicochemical properties, enabling the development and use of injectable hydrogels for different biomedical applications. The adhesive networks are constructed by

fabricating a family of engineered polymeric backbones. Owing to chains capability of being intrinsically adhesive to host tissue and forming a hydrogel network via a hybrid cross-linking mechanism, adhesion is achieved through a synergy between interfacial chemistry and bulk mechanical properties. The functionalities of our bioadhesives are demonstrated for various applications, such as tissue adhesives, surgical sealants or injectable scaffolds.

5.2 Hydrogel design concept

The majority of researches have proposed different strategies for adhesion increase mainly by the improvement of interfacial interactions. However, the obtained adhesion improvement is quite insignificant [27]. Recently, a few hydrogel systems have been proposed with interestingly high adhesive properties based on tuning the dissipative properties of hydrogels [24, 25]. However, the robust bonding of these hydrogel systems requires time-consuming surface modification of solids, porous surface structure, or inorganic solid surfaces, which is clearly not suitable to biological surfaces and clinical applications. We could propose an adhesive composite double-network hydrogel system to biological surfaces like articular cartilage and meniscus (Chapter 3). The adhesive performance of the hydrogel comes mainly from various toughening mechanisms which contributes to tough interfacial attachment.

Although the integration of the proposed dissipative network to the soft tissues surfaces increased adhesion strength to unprecedented values (Chapter 3), there are still some limitations in the hydrogel performance as a biomaterial:

a. In the hydrogel design, the tissue surface is the dominant part for the hydrogel-tissue attachment. It means that the quality of interface mainly depends on the chemistry and morphology of the tissue surface. Therefore, it is not possible to obtain sufficient adhesion on various biological surfaces. An intrinsically adhesive design should be developed.

b. The swelling ratio of the proposed composite hydrogel (even that of the single-network PEGDMA) is very high, which imposes serious limitations on many biomedical applications as well as maintaining hydrogel properties for this hydrogel.

c. From a practical point of view, the processability of the composite hydrogel should be highly improved in order to be able to be used in a real application.

d. The interface design is not included in the proposed hydrogel design in Chapter 3.

e. The degradation kinetics of the hydrogels needs to be controlled and be tunable.

f. Hydrogel curing should be fast as a fast adhesion formation is a prerequisite for clinical applications and is usually not achieved with actual hydrogels.

5.3 Introduction

Intrinsically adhesive hydrogels have various functions in biomedical areas particularly in minimally-invasive surgical treatments [165, 166]. In these medical situations, bioadhesives have to present not only strong adhesion to wet tissues but specific ranges of injectability, degradability, swelling, biocompatibility and mechanical match [33, 167]. This is particularly challenging as the adhesive mechanism of the hydrogel should also allow proper material functionality in its bulk. The adhesion of hydrogels could be enhanced by strong bonds with the tissue as well as the material's capacity to dissipate energy [24, 27, 168]. Dissipative double-network hydrogels show high adhesion when either the tissue or the hydrogel substrate is chemically treated, so that the interfacial bonds can be created. However, it is difficult to use these adhesive systems in minimally-invasive biomedical situations, in which hydrogel must be injected and formed in situ and tissue treatment would impose serious limitations. In addition, the physicochemical characteristics of the bioadhesive should satisfy the required properties of the targeted clinical application [168-170]. In particular, the available tissue bioadhesives such as PEG-based, fibrin-based and cyanoacrylate-based glues suffer from insufficient adhesive properties, mechanical properties and high cytotoxicity, respectively [5, 171].

Inspired by the adhesive tenacity of sandcastle worm and mussel, we propose a design strategy that not only provides strong interfacial bonds, but also presents a broad range of mechanical stiffness and dissipation. Despite the development of many mussel-inspired bioadhesives, which are based on interfacial bond strength of the catechol moieties, their tissue adhesion is weak [23] (see Supplementary Figure 5.1). Limited multiscale properties and adhesive strength are considerable limitations particularly in regard to load-bearing applications [23]. This is mainly attributed to the weak control of mechanical processes (i.e., supramolecular-level dissipative mechanisms), as the interfacial energy of the adhesive mussel foot proteins is three orders of magnitude lower than the overall adhesion energy of the mussel plaque [172, 173]. Although the origins of the elastic and

dissipative mechanisms in mussel plaque are not well known [173], their synergetic contribution to strong attachment tenacity of these sea creatures is significant [173, 174]. Correspondingly, we propose a design paradigm through systematic control of interfacial chemistry, material processing and network mechanics.

We report here a design platform of intrinsically-adhesive hydrogels for biomedical needs with various adhesive and physicochemical requirements. The developed family of hydrogels form strong chemical bonds with nucleophiles at the interface when the injectable precursor is applied to the tissue surface. The polymeric backbone of the designed hydrogels is crosslinked with covalent and non-covalent interactions and presents broad and tunable physicochemical properties. Therefore, the bioadhesive provides both a high level of adhesion to soft tissues and flexibility in physicochemical performance, which can be engineered to be compatible with the host tissues. Indeed, the proposed platform can be applied for soft and deformable (e.g., skin, liver, etc.), and stiff and load-bearing (e.g., cartilage, meniscus, etc.) tissues alike.

To reach a synergy between interfacial chemistry and bulk mechanical properties, we synthesized a family of polymeric backbones including methacrylated catechol-containing hyaluronic acid (MeCHa), methacrylated phosphoserine-containing hyaluronic acid (MePHa) and methacrylated phosphoserine-containing gelatin (MePGa). The designed polymers are polymerized via covalent bond formation, resulting in a hydrogel matrix with intrinsic tissue adhesion properties. Through a hybrid cross-linking strategy, the stiffness and dissipative potential of the designed network are carefully controlled by covalent cross-linking as well as by various non-covalent and physical interactions in the matrix chains (Figure 5.1a). Incorporation of reinforcing components (e.g., fibrillary collagen, fibrillated cellulose) into single network (SN) hydrogels contributes to even higher adhesion due to the resulting high level of energy dissipation in the composite network. Indeed, the fiber pullout mechanism as well as interfacial fiber-fiber and fiber-matrix interactions enhance the mechanical and physicochemical performance of the adhesive network [175, 176].

5.4 Materials and Methods

5.4.1 Materials

For synthesis of the modified polymer chains, sodium hyaluronate (HA) was purchased from Contipro with three molecular weight of 15-30, 30-50 and 50-90 kDa. Gelatin Type A from porcine skin (ref. G2500) was obtained from Sigma-Aldrich. Methacrylic anhydride (ref. 276685), Sodium hydroxide (ref. 71690), dialysis sacks (MWCO 6000-8000 Da) and hydrochloric acid were purchased from Sigma-Aldrich. For Dopa and phosphoserine modification, dopamine hydrochloride (ref. H8502) was obtained from Sigma-Aldrich and phosphoserine (ref. 17885-08-4) was provided by Flamma. N-(3-Dimethylaminopropyl)-N′-ethylcarbodiimide hydrochloride (EDC, ref. 03450, purum, $\geq$ 98.0%) and deuterium oxide (D2O, ref. 151882) were also purchased from Sigma-Aldrich. Sulfo-NHS (N-hydroxysulfosuccinimide, ref. 24510) was supplied from Thermo Fisher Scientific. For radical polymerization of methacrylated polymer chains, Lithium Phenyl(2,4,6-trimethylbenzoyl)phosphinate (LAP, ref 6146) was used as photoinitiator, obtained from Tocris Bioscience. For preparation of composite hydrogels, the Collagen fibers were synthesized from collagen Type I from rat tail (C3867), obtained from Sigma-Aldrich, and the Nanofibrillated Cellulose (NFC) was supplied from EMPA (Swiss Federal Laboratories for Materials Science and Technology, Dübendorf, Switzerland). The enzymatic biodegradation of bioadhesives was studied by using hyaluronidase (type II, ref. H2126, Sigma-Aldrich) and collagenase type II (Thermo Fisher Scientific, ref. 17101015). All animal tissues (liver, kidney, lung, heart, meniscus, cartilage and eye) were procured from a local abattoir.

5.4.2   Fabrication of bioadhesive hydrogels

MeCHa-Gel synthesis. The synthesis of MeCHa was performed using a two-step functionalization procedure. First, the methacrylation of hyaluronic acid was carried out in aqueous solution at alkaline pH and catechol groups were subsequently attached by reaction with dopamine under acidic conditions. The order of the functionalization steps is important due to the synthesis pH conditions and maintaining the dopamine adhesive performance. Briefly, 1 g of HA was dissolved in 50 ml of deionized water in a glass flask with a magnetic stir bar and stirred vigorously for 30 min at room temperature. The flask was then placed in an ice container and the temperature was kept at around 4 °C under a fume hood. While stirring, the pH of the HA solution was adjusted to 8.5 using 1.0 M NaOH. Methacrylic anhydride was added dropwise to the solution and the pH was adjusted to 8±0.5. The pH will not remain steady as it has a tendency to acidify quite rapidly. The molecular weight of backbone and the concentration of methacrylic anhydride affect the degree of methacrylation. For example, by addition of 1.5 mL of methacrylic anhydride, 48% of methacrylation was achieved for

50-90 kDa hyaluronic acid. After 3 hours of regular pH control, the solution was left stirring at 4 °C overnight while the flask opening was covered with parafilm. Thereafter, the reaction solution was transferred to 50 mL conical tubes and spun for 5 min at 1200 g. Unreacted chemicals and impurities were removed through 6-8 kDa dialysis membrane tubing for three days. The dialysis water was changed twice daily. Afterwards, the solution was frozen at -80 °C overnight, and lyophilized for at least three days.

Dopamine functionalization procedure of methacrylated hyaluronic acid was conducted using N-(3-Dimethylaminopropyl)-N′-ethylcarbodiimide hydrochloride (EDC) as an activation agent of the carboxyl groups on the hyaluronic acid. The reaction was performed at room temperature under nitrogen atmosphere and pH control in order to avoid the irreversible oxidation of dopamine molecules. Briefly, 0.5 g of methacrylated HA was dissolved in 50 ml of phosphate buffered saline (PBS) solution in a three-neck round-bottom flask with a magnetic stir bar and the pH was adjusted to 5.5 using hydrochloric acid (HCl). The solution was then purged with nitrogen for one hour. Then, 175 mg of EDC and 240 mg of dopamine hydrochloride were added into the reaction mixture (Mw = 50-90 kDa) and the pH of the reaction solution was maintained at 5.5 for 150 minutes. The functionalization process was performed under nitrogen atmosphere. The reaction mixture was afterwards dialyzed using dialysis tubes against acidic water with pH of around 5.5 for three days until all unreacted chemicals were removed. The dialysis water was changed twice daily. Further purification can also be carried out by another dialysis in deionized water. The filtered samples were finally frozen in a -80 °C and lyophilized for 3 days. The modified MeCHa product was stored at 4 °C under vacuum and protected from the light.

MePHa-Gel synthesis. Before phosphoserine functionalization of MePHa chains, methacrylation of hyaluronic acid was performed as described previously. Subsequently, 1 g of the lyophilized polymer was dissolved in 50 mL of the buffer and the pH was adjusted to 5. The carboxyl sites on the polymer backbone were activated by EDC reaction (3.5 mg.ml^{-1}) under continuous stirring for 15 min. By addition of phosphoserine (25 mM), the solution was further reacted for 6 hours. The resulting solution was then filtered and dialyzed for 4 days by using 6-8 kDa dialysis membrane and lyophilized for 3 days.

MePGa-Gel synthesis. MePGa polymer was also synthesized using a two-step modification process including the backbone methacrylation and subsequent phosphoserine conjugation. Gelatin

methacryloyl was prepared based on previously reported methods [37]. Briefly, 5 g of gelatin type A was fully dissolved in 50 ml of Dulbecco's phosphate buffered saline (DPBS) at 60°C for 30 min. 2 ml of methacrylic anhydride was added dropwise (0.5 ml/min) and the reaction mixture was left under vigorous stirring at 50°C for 2 hours. The solution was then 4 times diluted with DPBS to stop the reaction. The dialysis was performed against distilled water at 50°C using 12-14 kDa dialysis membrane tubing for 5 days, followed by 4 days of lyophilization.

Subsequently, 0.5 g of the methacrylated gelatin was dissolved in 25 mL of MES buffer at 50 °C and the pH was adjusted to 5. The modification was conducted based on EDC/NHS activation mechanism (3.5 mg.ml^{-1}) of the carboxyl groups of the backbone for 15 min at 37 °C. Phosphoserine was added to the reaction mixture (25 mM) and stirred continuously for 8 hours to form amide linkages. The reaction mixture was filtered and dialyzed in distilled water for 5 days. Finally, the samples were lyophilized for 4 days to obtain the solid porous product which could be stored at 4°C.

5.4.3 Synthesis procedure of SN hydrogels

MeCHa-Gel, MePHa-Gel and MePGa-Gel precursors were fabricated by dissolving the lyophilized polymer and the LAP photo-initiator in phosphate buffered saline (PBS). The final concentrations of LAP photo-initiator was 0.02% w/v in the resulting solution. Following EDC/NHS activation, the bioadhesive precursors at different concentrations were homogenized, and either injected or poured into different molds made of Teflon. MePGa precursor was vortexed at 37°C to be well homogenized before injection. The precursor mixtures were irradiated with light of wavelength 405 nm and low intensities 1-5 mW.cm^{-2} to cross-link the polymeric network.

5.4.4 Collagen fibrils fibrillogenesis

The collagen fibrils were prepared by mixing 5 ml of collagen solution with 5 ml of acetic acid solution (0.1 M) at 4 ℃. The pH of the mixture was adjusted to 7.4 with NaOH (1 M). The mixture was incubated at 37 °C for 4 hours to obtain the resulting collagen solution with 0.3% w/v concentration.

5.4.5 Fabrication of composite hydrogels

The NFC-reinforced hydrogel precursor was synthesized by dissolving of the photo-curable polymer (10 wt%) in phosphate buffered saline and mixing with NFC (0.3 w/v %) and LAP (0.02% w/v). To

prepare the NFC fibers, the slurry of bleached softwood cellulose pulp was fibrillated with high-shear homogenization. The hydrogel precursor was homogenized by using an Ultra-Turrax at 10000 rpm for 5 min. The mixture was then transferred into the molds and cross-linked. The collagen-reinforced hydrogel precursor was synthesized by mixing the photo-curable polymer (10 wt%) and LAP (0.02% w/v) in the prepared collagen solution. The mixture was then homogenized and subsequently cross-linked. The diameter of NFC fibres varies between 0.1-10 μm while the diameter of collagen fibers has a range of 50-100 nm [153, 175].

5.4.6 NMR analysis

The chemical structure bioadhesive polymers and the modification degree of conjugates on the polymeric backbone were analyzed using ^{1}H NMR spectroscopy. The spectra were obtained by using a 400 MHz Bruker Avance NEO. Briefly, 10 mg of the modified hyaluronic acid-based polymers were dissolved in 600 μl of D2O at room temperature. The solution was then transferred to NMR tube for the analysis. The same procedure was used for the control samples. For the gelatin-based polymers, 18 mg of the samples were dissolved in 500 μl of D_2O, and the NMR analysis was performed at 40°C.

5.4.7 Mechanical characterization

Adhesion measurement, tensile interfacial strength. The adhesion measurements under tensile loading were conducted on articular cartilage tissue as the model tissue (a load-bearing soft tissue) in our study. The cartilage-on-bone samples (osteochondral plugs) were cut in cylindrical shape with a diameter of 6.6 mm from the femoro-patellar groove of animal knee. The tissue sample was placed in Teflon molds where the bioadhesive precursor was injected and cured on the tissue surface, so that a cylindrical hydrogel formed on the tissue. We used a custom-made test to measure the interfacial adhesion strength between the bioadhesives and the cartilage surface as described in our previous work 4. The mechanical testing was performed using an Instron E3000 linear mechanical testing machine (Norwood, MA, USA) with a 50 N load cell. The tissue samples were gripped from the bone part and the tensile load was applied to the hydrogel. The tests were conducted with a constant rate of 0.1 mm.s^{-1}. The interfacial adhesion strength was calculated by dividing the maximum obtained load to the nominal contact area.

Compression, tension and energy dissipation. Compression tests of the bioadhesives were performed by preparing cylindrical samples with 5 mm diameter and 2.2 mm height. The compressive loading regime was applied at a displacement rate of 0.1 mm.s^{-1} and the load-displacement was recorded. The samples in swollen sate were loaded by 10 compression cycles. The compressive modulus of the hydrogels was obtained by linear interpolation of the stress-strain curve from 15% to 25% of strain (mm/mm) in the last loading cycle. Tensile properties of bioadhesives were obtained by preparing dumbbell-shaped hydrogel specimens with 2 mm thickness, 5 mm neck width and 4.5 mm gauge length. After placing the hydrogels in the test grippers, they were pulled with a tensile stretch rate of 0.1 mm.s^{-1}. The hydrogels were initially stretched to 25 % strain followed by 10 cycles. Similar to compression experiments, the tensile modulus was calculated from the slope of the best linear fit to the stress-strain curve. The bulk energy dissipation of the specimens was measured from the hysteresis loop area in the stress-strain curve during the loading-unloading process (n = 3).

5.4.8 *In vitro* swelling ratio and water content measurement

For the swelling study, hydrogel precursors were prepared and injected into Teflon molds as described before. Cured hydrogels were immersed into PBS followed by incubation at 37°C. The swelling ratio was determined by the following equation where Ws is weight of the swollen hydrogel in equilibrium state and W_0 is the initial weight of the hydrogel after synthesis.

$$SR\ (\%) = (W_s - W_0) / W_0 \times 100 \qquad (1)$$

Equation (2) was also used to calculate the equilibrium water content (EWC) of hydrogels where W_d is the weight of the dried hydrogel.

$$EWC\ (\%) = (W_s - W_d) / W_s \times 100 \qquad (2)$$

(n ≥ 3)

5.4.9 *In vitro* enzymatic biodegradation

Cylindrical MeCHa-Gel, MePHa-Gel and MePGa-Gel specimens were formed with 5 mm diameter and 2.2 mm thickness as described before. In particular, MeCHa-Gels were prepared with different molecular weights (15-130 kDa), polymer concentrations (5, 10 and 15wt%) and methacrylation

degrees (23, 48 and 80%). The prepared hydrogels were soaked in PBS at 37 °C to reach the equilibrium swelling and the initial weight of the samples was measured. The MeCHa- and MePHa-Gel samples were then incubated in biodegradation media with 10 U/mL of hyaluronidase type II, and MePGa-Gel bioadhesives were incubated with 10 U/mL of collagenase type II at 37 °C. Moreover, the enzymatic degradation effect was studied at different enzyme concentrations (0, 1, 2 and 10 U/mL). To further study the contribution of synthesis parameters to degradation kinetics, in vitro tests were conducted on MeCHa-Gel up to 84 days. The weight of the samples was recorded at specific time points and the enzymatic degradation kinetics was reported based on the mass loss ($n \geq$ 4).

5.4.10 *In vitro* shear test

The shear adhesive strength of our bioadhesives to soft tissues was evaluated on various types of bovine tissues (organs) including lateral meniscus, heart, lung lobe, kidney and liver. The measurements were performed using a shear test setup based on ASTM F2255 standard for strength properties of tissue adhesives in lap shear [164]. Briefly, tissue samples were prepared with 25 mm width and a thickness of less than 5 mm. A thin layer of bioadhesive (25 μl) was applied to the overlap area between the wet tissue sample and the coated glass substrate (10 mm × 25 mm). The tissue surface of the prepared meniscus samples (cut from the central region of the lateral meniscus) was smaller due to the native tissue dimensions. While applying 1 N load to the bond area, the bioadhesive was photo-cured between the substrates for 60 seconds. The tests were conducted using an Instron E3000 mechanical testing machine equipped with a 50 N load cell. A constant loading rate of 1 mm.s^{-1} was applied and adhesion strength was determined by dividing the maximum load by the overlap area. Commercially available TISSEEL™ adhesive (Baxter International Inc.) was also used for comparison. It was prepared according to the instruction provided by the manufacturer and tested on different tissues as described previously ($n \geq 3$).

5.4.11 *Ex vivo* sealing of cornea, burst pressure test

The adhesive performance of our bioadhesive family was investigated for sealing of the defects in eye cornea. An *ex vivo* test was performed to measure the burst pressure on freshly explanted calf eyes. Full-thickness corneal defects with 3 mm diameter were created by a biopsy punch in the cornea layer. The punching procedure was controlled by pressurizing vitreous humour of the eye using liquid

injection. Afterwards, MeCHa, MePHa and MePGa precursors were applied inside the defects and photo-cured in situ. The burst pressure test was conducted by pressurizing the anterior chamber under the eye corneal layer. The pressure was increased on the bioadhesives through air injection with a constant rate using a syringe pump. PASCO CapstoneTM software was used to record the applied pressure measured by a pressure sensor until the bioadhesives burst [177]. Moreover, the ex vivo experiments were performed by applying Fibrin TISSEEL^{TM} adhesive. The burst tests were conducted with empty defects as negative control. (n = 3)

5.4.12 Biocompatibility and proliferation evaluation

Cytocompatibility of all bioadhesive hydrogels was evaluated through a proliferation analysis. Briefly, bovine chondrocytes were cultured on a 6-well plate while each well contained 100'000 cells and 6 ml standard culture medium supplemented with Fetal Bovine Serum (10 vol%), Penicillin Streptomycin (1 vol%) and L-Glutamine (1 vol%). Sterilized SN and composite hydrogels were prepared with 2.5 mm thickness and placed in 70 µm cell strainers on the top of the wells. PrestoBlueTM assay (A13261, Life Technologies) was used to assess the cells proliferation based on manufacturer protocol. The evaluation was carried out every 2 days and over a 9 day period. The same procedure was followed for positive control samples without hydrogels. After aspiration of medium at each time point, the wells were filled with 1 ml medium containing 10 vol% PrestoBlueTM, and incubated at 37 °C for 30 min. Subsequently, 100 µl of the samples were plated in a black-walled 96-well plate in triplicate and the fluorescence was measured at 595 nm using a microplate reader (Wallac 1420 Victor2, PerkinElmer. (n = 3)

5.4.13 *In vivo* study

Animal surgeries were approved by the Faculty of Medicine, Institutional Animal Care and Use Committee (FOM IACUC) at the University of Malaya. 3 adult male Boer breed goats were used with an average weight of 33 kg. The goats were subjected to health screening including blood and urine tests. Prior to the surgeries, an 18 hour pre-operative fasting was considered for the animals with free access to drinking water. General anesthesia was induced by intravenous ketamine (3-5 mg/kg) and diazepam (0.2 mg/kg) injection. Surgeries were performed under aseptic conditions. Preemptive analgesia was provided by intravenous injection of meloxicam (0.2 mg/kg). The animals

were intubated and connected to oxygen flow for the duration of the surgery. The anesthesia was maintained by isoflurane. The cornea was also protected with ophthalmic ointment.

After general anesthesia, the knee joint was approached with a medial parapatellar incision. For each surgery, two full-thickness cartilage defects were made on the medial femoral groove of the left knee joint with a 5 mm diameter chondrotome. Defects were then filled by applying sterilized MePGa-Gel precursor and immediate photo-curing *in situ* as described before. The control defects were left untreated. After wound closure, goats stayed under observation until complete recovery. We carried out the *in vivo* study without any immobilization and the goats were allowed to roam freely within their barn. Goats received meloxicam (0.1 mg/kg) by subcutaneous injection once a day for 2 days after surgery. Animals were sacrificed after 2 days of implantation and the left knee joint was harvested. The presence of the implanted adhesive hydrogel in the defect site was examined.

5.4.14 *In vitro* tissue engineering by 3D cell encapsulation

Primary bovine chondrocytes were expanded and passaged in standard T75 flaks at 37°C and 5% CO_2 in DMEM supplemented with 10 vol% Fetal Bovine Serum (FBS), 1 vol% Penicillin Streptomycin (PS) and 1 vol% L-Glutamine. Chondrocytes at around 80% of confluency were suspended in the hydrogel precursors at 5.5% polymer content with a seeding density of 10 million cells/ml. The hydrogel precursors were then photo-cured in cylindrical molds (5 mm diameter and 2.2 mm height) by light exposure at an intensity of 2 mW/cm2 and 405 nm wavelength. The cell-laden constructs were cultured in the freshly prepared chondrogenic differentiation medium containing 50 µg/mL vitamin C, 10 ng/ml TGF-β3 and diluted ITS IV (P07-03410, PAN Biotech) in serum free culture medium (DMEM with 1 vol% PS and 1 vol% L-Glutamine) . The culture media was changed every 2-3 days for up to 4 weeks and cells biological response, matrix deposition and tissue formation were evaluated.

Cell viability and distribution analysis.

The viability of encapsulated cells was assessed by using a Live-Dead Assay Kit (Biotium, Fremont, CA) based on the manufacturer instruction. The Live-Dead staining solution was prepared by adding calcein AM and ethidium homodimer to PBS at 0.2 µl.ml^{-1} and 0.4 µl.ml^{-1} concentration, respectively. To observe cells distribution and obtain reliable viability analysis, the cell-laden constructs were cut into halves and subsequently incubated in the staining solution for 20 min

protected from light. The hydrogel constructs were then washed with PBS before imaging. The live and dead cells were analyzed under an invert LSM 700 confocal microscope (Carl Zeiss, Jena, Germany) by taking florescence images at wavelengths adjusted for green and red dyes. In addition to live/dead visualization, a FIJI script was written to quantify the viability of cells from the obtained z-stacks confocal images.

Biochemical analysis.

DNA content and sulfated glycosaminoglycan (sGAG) production of the cell-laden constructs were quantified at different time points (day 1, day 14 and day 28). The enzymatically digested samples were used for DNA and sGAG quantification. Accordingly, we transferred each samples in a 1.5 ml eppendorf tube and added 500 µl of papain digestion buffer containing 6 µl.ml-1 papain (Sigma P-3125). The papain solution was prepared by dissolving 7.1 g of sodium phosphate dibasic (Na2HPO4), 1.86 g of Ethylenediaminetetraacetic acid (EDTA), and 870 mg of L-cysteine HCl in 500 ml of dH2O. The pH of the resulting solution was adjusted to 6.5. The samples were crushed and mixed with a pestle and then incubated at 60 °C overnight to ensure complete digestion. The sGAG content was analyzed using the 1,9-dimethylmethylene blue (DMMB) dye-binding assay with shark chondroitin sulfate (CS) as standard. Accordingly, 20 µl of the diluted samples were plated in clear 96 well plates followed by adding 130 µl of DMMB dye to the wells (in triplicate). Sample absorbance was immediately measured at 590 nm using a microplate reader (Wallac 1420 Victor2, PerkinElmer). The obtained data was compared to the standard curves of CS and the sGAG content was determined. DNA analysis was performed by the Hoechst fluorescence assay (Hoechst 33258, Thermo Fisher Scientific) with a sample/dye ratio of 10 to 140 µl. The prepared samples were first plated in black 96 well plate followed by immediate addition of Hoechst dye and measuring the emission signal of samples at 460 nm by the microplate reader. The DNA content of the samples was finally determined by using a standard curve extracted from sequential dilutions of Calf Thymus DNA (Thermo Fisher Scientific) as calibrators.

RNA extraction and gene expression analysis.

The expression of chondrogenic markers was compared at each time point of 3D culture using RT-PCR method. Briefly, hydrogel constructs were transferred to 1.5 ml eppendorf tube and 300 µl of Trizol was added. The samples were smashed and homogenized by with a pestle while keeping the sample in cold ice. Total RNA was isolated using a NucleoSpin RNA Kit (Macherey-Nagel) based

on the manufacturer's instructions. The amount of extracted RNA was obtained with a Nanodrop Lite Spectrophotometer (Thermo Scientific). After RNA isolation process, 1 µg from each sample was taken for reverse transcription into complementary DNA (cDNA) using TaqMan® Reverse Transcription Reagents (Applied Biosystems). SybrGreen® Mastermix (Applied Biosystems) was used for quantitative RT-PCR using a StepOnePlus™ Real-Time PCR System (Applied Biosystems). The expression of collagen type II (COL2a1), aggrecan (ACAN), and ADAMTS5 genes were examined (Supplementary Table S5.1). RPL13a was used as a reference gene. The initial denaturation and polymerase activation occurred at 95 °C for 1 min, followed by 40 cycles of denaturation at 95 °C for 5 s, and extension at 60 °C for 30 s. The comparative threshold cycle ($\Delta\Delta CT$) method was used to calculate the relative gene expression.

5.5 Results

5.5.1 Characterization and adhesion mechanism of hydrogel family

The developed family of hydrogels adhere strongly to articular cartilage, as a soft tissue example (Figure 5.1b). All SN matrices have considerable adhesion strength ($\geq$ 50 kPa) with a water content of 90 wt%. The adhesive performance is even further enhanced in the composite form of these hydrogels. For example, collagen and Nanofibrillated Cellulose (NFC)-reinforced MeCHa-Gel improve the adhesion strength of the single-network MeCHa-Gel by 32% and 56%, respectively. This is mainly attributed to better energy dissipation capacity in the collagen- and NFC-reinforced hydrogels, which results in higher synergetic contribution between strong interfacial bonds and bulk dissipation. The higher strength values of the NFC-reinforced over the collagen-reinforced composites hydrogels indicate the presence of more sacrificial bonds in fiber-matrix interface, dissipating more energy. The bioadhesive family exhibits superior adhesion strength at various polymer concentrations compared to the values obtained with commercial Fibrin TISSEEL™ adhesive, as shown for MeCHa-Gel (Figure 5.1c).
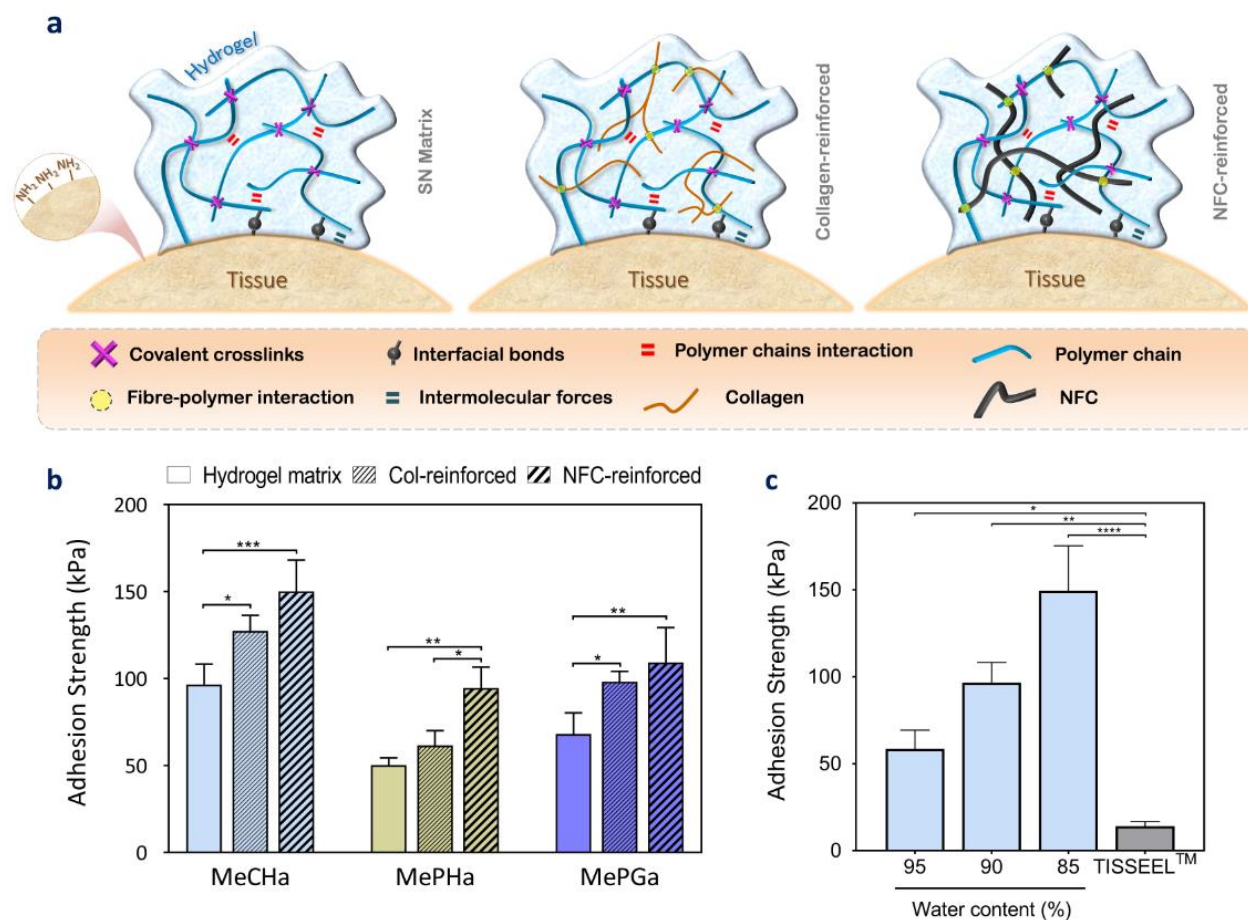
Figure 5.1. Adhesion performance of intrinsically-adhesive hydrogel family. (A) Schematic illustration of bioadhesives and network design. The intrinsically-adhesive hydrogels create interfacial chemical bonds with nucleophiles at tissue interface, including covalent bonds and intermolecular forces. The cross-linkable chains form the hydrogel network. Fast covalent cross-linking and different sacrificial bonds provide a wide window of reachable stiffness and dissipation in the hydrogels. The network interactions are augmented by nanofiber-reinforcement so that the adhesive and physicochemical properties can be well controlled. Effect of collagen fibers with small fibers diameter (< 100 nm) and nanofibrillated cellulose with larger size (0.1-10 µm) are investigated. **(B)** Tensile adhesion strength of the single network and composite bioadhesive family to bovine articular cartilage (tissue model). **(C)** Adhesive strengths of SN MeCHa-Gel with different water content (85-95 %). The results report adhesion values obtained from tensile adhesion tests on bovine articular cartilage. Data represent means and standard deviation of the mean (n ≥ 3, *P <0.05, **P <0.01, ***P <0.001, ****P <0.0001)

To form a fast light-activated adhesive system, the polymer backbone is firstly chemically functionalized with methacrylate groups. Accordingly, upon the visible light exposure and in the presence of LAP photo-initiator, cross-linking of the adhesive occurs in only 30-150 sec depending on the target hydrogel composition. Moreover, illumination with a long wavelength light (405 nm) in a low range of light intensity (1-5 mW.cm^{-2}), along with performing biocompatibity tests and in vitro 3D culture experiments, addresses the biosafety concerns associated with photo-polymerizable hydrogels in many biomedical applications [178]. The backbone is also modified with a second molecule to enhance interfacial bonding to various tissues. Therefore, the SN hydrogel can adhere intrinsically to tissue substrates. The obtained range of adhesion strength and fast curing time differentiate our bioadhesive family from various injectable tissue adhesives (Supplementary Figure S5.2). The timely efficient one-pot polymerization process facilitates the clinical usage of the proposed bioadhesives for demanding surgical situations.

The methacrylated catechol-containing hyaluronic acid (MeCHa) chains are fabricated with an original two-step modification of hyaluronic acid, including esterification of hydroxyl groups on the polymer backbone with subsequent chemical conjugation of Dopa at the carboxyl sites of the backbone. The careful pH control of aqueous environment and the order of functionalizations avoid Dopa oxidation during the reaction. Similarly, by substituting the adhesive component or the polymeric backbone, methacrylated phosphoserine-containing hyaluronic acid (MePHa) and methacrylated phosphoserine-containing gelatin (MePGa) chains are synthesized with methacrylation of the backbones (hyaluronic acid and gelatin) and subsequent attachment of phosphoserine molecule (see Figure 5.2 and Materials and Methods). Phosphoserine is predominantly found in phosphoproteins which demonstrate functions in improving adhesive and cohesive properties such as in marine bioglues [120, 179, 180].
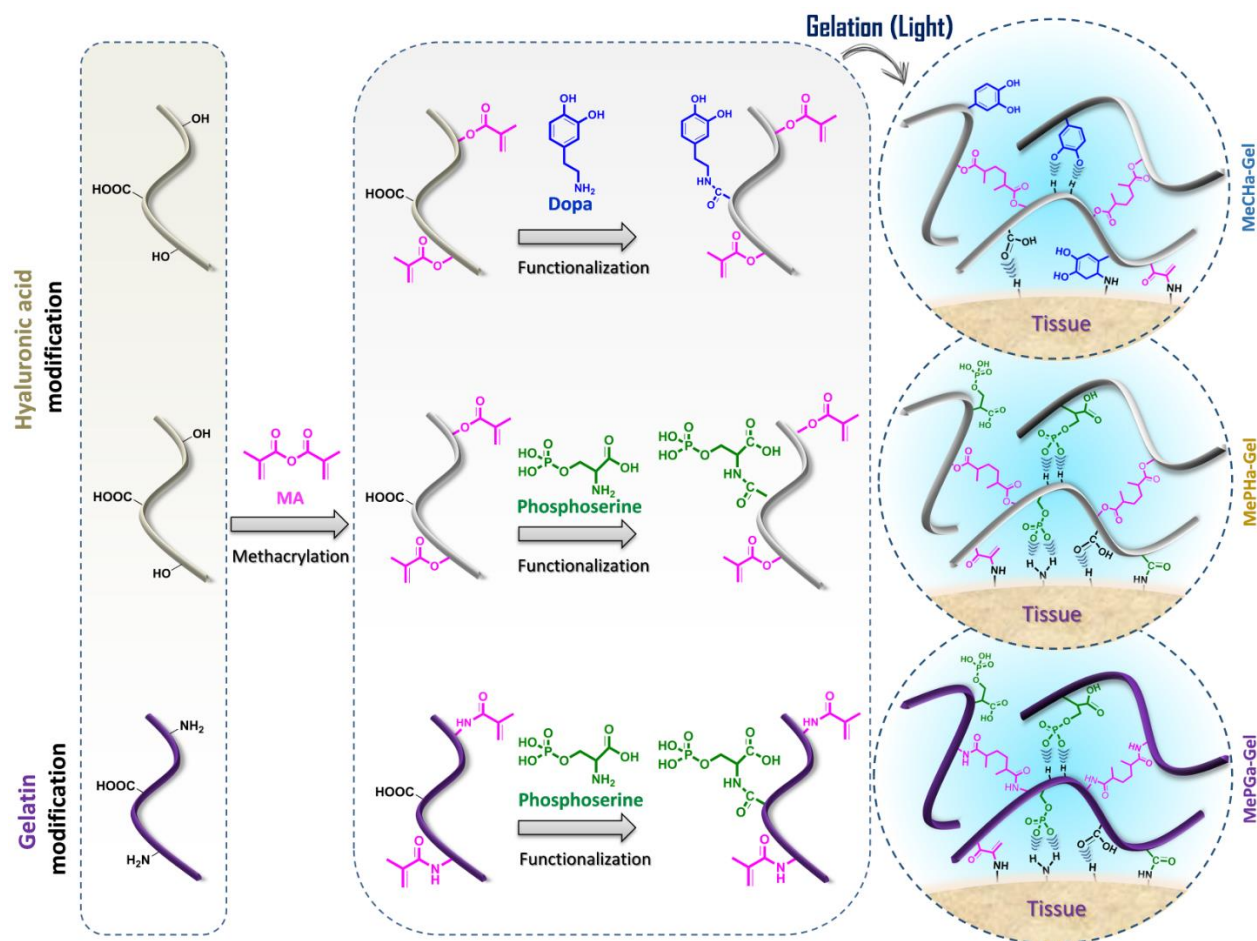
Figure 5.2. Design and synthesis route to MeCHa-Gel, MePHa-Gel and MePGa-Gel. The adhesive family is fabricated by changing the polymeric backbones or the modified components. The chains (i.e., hyaluronic acid, gelatin) are first chemically modified with methacrylate groups. The second modification includes conjugation of the functional groups (i.e., dopa, phosphoserine) to the processed chains to enhance the interfacial interactions. The photo-triggered gelation process is driven by fast cross-linking, and various intrinsic interfacial interactions can be formed via covalent bonds (e.g., amide formation, Michael addition, Schiff base reaction, etc.), electrostatic interactions and intermolecular forces (e.g., hydrogen bonds, etc.).

The contribution of interfacial chemistry and hydrogel mechanics to overall adhesion is demonstrated for MeCHa-Gel, as an example (Figure 5.3). The hydrogel design allows control over the interface (e.g. chemical bond formation) and bulk mechanical properties (e.g. stiffness and dissipation potential) using the same hydrogel composition and without the surface treatment of host tissue or hydrogel. By varying the pH of the precursor and the illumination time it is possible to evaluate the

individual contribution of interfacial and bulk properties, respectively, on the obtained adhesion as well as the produced synergy between them. The adhesive systems with either robust hydrogel-tissue chemical interactions or superior dissipative mechanism present weaker adhesion (less than 3 times) due to the lack of synergy. The presence of interfacial covalent bonds at low mechanical dissipation in the hydrogel results in 29.3 ± 4.4 kPa adhesion strength, and higher mechanical dissipation without strong interfacial bonds contributes to 13.7 ± 3.7 kPa adhesion strength. However, the adhesive system with both strong chemical bonds at the tissue interface and high dissipative performance in the hydrogel exhibits 95.5 ± 11.7 kPa adhesion strength.

In addition to physical interactions, electrostatic forces and hydrogen bonds, the interface energy is augmented with strong covalent bonds. In MeCHa-Gel system, the oxidized catechol (dopa-quinone) and the activated carboxyl groups in the MeCHa backbone can form covalent bonds with primary amine groups, which are abundant in the tissue substrates. In MePHa- and MePGa-Gels, the amine-phosphate interactions can be formed, including the binding of negatively charged phosphate to positively charged amine surface groups, multiple hydrogen bonding opportunities, and amide formation by reaction of ester and amine groups. Furthermore, covalent bonds can be finely formed between methacrylate groups of hydrogel chains and amine functional groups in the tissue [181-183] (see Figure 5.2).
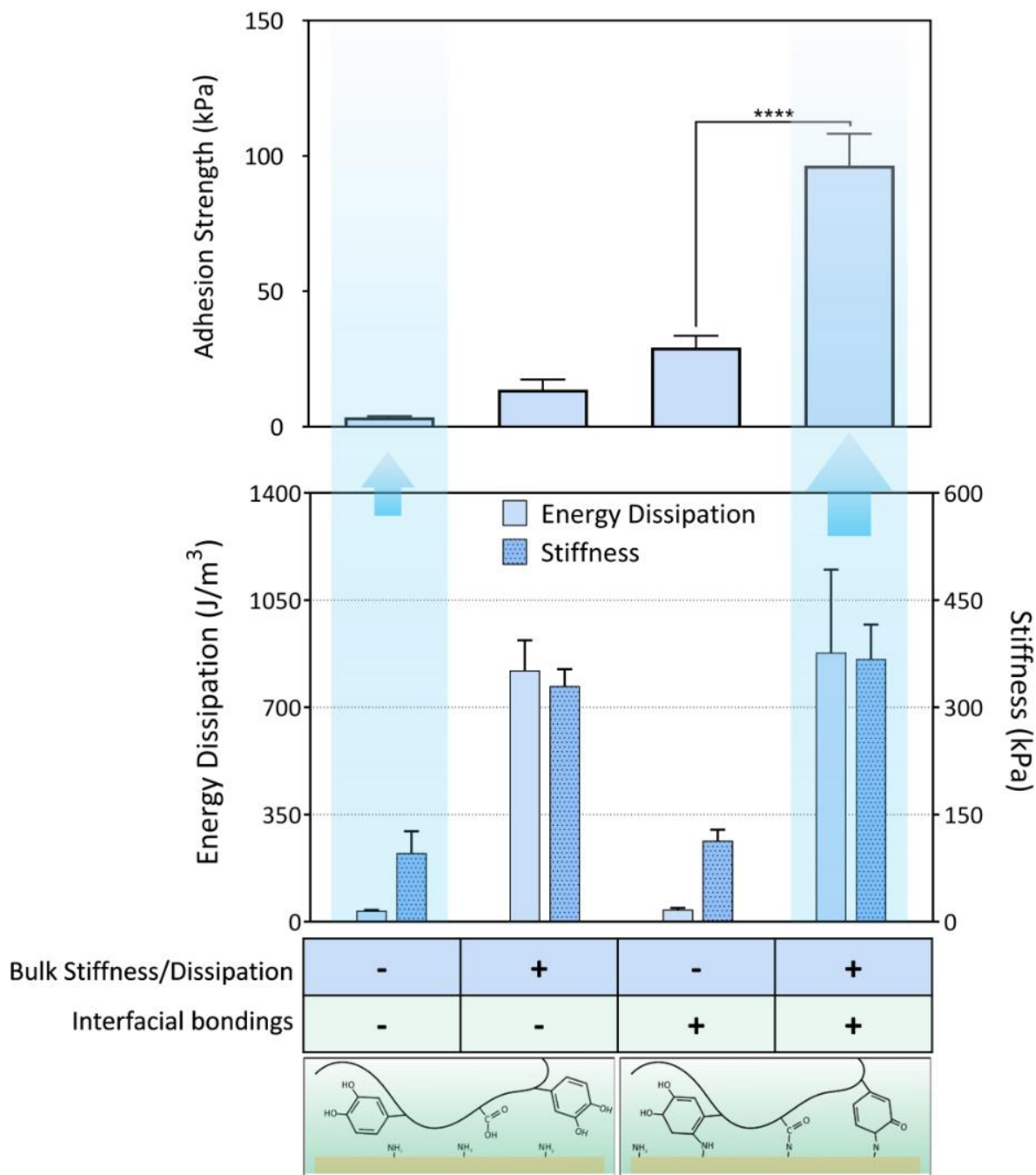
Figure 5.3. Synergetic adhesion mechanism of the MeCHa-Gel. Interfacial bonding, **(-):** preparation of MeCHa precursor at pH=5.9 without carboxyl activation, limited covalent bonds formation between hydrogel and tissue, **(+):** preparation of MeCHa precursor at pH=7.5 with carboxyl activation, covalent bonds formation between hydrogel and tissue (e.g., amide formation, Michael addition, Schiff base reaction). Bulk stiffness/dissipation, **(-):** hydrogel illumination for t=20 sec, **(+):** hydrogel illumination for t=1 min. (n $\geq$ 3)

5.5.2   Physicochemical characterization of hydrogel family

Due to the versatility of the design parameters, the physicochemical properties of the hydrogels could be tuned over a broad range of properties. The range of the physical properties in the designed adhesive hydrogels were investigated (Figure 5.4 and Supplementary Figure S5.3). Tailoring the swelling performance of hydrogels might be of high importance in many medical applications [184, 185]. While high level of swelling imposes limitations on numerous hydrogel systems, the swelling of our hydrogels system can be finely controlled. Indeed, the cross-linking mechanism of the modified chains and their network configuration hinder excessive swelling of the neat hydrogel matrices. Additionally, the fiber-reinforced hydrogels further reduce the swelling of the hydrogel composites due to the fiber-matrix interactions. Unlike MeCHa- and MePHa-based hydrogels, negative but negligible swelling is observed in MePGa-based hydrogels (Figure 5.4a). Mechanical properties (i.e., hydrogel stiffness, energy dissipation and energy loss) of our adhesive family were characterized under compression and tensile deformations (Figure 5.4b,c). Across all hydrogel compositions, the NFC-reinforced hydrogel showed the highest mechanical properties, followed by collagen-reinforced, and lastly, the neat hydrogel. Furthermore, the hydrogel properties are acquired at high water content (80-95 wt%) which mimic most native tissues [186]. The stiffness and mechanical dissipation of the SN hydrogels are further enhanced in the composite form. For example, NFC-reinforcement contributes to approximately 95% increase in compressive modulus (from 368.2 ± 49.0 kPa to 719.3 ± 13.1 kPa), 68% in tensile modulus (from 172.9 ± 31.3 kPa to 291.0 ± 21.2 kPa), 107% in energy dissipation (from 879.5 ± 270.6 kJ.m-3 to 1822.5 ± 222.2 kJ.m-3) for MeCHa-Gel. The gelatin-based adhesives have lower stiffness than hyaluronic acid-based adhesives, however they exhibit higher dissipative properties. The chain mobility and higher number of sacrificial bonds in gelatin-based bioadhesives contribute to a more flexible network with higher capability for energy dissipation. We associate this superior mechanical dissipation with the augmented adhesion performance of the MePGa-Gels compared to MePHa-Gels (see Figure 5.1b). The mechanical properties of the adhesive can be customized by varying the adhesive polymer concentration, degree of modifications, curing condition (i.e. light intensity, illumination time, photo-initiator concentration), polymer chain length and tailoring the reinforcing network, (Supplementary Figure S5.4). Different formulations can be derived by manipulating the synthesis parameters, so that the physical properties of the hydrogels can be tuned. The obtained stiffness in different formulations

could be comparable with the required properties for various soft tissues (e.g., liver, kidney, stomach, skin, heart, lung, muscle, articular cartilage, etc.) [187].

The adhesive hydrogels show tunable biodegradability rates modulated via hydrogel composition and synthesis parameters based on the target application. MeCHa- and MePHa-Gels are enzymatically degradable by hyaluronidase enzyme, hydrolyzing the bonds between N-acetyl-D-glucosamine and D-glucuronic acid [188]. MePGa-Gels are also enzymatically degradable by collagenase enzyme breaking the peptide bonds in the backbone of the chain. MePGa-Gels degrade faster than MeCHa- and MePHa-Gels at the same enzyme concentration and under the same test conditions (Supplementary Figure S5.5a). The degradation of hydrogel networks can be controlled and may take anywhere from days to months based on the synthesis parameters (Supplementary Figure S5.5 b-f). For example, the MeCHa-Gel with a backbone molecular weight of 15-30 kDa exhibits around three times faster degradation rate than that found with a molecular weight of 30-50 kDa. Moreover, the enzyme concentration can vary the biodegradation kinetics. MeCHa-Gel fully degrades after one week of incubation in 10 U/ml enzyme solution while only $40.6 \pm 5.4\%$ degradation is observed after 12 weeks, when the adhesive is incubated in 1 U/ml enzyme concentration (Supplementary Figure S5.5 f).
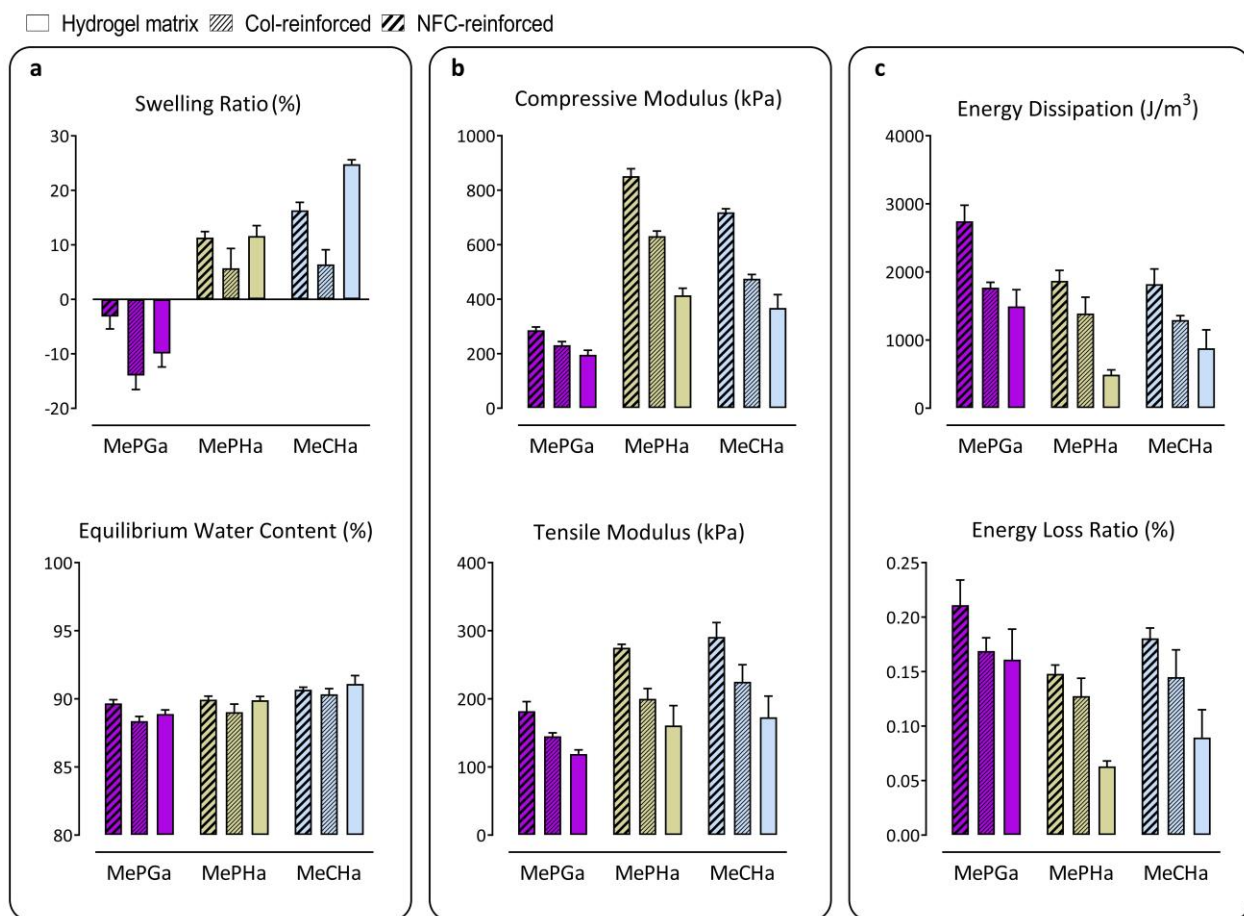
Figure 5.4. Physical characterizations of the adhesive hydrogels system (with 10 wt% initial water content). **(A)** Swelling ratios and equilibrium water content, **(B)** compressive and tensile modulus and **(c)** energy dissipation and energy loss ratio of the hydrogels with various network composition.

5.5.3 Various applications of hydrogel family

The developed adhesive family forms strong contacts to a broad variety of tissue substrates. With the superior and customizable properties, our bioadhesive can be used as a fast-curing tissue adhesive, a surgical sealant or an injectable implant. We evaluated the adhesive performance with different lap-shear, burst pressure and tensile adhesion tests. *In vitro* shear properties of bioadhesives were analyzed using a modified lap-shear setup (Supplementary Figure S5.6). Robust shear adhesion to various soft tissues was measured, including bovine lateral meniscus, heart, lung, kidney and liver (Figure 5.5a). Compared to Fibrin glue TISSEEL as a commercially available adhesive, the interfacial

shear strength of our hydrogels is significantly higher. For example, MeCHa-Gel exhibits an increase in shear adhesion, which is approximately 10 times higher for meniscus, 9.5 times higher for heart, 13.5 times higher for lung, 5.5 times higher for kidney and 5 times higher for liver (Figure 5a). The range of strength values varied widely across different tissue substrates. This mainly results from the differences in the density of functional groups present on the tissue surface as well as the mechanical properties of the tissues.

As another potential clinical application, we further evaluated the function of our developed biomaterials as adhesive sealants. In particular, the performance of the adhesives is evaluated for sealing of corneal incisions by an ex vivo burst pressure test (Figure 5b and Supplementary Figure S5.7). The fine control on the hydrogel properties (e.g., swelling as well as the modulated mechanical performance) make our adhesives promising for the repair of corneal injuries [57, 189]. We performed the adhesion tests on fresh calf eyes by creating full-thickness corneal defects. Transparent MeCHa, MePHa and MePGa precursors were then injected inside the defects and cured quickly (1 min). The burst pressure was measured by pressurizing the anterior chamber of the eye until it bursts. The recorded burst pressures of the adhesive hydrogels (78.4 ± 8.6 kPa for MeCHa-Gel, 54.8 ± 3.6 kPa for MePHa-Gel and 48.0 ± 9.9 kPa for MePGa-Gel) are significantly higher than that of the commercial adhesives such as fibrin glue TISSEEL (9 ± 2.2 kPa) and PEG-based ReSure Sealant (15.4 ± 6.3 kPa). These commercial adhesives exhibit insufficient adhesion to corneal tissue and lack the required mechanical properties [32, 33]. The empty corneal defects were also tested as a control.

Finally, to further demonstrate the functionality of the bioadhesive as an injectable scaffold with fast adhesion formation, we implanted the adhesive hydrogel (MePGa-gel) into full-thickness cartilage defects in knee joints in a large animal model. *In vivo* tests were performed on goats as an appropriate animal model for cartilage defect trials with a joint anatomy and loading conditions close to humans [34]. The performance of the intrinsically-adhesive scaffold can therefore be shown in a load-bearing orthopedic application. Cartilage defects with 5 mm diameter were created on the medial femoral groove of the (left) knee joint. Subsequently, the hydrogel precursor was injected in the defects and photo-crosslinked in situ (Supplementary Figure S5.8). With no immobilization of the joint, the goats were allowed to roam freely throughout the duration of the study. The integrity of hydrogels is

maintained after 2 days of implantation (Figure 5.5c), which indicates stable and strong adhesion between the scaffold and the surrounding tissue.
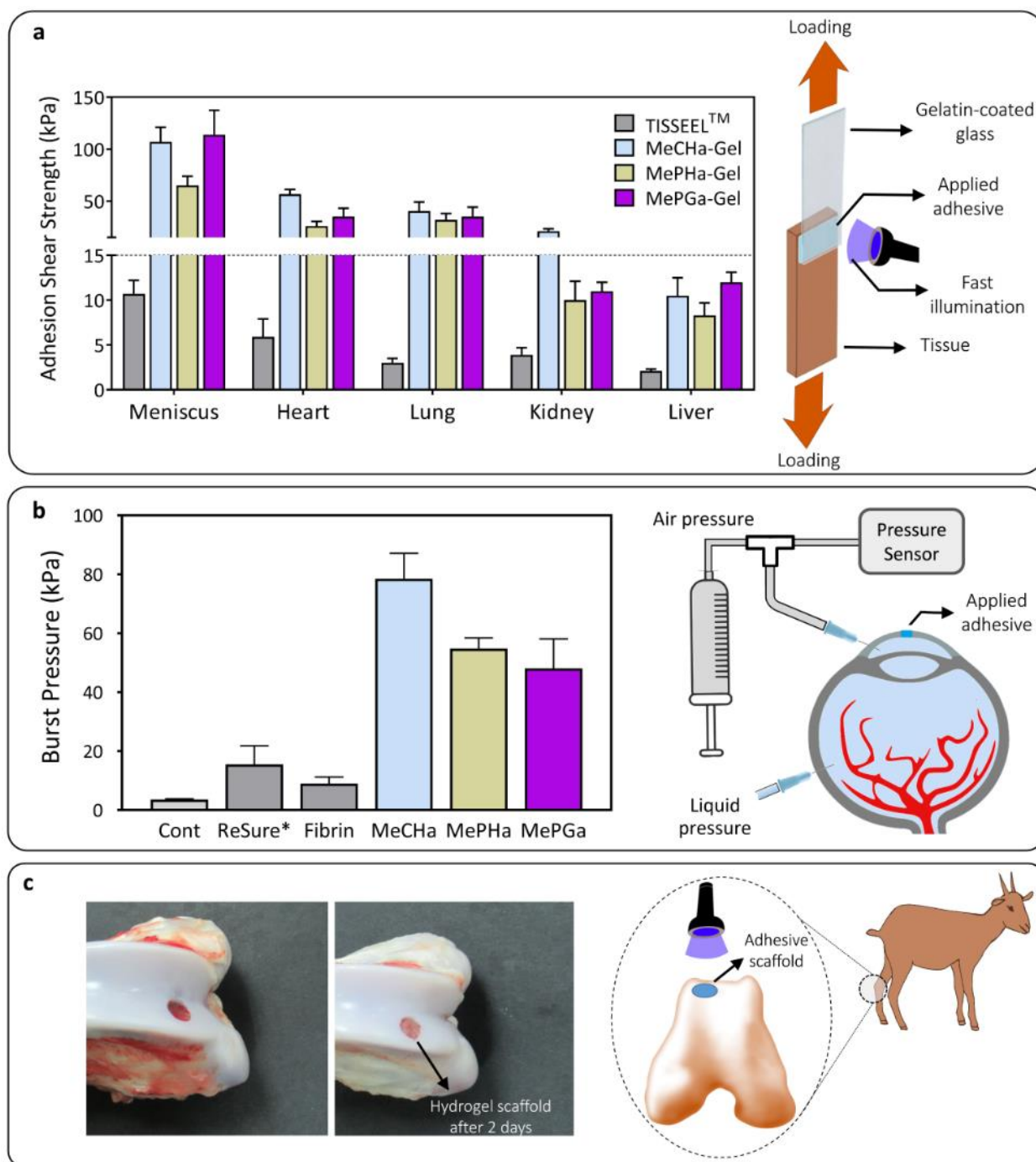
Figure 5.5. Adhesion performance of the bioadhesive hydrogel family. (A) Interfacial shear strength between soft tissue substrates and MeCHa, MePHa and MePGa bioadhesives with 87 wt% water content and fast (30 seconds) of curing time. The tests are conducted on fresh bovine tissues using a lap shear

adhesion setup. The results are compared to shear strength values of Fibrin glue TISSEEL^{TM}. **(B)** *Ex vivo* burst pressure test of bioadhesives for sealing of corneal defects. The sealed cornea is tested by pressurizing the anterior chamber of the explanted calf eyes using a burst pressure setup and a pressure sensor. The results are compared to ReSure and Fibrin Tisseel^{TM} tissue adhesives. **(C)** *In vivo* implantation of the bioadhesive scaffold in full-thickness cartilage defects in large animal model. The integration of the adhesive hydrogel is observed after two days of implantation with no immobilization (n ≥ 3).

5.5.4   Biocompatibility and in vitro tissue engineering

The adhesive family of hydrogels developed in this study showed good biocompatibility. The in vitro cytotoxicity of the hydrogels was first assessed by a proliferation test using bovine chondrocytes for 9 days. The cell proliferation in the presence of all SN and composite bioadhesives (evaluated by PrestoBlueTM assay) is comparable to that found with the control group at different time points, confirming that the bioadhesives have no significant negative effect on cell proliferation (Supplementary Figure S5.9)

In addition to physicochemical and adhesive performance of our engineered bioadhesives, they may also be used as injectable cell-laden scaffolds for tissue engineering and drug delivery applications. In order to further demonstrate this capacity, we conducted an in vitro experiment to study the differentiation capacity of chondrocyte cells encapsulated in the adhesive MePHa- and MePGa- Gels. The viability, proliferation, chondrogenic differentiation and matrix production of embedded cells as well as the physical properties of the 3D hydrogel constructs were analyzed over 4 weeks. The cells encapsulated in both adhesive hydrogels exhibit high viability at all time points, with more than 84% live cells after 4 weeks (Figure 5.6a and Supplementary Figure S5.10). The assessment of total DNA content shows conspicuous increase, indicating proliferation of cells inside the hydrogel constructs (Figure 5.6b). Moreover, S-GAG accumulation was significantly increased after 2 and 4 weeks of 3D culture (Figure 5.6c). While gelatin-based MePGa-Gel exhibit slightly less viability and DNA content than hyaluronic acid-based MePHa-Gel, it induces more S-GAG deposition. This indicates superior chondro-inductive property of the MePGa-Gel. GAG production enhances the mechanical performance of the seeded hydrogels. The stiffness and energy dissipation capability of the constructs

highly improved during the culture time. However, enhancement of the mechanical properties was more substantial for MePGa-gel after 4 weeks (1.51 ± 0.24 MPa stiffness and 7338.52 ± 1653 kJ/m3 energy dissipation), which is close to that found in native cartilage [35]. The gene expression of the main anabolic (Collagen type II and Aggrecan) and catabolic (ADAMTS5) chondrogenesis markers were also studied by using real-time reverse transcriptase polymerase chain reaction (RT-PCR) analysis. The collagen type II (COL2A1) and aggrecan (ACAN) indicators are highly upregulated in both hydrogels ($p < 0.001$) over 4 weeks of 3D culture. In addition, ADAMTS5 is dramatically downregulated in the hydrogel constructs. This is favorable for cartilage regeneration as ADAMTS5 is associated with the degradation of extracellular matrix constituents [190]. MeCHa-Gel is mainly proposed for tissue adhesion and sealing applications and was not used in chondrocyte encapsulation study due to lower viability of chondrocyte in this hydrogel.
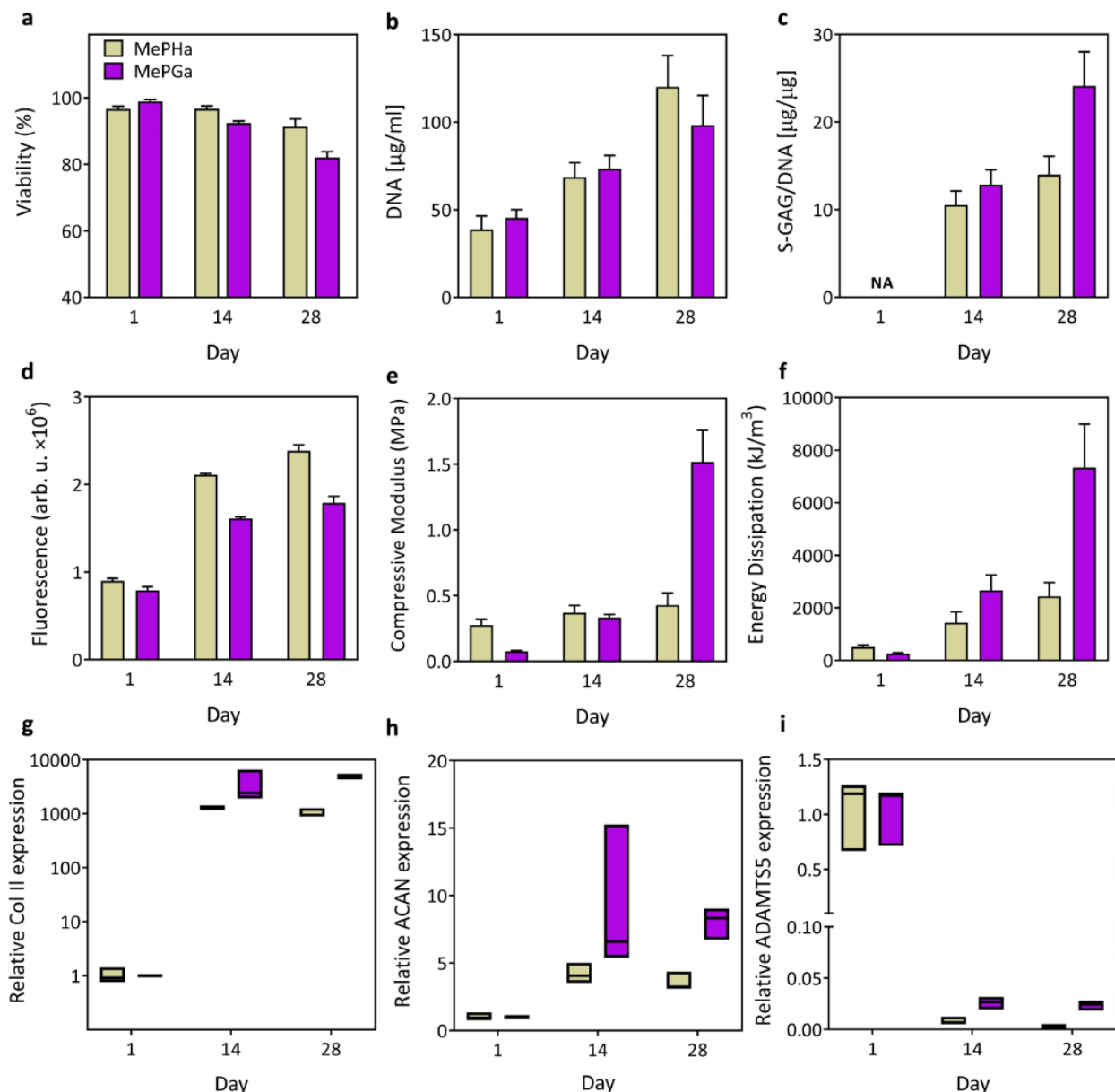
Figure 5.6. *In vitro* **evaluation of the chondrocytes biological response encapsulated in adhesive hydrogels (WC: 95%) over 4 weeks of 3D culture. (A)** Viability of chondrocytes in MePHa-Gel and MePGa-Gel constructs using live/dead assay. **(B, C)** Biochemical analysis: DNA and sGAG/DNA content in hydrogel constructs. **(D)** Cell proliferation using PrestoBlue™ assay. **(E, F)** Mechanical characterization. **(G-I)** Gene expression analysis: collagen type II (COL2A1), aggrecan (ACAN) and ADAMTS. (n = 3)

5.6 Discussion

A family of injectable and internally-adhesive hydrogels with a fast curing process was reported based on a bioinspired design paradigm. Different polymeric backbones were synthesized through an original two-step modification process to include cross-linkable and adhesive components. With a unique control on interface and bulk properties, the adhesion mechanism of the developed hydrogels was shown, and the synergy of interfacial bonds and mechanical properties was studied. The hydrogels were further modified to include secondary networks of various nanofibers. In addition to strong and fast adhesion formation on a variety of soft tissues in wet environment, the physicochemical properties of the hydrogels could be also tuned over a broad range of properties. Different design aspects of the bioadhesive family were therefore addressed. The hydrogels have tunable swelling behavior so that they can be applied without significant volumetric increase in wet physiological environments. A wide range of compressive and tensile stiffness and dissipation can be attained. Therefore, the mechanical requirements for the repair of various tissues, including load-bearing soft tissues, can be addressed. The biodegradation kinetics of the hydrogels is controlled through decoration of chains and hydrogel fabrication. With various *in vitro*, *ex vivo*, and preliminary *in vivo* studies, the biocompatibility and potential biomedical applications of the injectable adhesive hydrogels were demonstrated for cells scaffolding, soft tissues repair and tissue sealing. The adhesion mechanism of our hydrogel family can further be used for unmet clinical needs, and also provides a promising path to the development of future biomimetic adhesive hydrogels.

Supporting Information for Chapter 5

Mussel adhesion mechanism

The adhesive performance of marine mussels has recently provided important chemical and physical insights into moisture-resistant adhesion. Water could be a main contributor to adhesive failure especially in the biological environment than on clean and dry surfaces. It may subvert adhesion through weakening interfacial bondings, swelling, etc. Therefore, the presence of moisture often leads to the deterioration of performance in adhesive polymers. However, adhesion mechanism of this animal allows strong attachment to different surfaces in wet environments.

There are several proteins in the byssal plaque of the mussel. All these proteins contain the post-translationally modified amino acid 3,4- dihydroxyphenyl-L-alanine (Dopa) and have widely different sequences. It is widely discussed that the presence of this amino acid is responsible for the mussel's ability to stick. The key part of the molecule is the catechol side-chain, made up of a benzene ring with two hydroxyl groups which can form bonds with different surfaces.

The primary adhesive interactions of mussel with the surface is commonly attributed to the presence of Mfp-3 (mussel foot protein-3) and Mfp-5, as Dopa content in these two proteins is much higher than the other proteins. However, it can be interestingly observed that Mfp-3 and Mfp-5 have relatively low molecular weight (6 and 9 kDa respectively). Moreover, It seems that the interactions between other existing proteins could be important in the adhesion performance of the mussel. In particular, Mfp-2, the most abundant plaque protein with a high molecular weight (45 kDa), interacts only with the adhesive Mfp-5; and Mfp-5 interacts only with Mfp-3 through strong protein-protein bindings. Interactions between Mfp-2s are ionic with Ca^{2+} and Fe^{3+} [120].

Molecular-level studies of Dopa interfacial behavior revealed strong and reversible interactions between Dopa and inorganic surfaces. The strength of the interaction between Dopa and an oxide surface appears to be highly pH dependent, as measurements performed at high pH resulted in significantly attenuated pull-off forces. Auto-oxidation of Dopa to Dopaquinone at alkaline pH is likely responsible for this observation, implying that the interaction with inorganic surfaces is stronger in the catechol form compared with quinone. However, Dopaquinone is able to contribute to

interfacial bonding with organic surfaces by covalent reactions between quinones and nucleophiles commonly present on organic surfaces (see Figure 5.2). Single-molecule studies performed at high pH resulted in covalent bond formation between Dopa and primary amine surfaces [69].

Inspired by mussel adhesion and its unique chemical versatility, new adhesive hydrogels can be designed for strong adhesion to both organic and inorganic surfaces. On inorganic surfaces the unoxidized dopa forms high-strength yet reversible coordination bonds, whereas on organic surfaces oxidized dopa is capable of adhering via covalent bond formation. It may be that the remarkable ability of mussels to adhere to both organic and inorganic surfaces is related in part to the equilibrium that exists between Dopa and dopaquinone at marine pH, allowing both species to interact with surfaces. It is also notable that strong bonds between dopa and organic and inorganic surfaces formed in the presence of water, presumably a crucial characteristic for a protein adhesive operating in the wet marine environment.
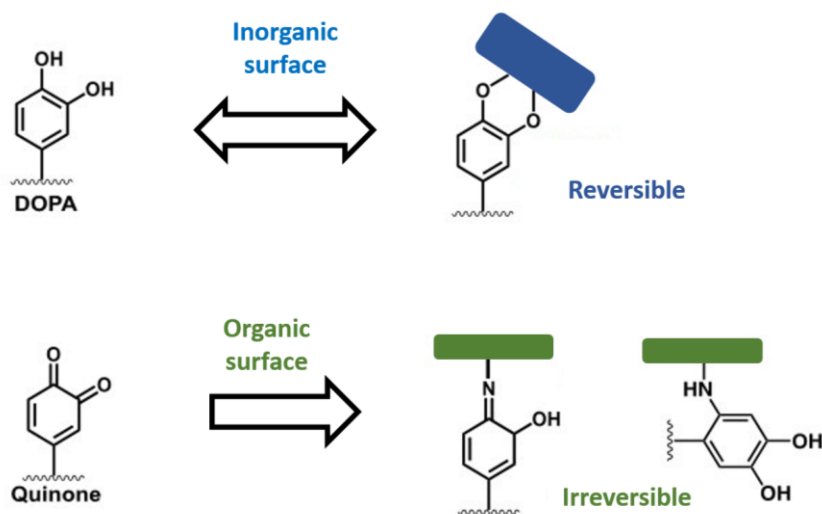
Supplementary Figure S5.1. The chemical versatility in chemical interactions of Dopa with inorganic and organic surfaces: Dopa interacts strongly and reversibly to inorganic surfaces while it forms covalent bonds on organic surfaces under alkaline pH conditions through C-N bond with amine functional groups (Lee et al. 10.1073/pnas.0605552103).
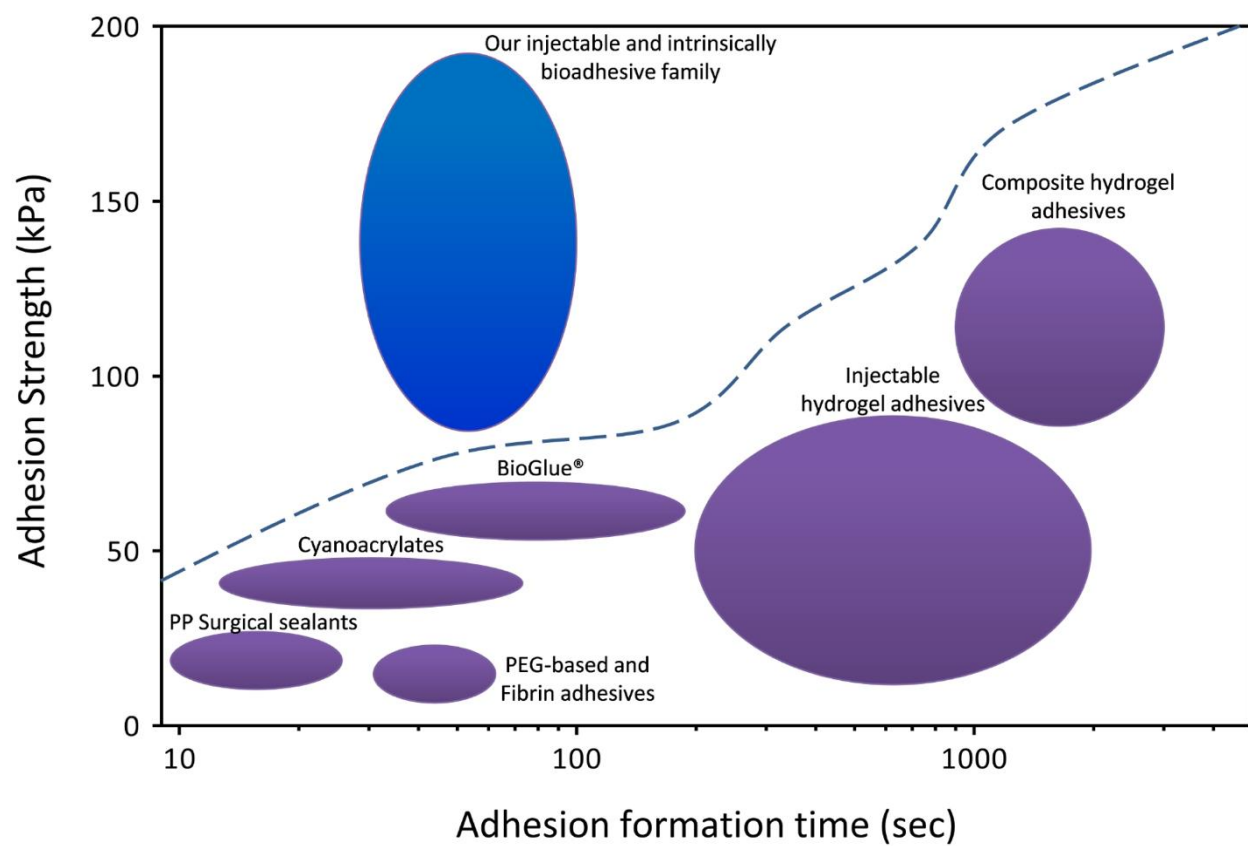
Supplementary Figure S5.2. Tensile adhesion strength tenacity and the required curing time of our bioadhesive family in comparison to available injectable tissue adhesives.
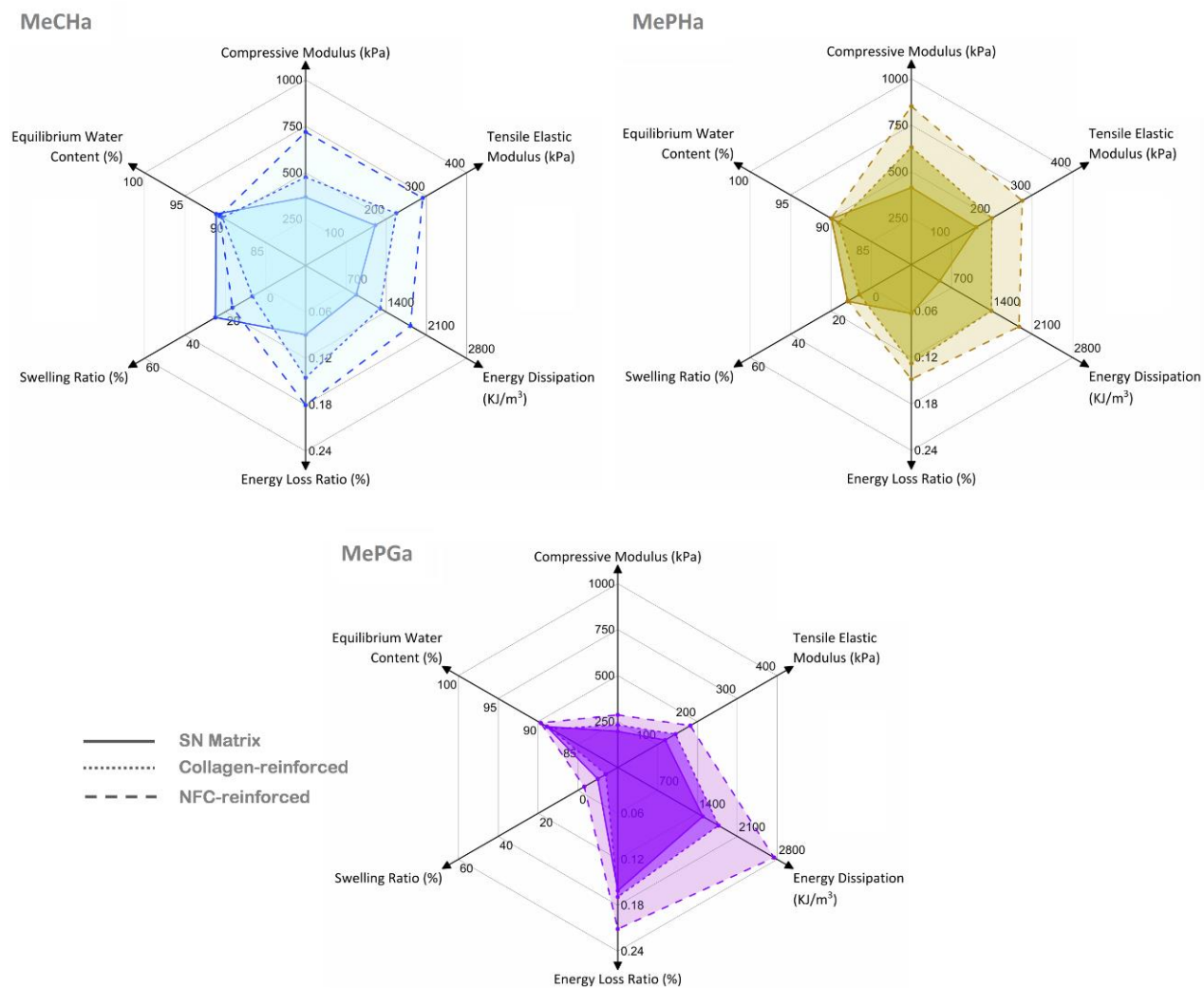
Supplementary Figure S5.3. Effect of fiber-reinforcement on physical properties of the adhesive hydrogels system (with 10 wt% initial water content).
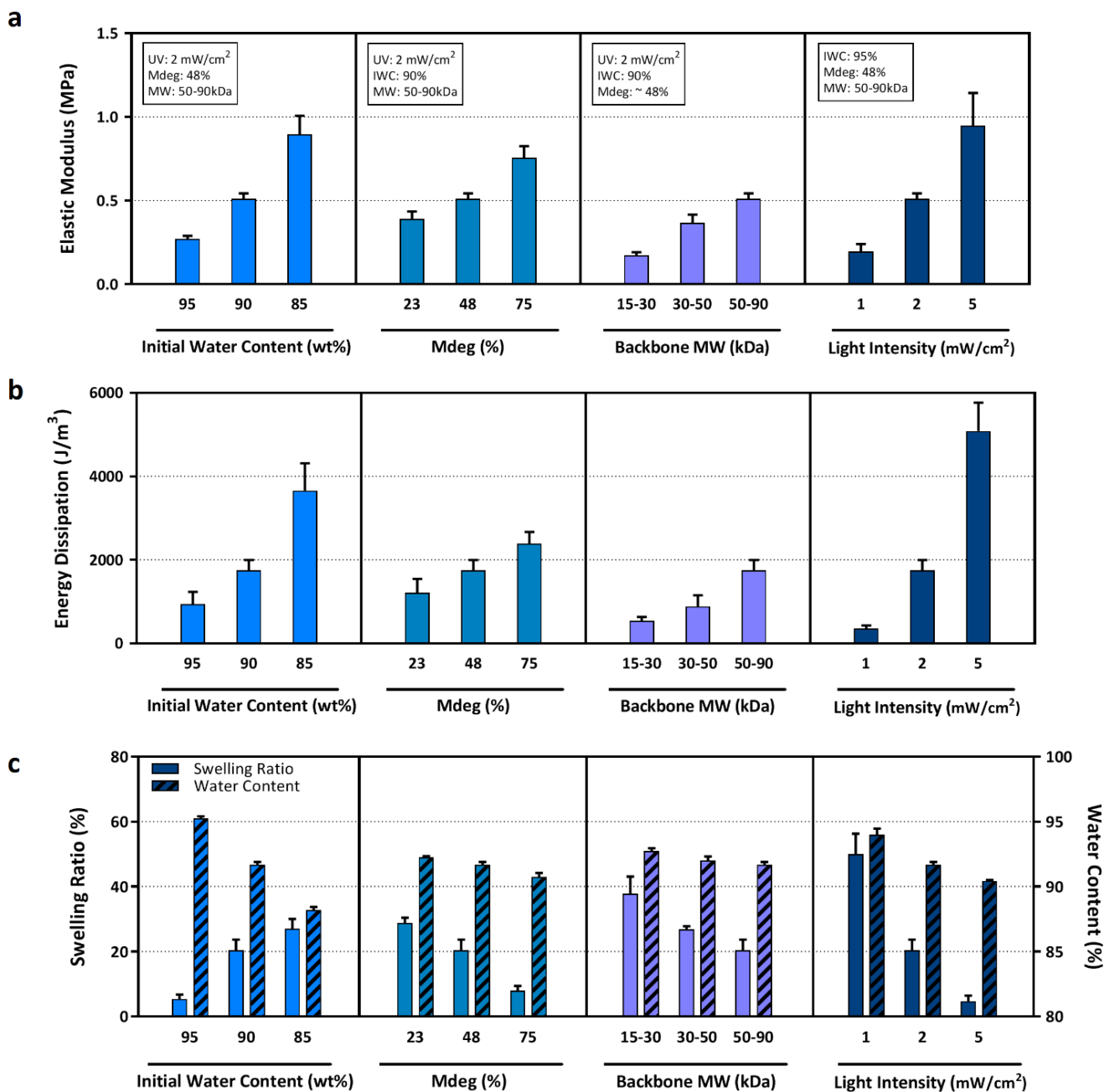
Supplementary Figure S5.4. Influence of different synthesis/fabrication parameters on functional properties of the MeCHa-Gel system. (**a**) stiffness, (**b**) energy dissipation and (**c**) swelling ratios and equilibrium water content (hatched) of hydrogels with modulated network structures. Results demonstrate that the physiochemical properties of bioadhesive hydrogels can be finely tuned by modulating the network structure. The analysis is conducted at various initial water contents (IWC), methacrylation degrees (Mdeg%), back bone molecular weight (MW) and light intensities at 405 nm. For evaluation of each parameter, the other parameters are kept constant.
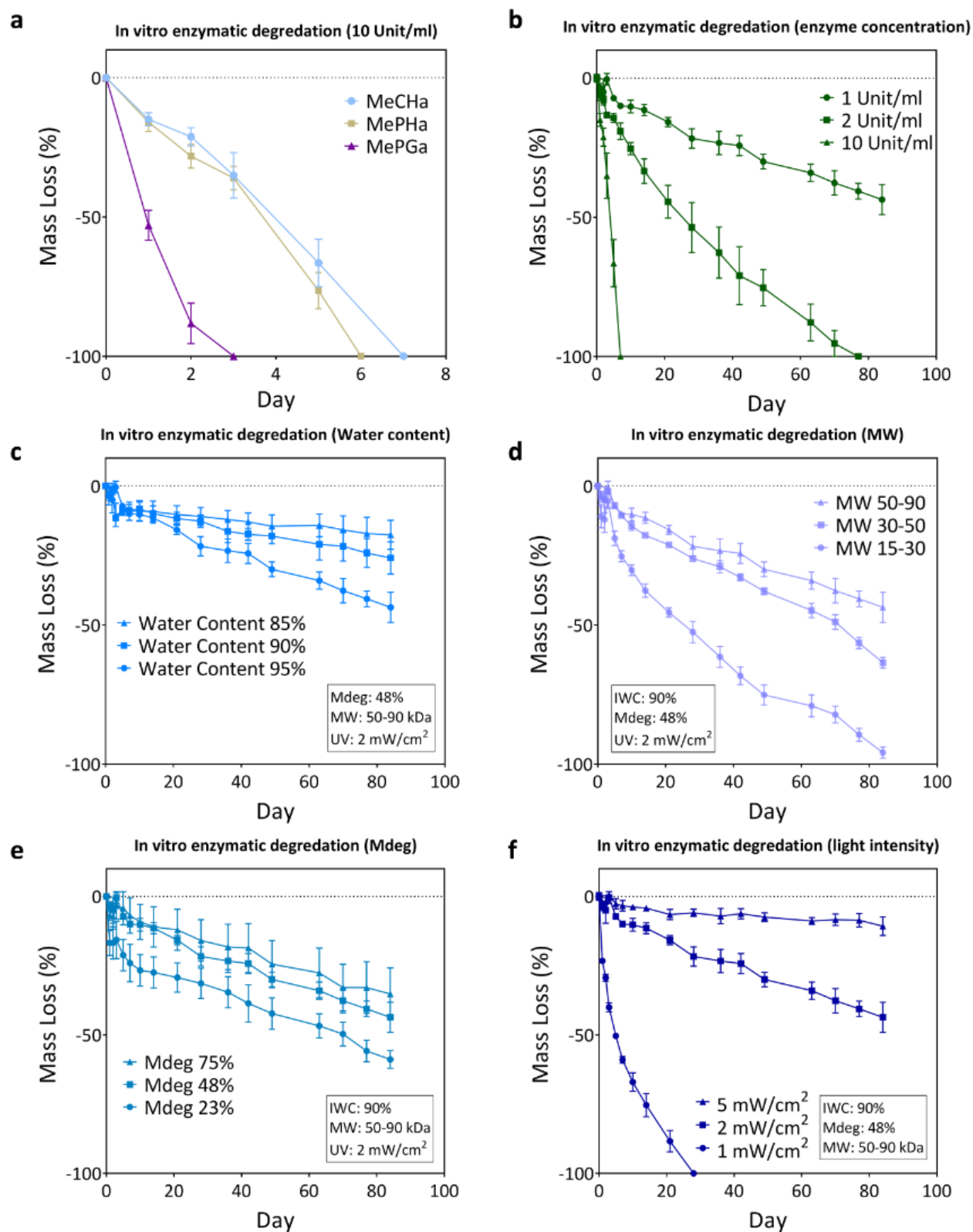
Supplementary Figure S5.5. (a) *In vitro* biodegradation of the 10 wt% MeCHa-, MePHa- and MePGa-

Gel matrices at 37°C. 10 unit/ml hyaluronidases solution was used for MeCHa- and MePHa-Gels, and 10

unit/ml of collagenase type II solution was used for MePGa-Gel. Full degradation is observed after 3-7 days of incubation for different hydrogels at relatively high enzyme concentration (10U/ml). (b) degradation of the MeCHa-Gel at different enzyme concentration (c-f) Analysis of various synthesis parameters on hydrogel degradation kinetics (MeCHa-Gel) at 1 U/ml enzyme concentration, including initial water content (IWC), molecular weight (MW), methacrylation degree (Mdeg) and light intensity. The biodegradation of the hydrogels can be tuned by modulating the network structure. Results demonstrate that lower water content (c), longer polymer chains (d), more crosslinking density (e), higher light intensity (f) and higher enzyme concentration increase the biodegradation time from days to months.
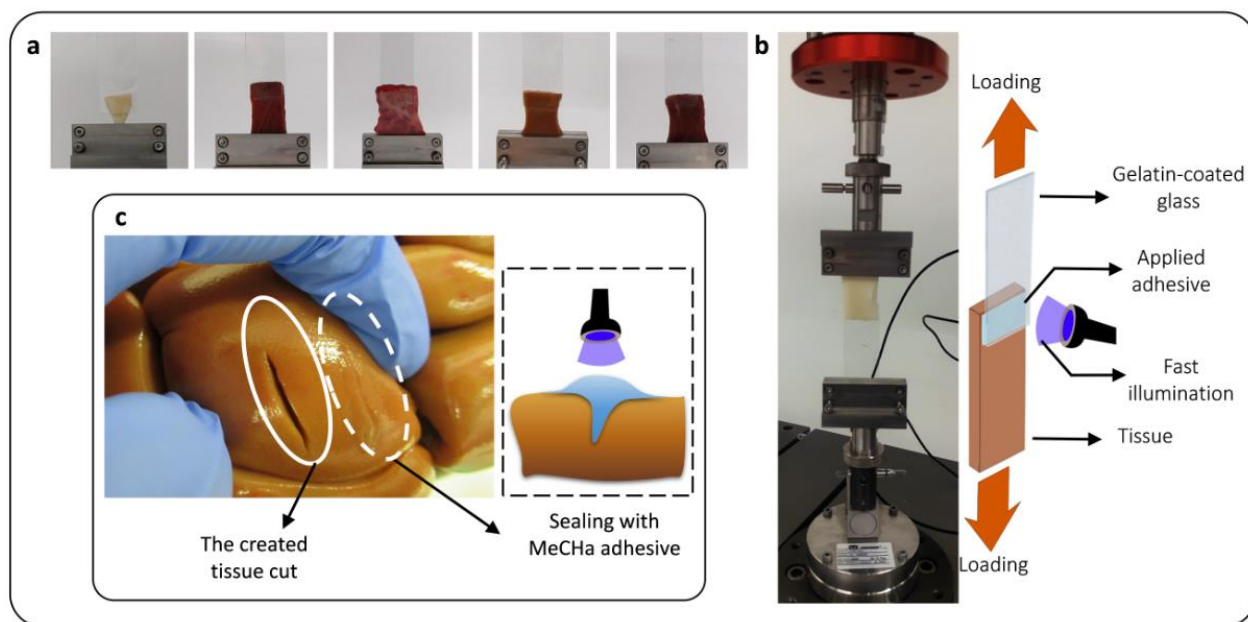
Supplementary Figure S5.6. (a, b) *In vitro* lap shear adhesion setup and schematic of the test procedure. The tests are conducted using bovine tissues including lateral meniscus, heart, lung lobe, kidney and liver (from left to right). The bioadhesives are applied to the overlap area between the tissue substrate and coated slide and subsequently photo-cured. (c) ex vivo demonstration for the sealing of soft tissue with the fast-curing bioadhesives (bovine kidney is shown as an example in this figure). A laceration is made on soft tissue, then the hydrogel precursor is applied on the tear and quickly polymerized with light. The adhesive precursor is prepared with longer backbone length (90-130 kDa) and high water content (88 wt%).
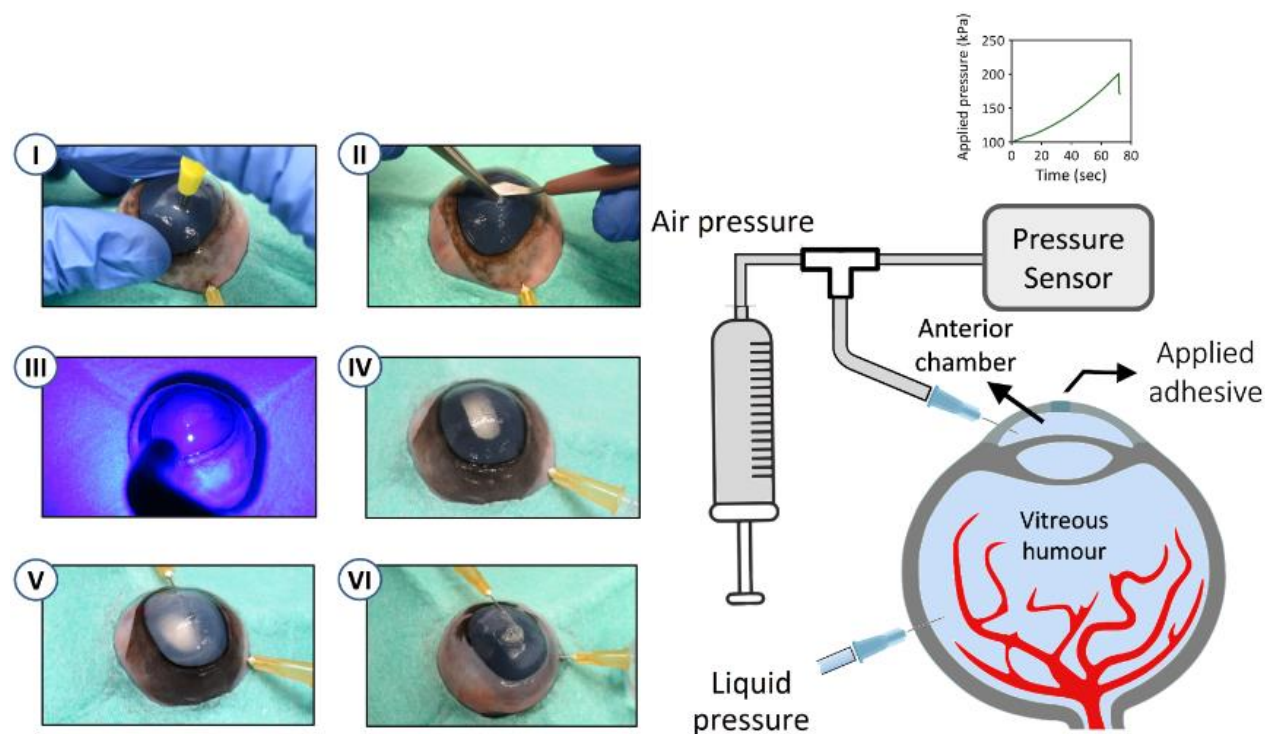
Supplementary Figure S5.7. *Ex vivo* test procedure for sealing of corneal defects in calf eyes and burst pressure measurement. The burst test included **(I)** creation of corneal defects by a 3 mm biopsy punch while the internal vitreous humour is pressurized, **(II)** removal of the stromal layer in the defect site, **(III)** injection of the bioadhesive in the defect with subsequent photo-curing process, **(IV)** cross-linked network and formation of the transparent hydrogel, **(V)** air pressurizing of the anterior chamber with a constant rate using a syringe pump and **(VI)** measuring the corresponding burst pressure of the bioadhesive by real time monitoring, and recoding of the maximum developed pressure as schematically shown on the right.
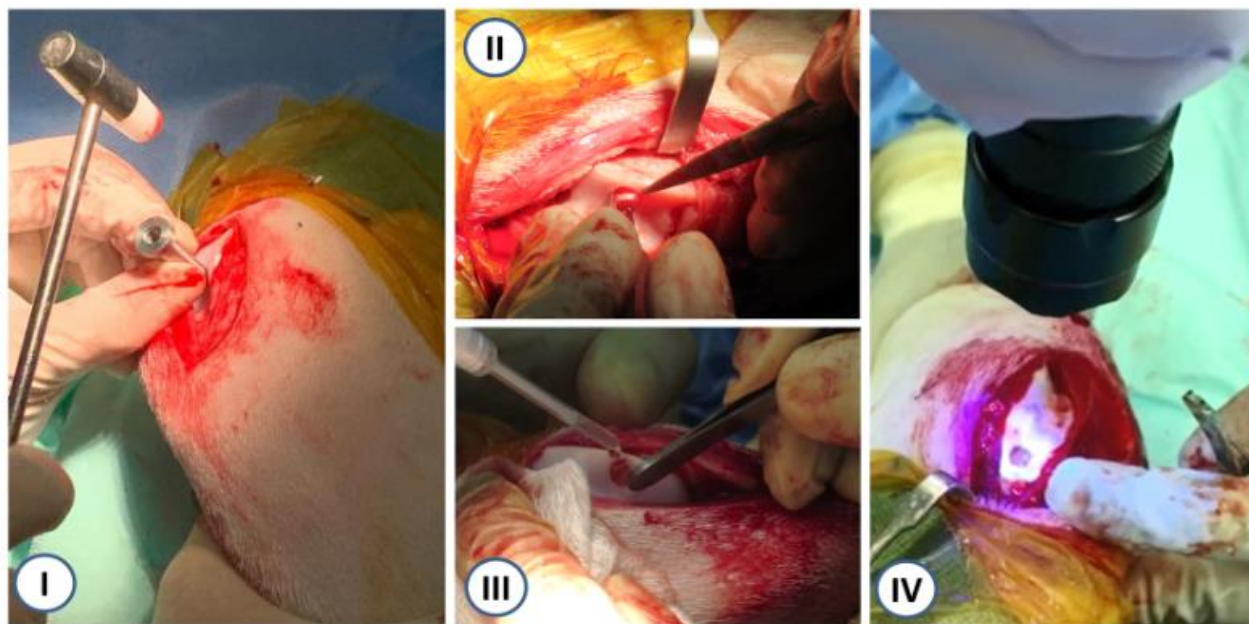
Supplementary Figure S5.8. *In vivo* implantation procedure of the bioadhesive hydrogel in cartilage defects in goat model: **(I)** creation of full-thickness cartilage defect in medial femoral groove in knee joint by a 5 mm chondrotome, **(II)** removal of the cartilage layer in the defect site, **(III)** filling the defect by applying sterilized bioadhesive precursor and **(IV)** immediate photo-curing in situ and formation of the adhesive scaffold. The control defects are left untreated.
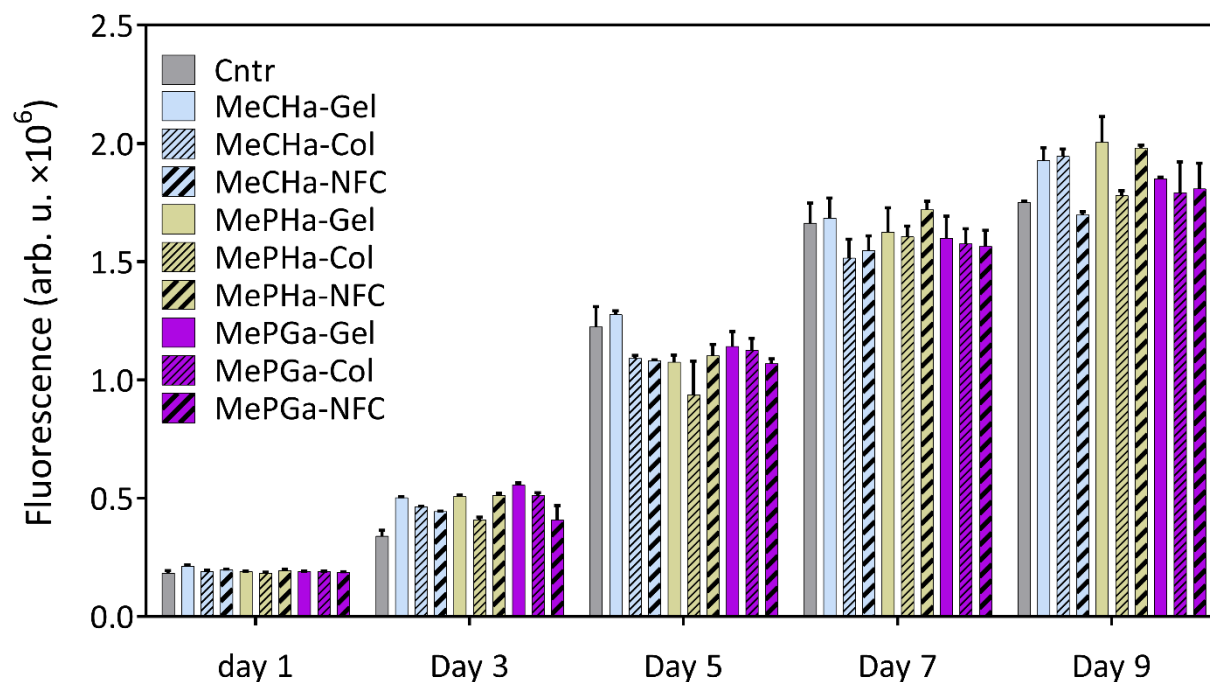
Supplementary Figure S5.9. Cytocompatibility test of the developed bioadhesives. No significant difference is observed in cells proliferation between the samples with the presence of SN and composite hydrogels and control group. The test is conducted for 9 days and the cells proliferation is assessed by the PrestoBlue^{TM} assay every 2 days. (n=3)
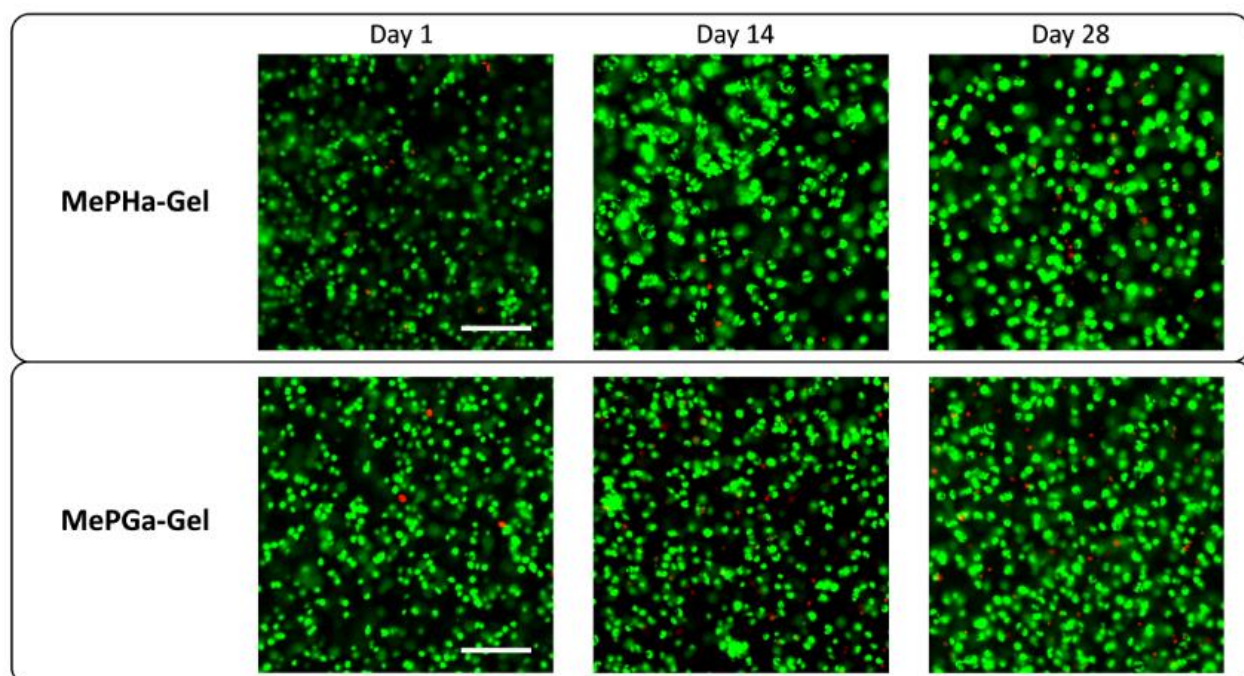
Supplementary Figure S5.10. Representative Live-Dead confocal images of bovine chondrocytes encapsulated in MePHa-Gel and MePGa-Gel at different time points after 3D encapsulation (day1, day 14 and day28). After 4 weeks of culture in chondrogenic medium, more than 80% cells remained alive in the hydrogel constructs. Live cells are imaged using the green stain, and dead cells are shown using the red stain. Samples are cut into two halves and images are taken from the cross-section. Results demonstrate that the cells are well distributed in the hydrogel constructs. Scale bars show 150 μm.
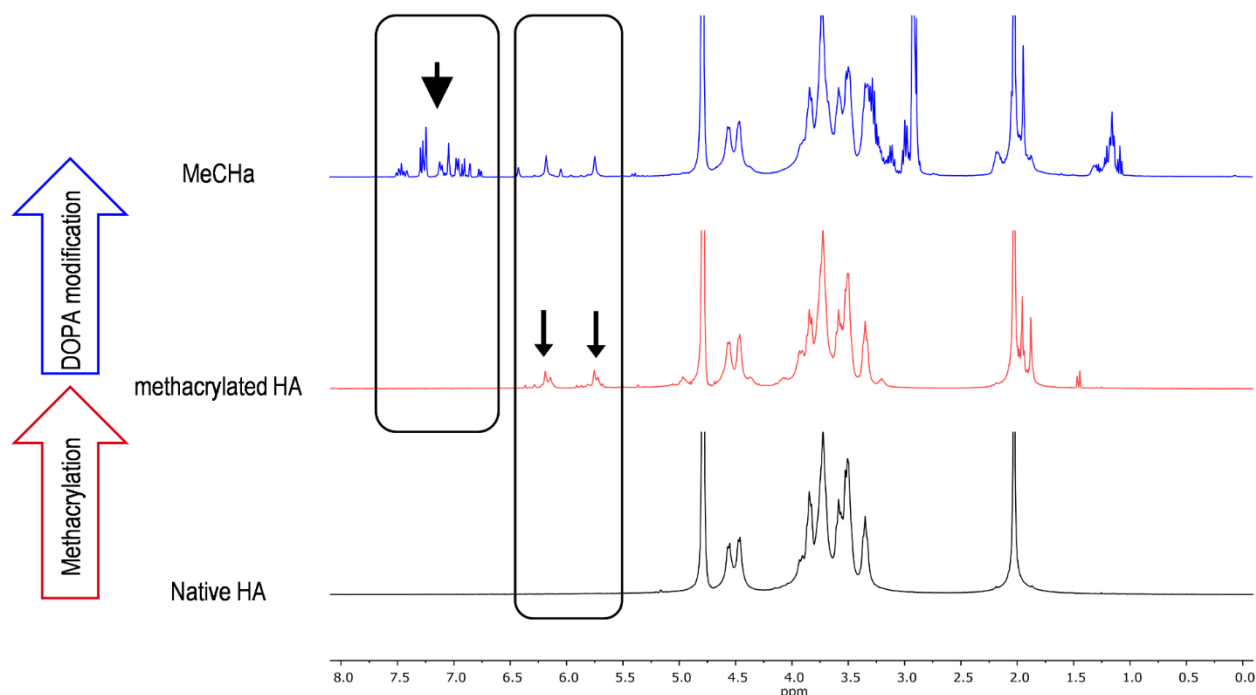
Supplementary Figure S5.11. Representative ^{1}H NMR spectra of the synthesized polymer during the two-step functionalization process (MeCHa). The hydroxyl group peaks are located at the chemical shift of 4.4-4.6 ppm. The degree of methacrylation was determined by integrating the peak area of the protons in the vinyl groups at the chemical shift of δ = 5.8 and δ = 6.25 ppm, relative to the carbohydrate methyl protons in the hyaluronic acid backbone at δ = 3.2-4.2 ppm. Each vinyl group peak corresponds to one proton and the peaks corresponding to the hyaluronic acid backbone correspond to 10 protons. In ^{1}H NMR spectrum of MeCHa, the multiplets at the chemical shifts of δ = 6.7-7 ppm in the MeCHa spectrum correspond to the protons in ortho and meta coupling position of the phenyl ring of Dopa and multiplet signals at δ = 2.87 ppm and δ = 3.22 ppm correspond to the protons of the aliphatic ethylene group. The grafting degree of Dopa per unit of hyaluronic acid was evaluated by comparison of the integrated peak areas of aromatic protons of Dopa at the chemical shift of 6.7-7.5 ppm. The sharp peak at the chemical shift of 4.79 ppm in the NMR spectra is associated with D$_2$O.

Supplementary Table S5.1. Bovine primers data used for gene expression analysis

Gene	Sequence	Primer content (nM)	Efficiency (%)
AGC-FWD	AGC AGC TCC AGG CCG CCT AT	250	98
AGC-REV	TGG CCT GTG GTG GCC AGA GT		
RPL13a-FWD	ATC CTG AAG CCC CAC TTC CA	250	94
RPL13a-REV	CCT TGC GTC TAC GGA TCT TGC		
COL2a-FWD	AAGAAGGCTCTGCTCATCCAGG	225	99
COL2a-REV	TAGTCTTGCCCCACTTACCGGT		
ADAMTS5- FWD	CTCCCATGACGATTCCAA	250	87
ADAMTS5- REV	AATGCTGGTGAGGATGGAAG		

Chapter 6 -   **Conclusions and Perspectives**

6.1 Conclusions

Strong adhesion of hydrogels to biological surfaces is of high interest in the biomedical field, and despite some claims found in previous researches, strong adhesion has never been demonstrated with truly injectable materials through a systematic strategy. Consequently, most recent advancements in highly adhesive hydrogel systems are focused on the preformed hydrogel patches and dry hydrogel tapes. In the past proposed highly adhesive strategies, the developed hydrogels are not intrinsically adhesive, but adhere to the targeted tissues thanks to specific developments such as chemically modifying the contacting surface for example.

We introduced in chapter 3 a composite double-network hydrogel through various toughening mechanisms. The bulk toughness and dissipative capability of the proposed design create a tough interface and high adhesion strength. However, it has some disadvantages which can impose limitations on the application of the hydrogel. Therefore, in Chapter 5, we proposed a universal framework for the design of injectable hydrogels that are intrinsically adhesive to various tissues surface. This is an innovative development which has potent implications in the way hydrogels are designed to reach high tissue adhesion, as it is not only a way towards synthesis of new biomaterials,

but a general design approach based on an understanding of adhesion mechanism. Therefore, our approach can even further be used to fabricate more advanced adhesive systems with novel performances.

Accordingly, we fabricated a family of original polymeric backbones (including methacrylated catechol-containing hyaluronic acid, MeCHa, methacrylated phosphoserine-containing hyaluronic acid, MePHa, and methacrylated phosphoserine-containing gelatin, MePGa) using a two-step functionalization process in order to make new hydrogels with available adhesive sites and the capability to form hybrid networks, as well as further enhancements through the fiber reinforcement for stronger synergetic effects. For example, in our MeCHa-Gel system, the oxidized catechol and the activated carboxyl groups in the MeCHa backbone can intrinsically form covalent bonds with primary amine groups in the tissue substrates with a control in the precursor synthesis and its aqueous environment. Simultaneously hybrid cross-linking mechanism between chemical groups, methacrylate sites and catechol sites form a network with enhanced bulk properties. The robust adhesion could be therefore achieved using the resulting synergy between interfacial chemistry and bulk mechanical properties. This is an innovative approach for injectable hydrogels not presented before. Moreover, the synergy effect is clearly demonstrated for the first time by varying the synthesis parameters (pH environment, curing condition, etc.) and with no extra surface treatment.

Both hydrogel-tissue interfacial and hydrogel bulk properties were analyzed for the adhesive hydrogel design. To propose a reliable biomaterial performance, the environmental parameters, gelation kinetics, water content, swelling ratio, long-term stability and biocompatibility should be taken into the design procedure, and controlled. Moreover, adhesion evaluation and interfacial characterization of hydrogel-tissue interface were performed through development of proper adhesion measurement methods. Based on the proposed design strategy, the biological and mechanical specifications as well as the specific adhesion targets were studied for development and tailoring of the injectable hydrogel. Evaluation of the bulk and adhesive properties and integration of hydrogel was performed through *ex vitro* and *in vivo* studies as well.

Such synergistically adhesive system, which is systematically presented in our work, is of high interest for the design of injectable hydrogels. The highly adhesive hydrogel presented in previous high impact researches are not able to exhibit such performance, as either the contacting surface of the preformed hydrogel (patches or tapes) or the host substrate requires to be chemically treated to be able to create interfacial bonds (i.e. no injectability and much less potential for *in situ* curing and

being minimally invasive). On the other hand, the past developments of injectable systems are not able to present a clear systematic strategy to achieve high adhesion, as they mostly rely on providing interfacial interactions, which by itself, cannot necessarily lead to a highly adhesive contact.

This thesis describes a paradigm shift towards the design of intrinsically adhesive networks for injectable hydrogels, and the observed adhesive, physicochemical and biomedical functions of the hydrogels, by engineering of original polymeric chains. The obtained hydrogel platform will be appealing for a broad range biomedical applications in biomaterials, tissue engineering and drug delivery.

6.2 Perspectives

Based on the proposed adhesive system and the obtained results, further studies could be proposed on the adhesive hydrogels in biomaterials field:

Investigation of fiber dimensions on adhesive performance for fiber-reinforced composite hydrogels: We demonstrated the role fiber-reinforcement on adhesive and physiochemical properties of different hydrogel systems. However, the analysis of dimensional parameters of fibers (i.e. fiber diameter, fiber length, aspect ratio, fibers orientation and distribution, surface chemistry and fiber modification, etc.) in the adhesive hydrogel system could be further studied and enhanced. A wide window of properties could be achieved by using different types of fibers as well as their structure and dimensions. Through using such an approach, the properties of composite hydrogels could be further tuned depending on various target applications. In particular, the biodegradable collagen fibers used in this work could be synthesized with different physical parameters and further studied to reach more advanced adhesive systems. Furthermore, development of adhesive hydrogel systems with gradient properties could be of high interest in the biomaterials field.

Photo-curing of adhesive hydrogels: The proposed hydrogel platform in this work is based on *in situ* network formation using photo-polymerization process. Therefore, the light penetration energy is a key parameter for proper polymerization of the adhesive hydrogels, and consequently, the resulting adhesive and physicochemical performance. This could be considered as a limitation for the hydrogel applications where a proper light exposure cannot be achieved. Such limitation can be the result of either:

(a) limited ultraviolet and visible light penetration inside biological tissues (for minimally-invasive applications such as gluing large pieces of tissues which needs to be in close contact, etc.) or

(b) insufficient light energy for full polymerization of a hydrogel bulk which leads to limited polymerization depth.

Therefore, further studies on photo-curing of adhesive hydrogels with novel methods is of particular interest. In this context, besides development of customized minimally-invasive medical devices, photo-polymerization using high penetration light irradiation could be a promising approach in this research field. It could be used for efficient curing of novel adhesive hydrogels from outside of tissue (or body) in various biomedical applications.

Towards clinical applications: One of the main goals in this research is to move towards a clinically translatable solution through an interdisciplinary study. The first part of this work was devoted to characterize and understand the governing physical phenomena behind the interfacial and toughening mechanisms. A bio-inspired design strategy was accordingly proposed for an adhesive hydrogel and implemented. Moreover, the adhesive system presents not only enhanced adhesive properties but other properties such as controllable swelling ratio, biocompatibility and processability. Therefore, the proposed hydrogel family demonstrates high potential to be used in different translational studies, as well as for further novel sets of applications in diverse fields including biomedicine, advanced degradable devices flexible electronics and soft robotics.

Appendix 1 - **Numerical Analysis**

As mentioned in Chapter 1 and 2, insufficient adhesion and bulk performance of high water containing hydrogels may impose serious limitations on their potential applications. Therefore, analysis of the contributory factors in adhesive capability of hydrogels and their synergetic effects could be of high importance especially for further material development. It was discussed in Chapter 3 that tough hydrogels have shown a marked potential to be used as adhesive biomaterials in the load-bearing situations.

Consequently, the analysis of adhesion and the contributory parameters for the adhesive systems could be highly beneficial. In this chapter, a finite-element model is developed to simulate the adhesion of hydrogels bonded on a defined surface with ABAQUS/Explicit. The bulk properties of the adhesive hydrogels, including stiffness and effective dissipative capability, as well as the interface quality and damage resistance in the hydrogel-tissue systems will be analyzed.

7.1 Objective

The goal of this study is to develop a finite-element model to perform a parametric study and analyze the contributory factors in hydrogel-tissue adhesion. Moreover, based on the preliminary evaluation, further material developments can be proposed and finally better understanding of the leading factors can be achieved.

The general approach for the finite-element analysis of hydrogel-tissue adhesion is demonstrated in Figure 7.1.
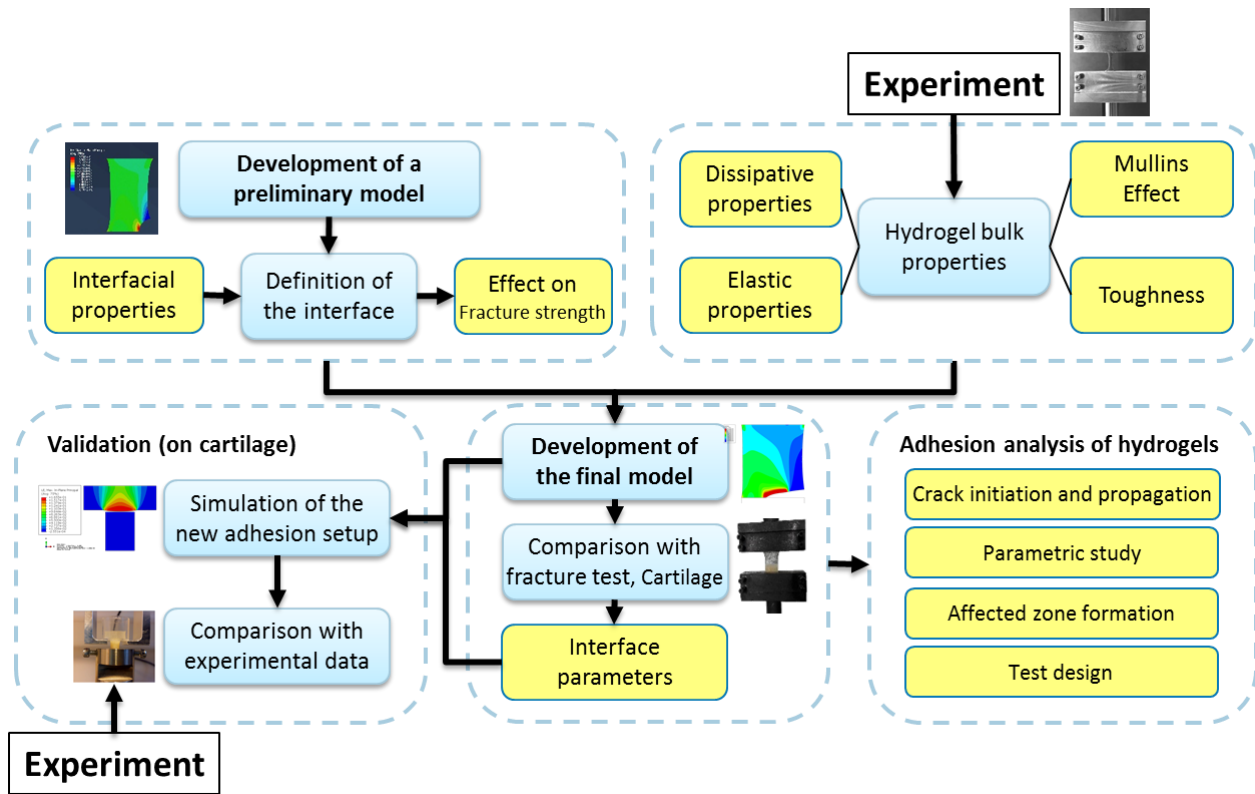
Figure 7.1. The approach for the numerical analysis of hydrogel-tissue adhesion.

The total interfacial toughness can be described as the sum of the intrinsic work of adhesion between hydrogel and tissue and the mechanical energy dissipated around the interface [24]. The intrinsic work of adhesion is the energy needed for breakage of the interfacial interactions between the hydrogel and the tissue surface (see Chapter 3 for more details on different mechanisms). It should be noted that there are also some contributions from friction on the interface (Figure 7.2).
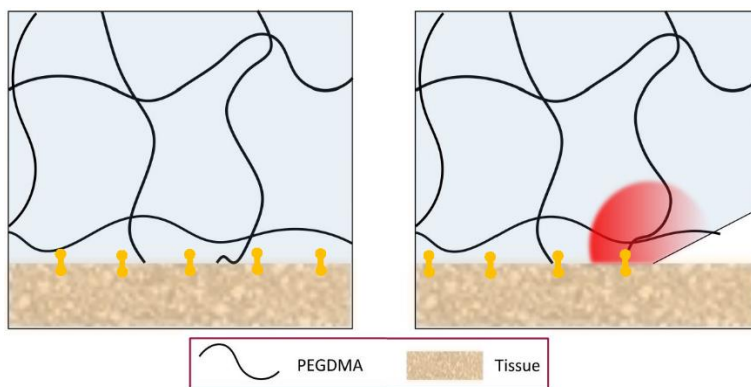
Figure 7.2. Representation of the adhesion of a single-network hydrogel and tissue, red: affected zone and yellow: interface interactions.

The developed fracture test for hydrogel specimens bonded to a layer of cartilage was used to obtain the experimental data (see Chapter 3). Different types of hydrogel (SN, DN, fiber-reinforced and fiber-reinforced DN hydrogels) were tested on bovine articular cartilage. A mould of 30×15×2 mm is used to prepare the specimens to be tested. A 15×15×2 mm sample of cartilage-on-bone is placed in the mould. Before the test, a notch of 4 mm was made between the hydrogel and the layer of cartilage. The fraction tests were performed using a Zwick servo-hydraulic testing machine and we obtained load-displacement curves for the different hydrogels used (Figure 7.3).
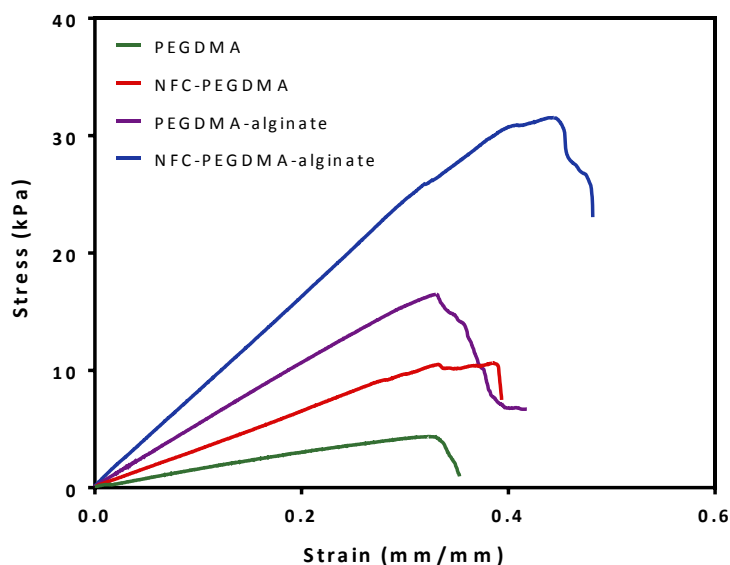
Figure 7.3. The stress-strain curves for the fracture tests of different hydrogels adhered to articular cartilage.

7.2 FE model

A finite-element model was used to simulate the adhesion test of hydrogels bonded on solid tissue substrates. The numerical simulation was carried out with ABAQUS/Explicit. The one-term Ogden hyperelastic material model and Mullins effect were employed to model the elastic properties and energy dissipation of the hydrogel. The cohesive layer at the interface was modeled as thin layer, characterized by a triangular traction-separation law with maximum strength and maximum separation distance. The interface was uniformly discretized with very fine mesh size and mesh insensitivity verification of the model was performed.

7.2.1 2D model

The model includes three parts:

- Hydrogel was defined as an hyperelastic material (15×15 mm);
- Hydrogel-tissue interface was defined as layer of cohesive elements (11×0.01 mm). It follows a damage law representing the quality of interaction between the hydrogel and the tissue surfaces [4]. The length of the interface layer corresponds to a 4 mm notch as presented in section 3.2.4.
- Tissue was defined as a rigid body (15×15 mm), as the tissue deformation is negligible in comparison to the deformation observed in the hydrogel.
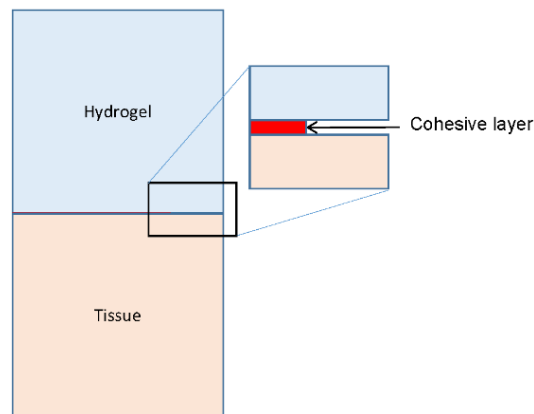
Figure 7.4. The 2D model.

7.3 Constitutive laws

7.3.1 Hydrogel model

Due to the large deformation in hydrogel, the elastic properties are modeled as an Ogden hyperelastic material. The model principal is based on using a strain energy density function. This material model is often used to describe the behavior of polymeric materials due to nonlinear deformation with respect to the applied load. Since we use a two-dimensional model the one-term Ogden model can be expressed as:

$$U_{ela} = \frac{2\mu}{\alpha^2}(\lambda_1^\alpha + \lambda_2^\alpha + \lambda_3^\alpha - 3)$$

where U_{ela} is the strain energy density, λ_i the i_{th} principal stretch, μ the shear modulus, and α the Ogden parameter. The parameters of the model were obtained by fitting the model to experimental data from mechanical tests.

7.3.2 Hydrogel-tissue interface definition

The interface is modeled as a thin cohesive layer with COH2D element. The interface is characterized by a triangular traction-separation law with maximum strength and maximum separation distance. The triangle cohesive interface models the interactions between hydrogel and tissue interface, which corresponds to the intrinsic work of adhesion. The intrinsic work of adhesion corresponds to the area under the curve as demonstrated in Figure 7.5.
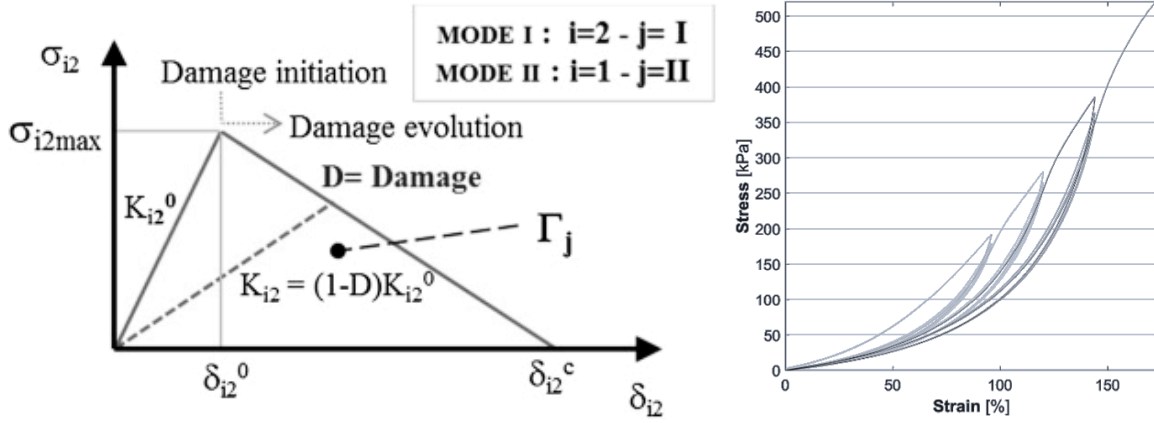
Figure 7.5. Traction-separation law followed by each element in the cohesive layer **(left)** and Mullins effect **(right)**; the one-term Ogden hyperelastic material model and Mullins effect were employed to model the elastic properties and energy dissipation of the hydrogel.

The hydrogel-tissue interface is defined with a thickness of 0.01 mm. Each cohesive element follows an increasing stress until it reaches a specified maximal stress σ_{max} coupled with a corresponding deformation (separation). Once the maximal stress is reached, the element starts to degrade. After reaching a maximal separation δ_{max}, the element disappears, showing the crack propagation between the hydrogel and the tissue.

7.4 FE on ABAQUS/Explicit

7.4.1 Assembly interactions

A tie interaction was used between the bottom surface of the hydrogel and the top surface of the cohesive layer as well as between the bottom surface of the cohesive layer and the top surface of the rigid body.

To prevent any interference between the parts, a surface-to-surface contact is defined between the bottom surface of the hydrogel and the top surface of the tissue.

7.4.2 Mesh properties

The hydrogel model is discretized by using a 4-nodes bilinear plane stress quadrilateral, reduced integration, hourglass control (CPS4R) element type. Considering the thin geometry that inspires the 2D FE model, a plane stress condition is employed. The Poisson's ratio of the hydrogel was set to give approximate incompressibility ($v = 0.49$). The meshing uses a free quad-dominated technique as shown in figure 7.6. The element size is refined at the bottom (0.1 mm) to match the mesh size of the cohesive layer.

The layer of the cohesive elements is defined using a 4-node two-dimensional element (COH2D) element type, which is specific to the cohesive element definition. The meshing is done by following a structured quad technique. As presented in the previous section, the thin layer is a juxtaposition of elements and is uniformly discretized with a fine mesh (0.1 mm). The part that models the tissue uses a discrete rigid: 2-node-2-D linear rigid link (R2D2) element type.
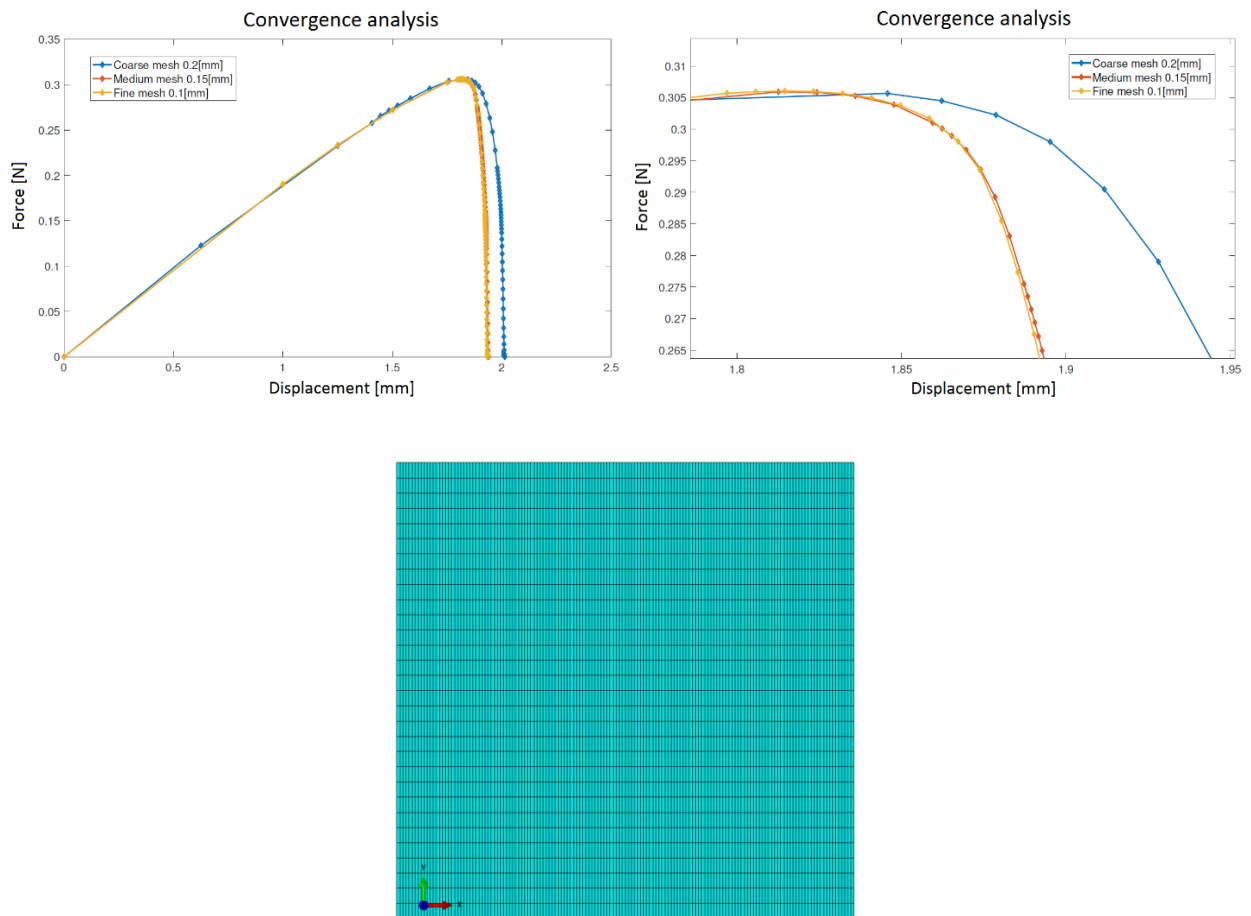
Figure 7.6. convergence analysis, zoom on the graph **(top)** and meshing of the hydrogel part in the 2D FE model **(bottom)**.

To verify the insensitivity of the mesh, a convergence analysis was performed by extracting the load-displacement for different mesh sizes. Three mesh sizes were used: a coarse mesh (0.2 mm), a medium mesh (0.15 mm) and a fine mesh (0.1 mm). As shown in figure 7.6, the error in the load displacement curve between a medium mesh and a fine mesh is almost negligible. Therefore, a medium mesh was selected to be sufficiently insensitive for the simulation. However, since the study is performed on a 2D FE model, the computational time remains small in both cases, allowing the use of a finer mesh.

7.5 Results and Discussion

7.5.1 Strain distribution

The distribution of strain is shown in Figure 7.7 during the crack initiation and propagation. We can observe that there is a stress concentration at the crack tip with higher strain values, built up around it in the hydrogel. The strain values in the affected zone increase until the crack starts to propagate. In fact, the stress is transferred to the cohesive elements, and once the intrinsic energy is reached, the cohesive elements disappear, thus simulating the crack propagation. When crack starts to advance, the size of the affected zone with high strain values remains the same until complete failure.
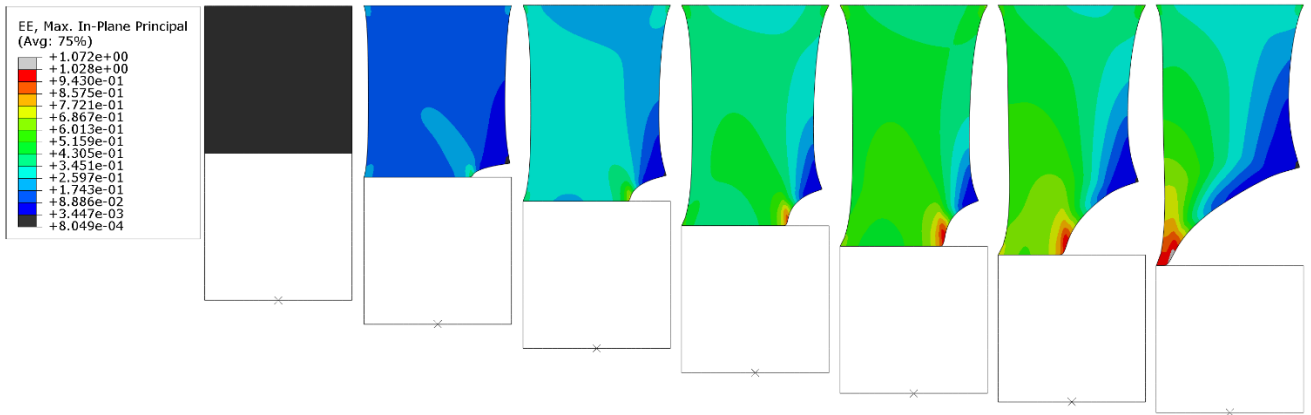
Figure 7.7. Snapshots of the simulation for intrinsic work of adhesion of 120 N.m.

The affected zone was studied for various intrinsic work of adhesion. By improving the interface quality between the hydrogel and the tissue substrate, we observe an increase in the size of the affected zone around the crack tip. Figure 7.8 demonstrates fracture tests for three different intrinsic energies, showing the evolution of the affected zones subjected to strains of 90-110% (red and orange colors in the figure). As the hydrogel-tissue interface requires more energy before the crack propagation, the hydrogel can undergo larger deformation and consequently transfer the stress to the bulk material. Moreover, the shape of crack openings indicates the critical role of interfacial energy in local deformation of the gel. It should be noted that the same dissipation of the hydrogel is used for the three simulations.
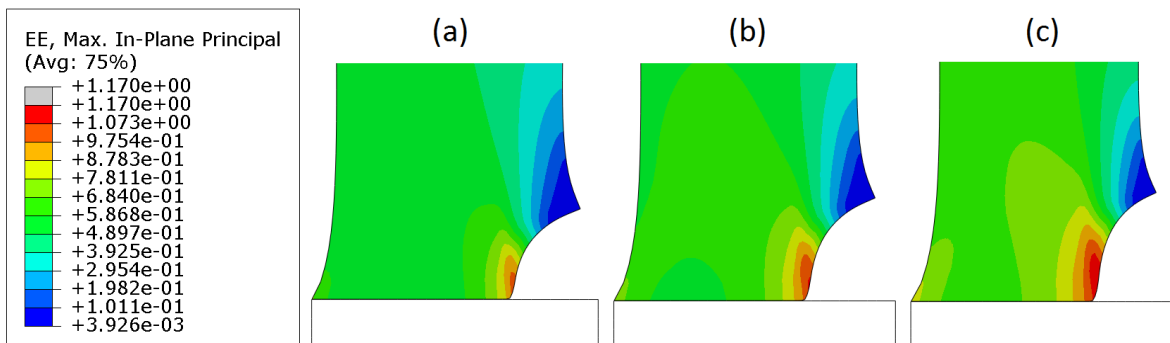
Figure 7.8. Compilation of three different simulations showing the affected zone at the critical point of crack initiation. The strain distributions are illustrated for the intrinsic work of adhesion of (a) 120 N.m, (b) 150 N.m and (c) 200 N.m.

7.5.2 Load-displacement

Recordings of the reaction force in combination with the displacement of the tissue during the simulation allows us to obtain load-displacement curves for each simulation, which are characterized by a triangular shape as a result of the loading until a maximal force is reached before the crack propagates. Figure 7.9 represents the different strain distributions along with the load-displacement curve and illustrates the different steps of simulation.
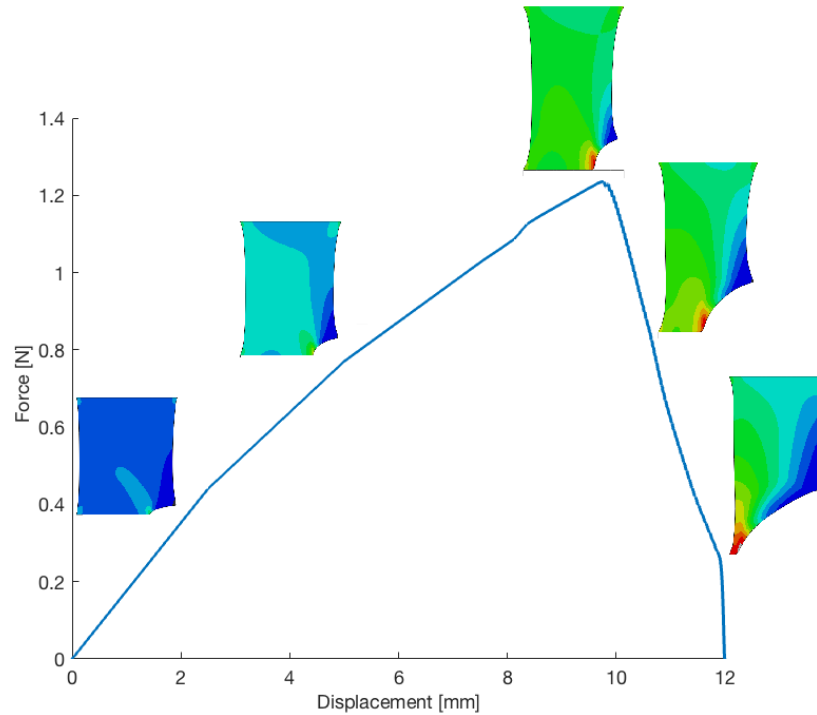
Figure 7.9. Strain distribution in hydrogel during the hydrogel detachment for an intrinsic work of adhesion of 120 N.m.

The maximal load and deformation increase at higher intrinsic energy (Figure 7.10). There is a critical load before crack initiation occurs. With a higher interface quality, more energy is required for the propagation while the hydrogels exhibit the same level of dissipation. Indeed, the fracture is brittle for a low intrinsic work of adhesion whereas it is more resilient for a higher intrinsic work.

The crack initiation energy corresponds to the area under the load-displacement curve during the hydrogel loading, i.e. from the point the deformation starts until the maximal load is reached. The propagation energy corresponds to the area under the curve during the crack propagation, i.e. the amount of energy required for crack advancing from the crack initiation until total failure of adhesion. Figure 7.10 shows the evolution of initiation and propagation energies at various intrinsic work of adhesion. Initiation energy corresponds to the surface area under force-displacement curve before crack advancing. Accordingly, the propagation energy, which corresponds to the surface area under force-displacement curve after crack advancing, is much noticeable at higher values of intrinsic work of adhesion due to larger local deformation of the hydrogel.
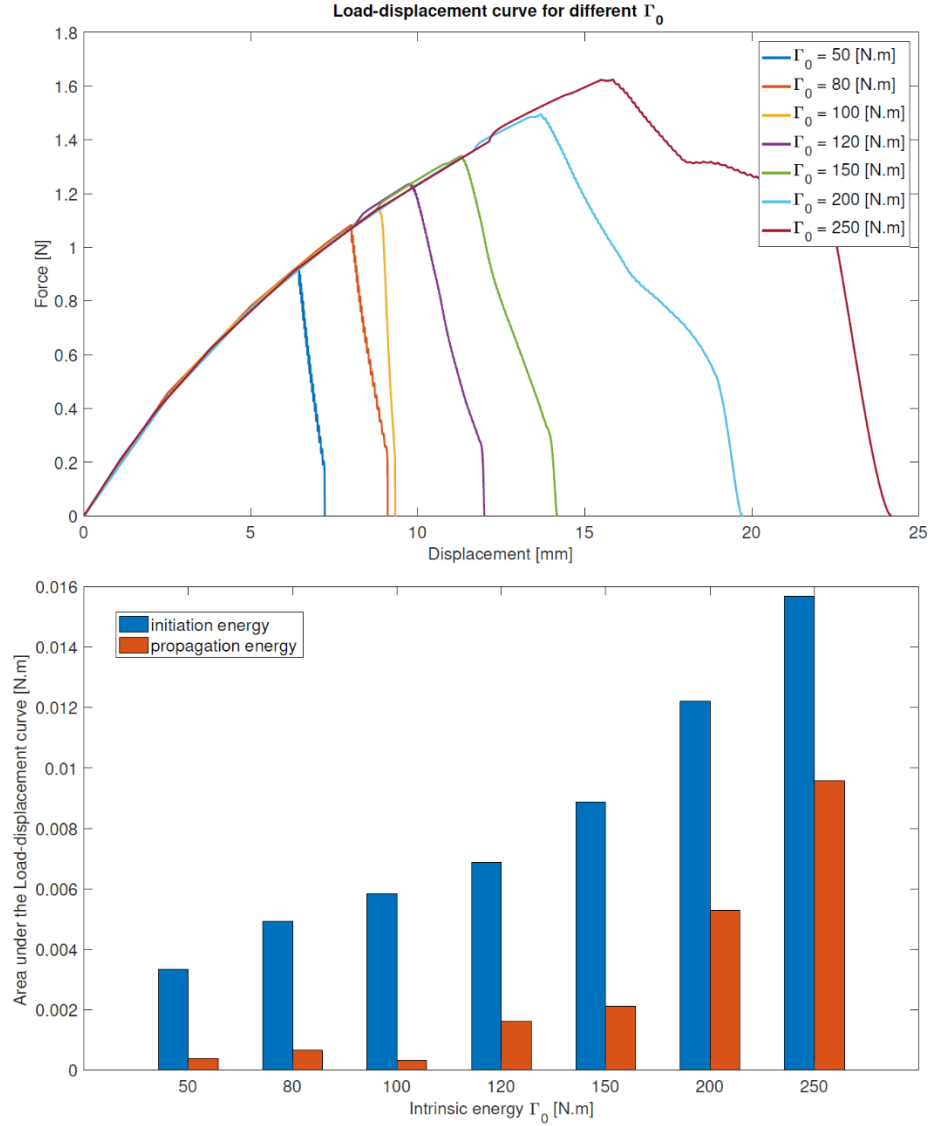
Figure 7.10. (top) Load displacement curves for different intrinsic works of adhesion and (bottom) initiation and propagation energy extracted from the area under the load-displacement curves.

Taking into account the amount of energy required to propagate the crack and the surface area of fracture, an approximation of the energy release rate (ERR) can be computed as follows;

$$\text{ERR} \ = \ \frac{\text{Propagation energy}}{\text{Surface area fracture}}$$

The ERR corresponds to the fracture toughness of the hydrogel-tissue interface. Figure 7.11 shows the ERR in function of the interface quality. The trend of the ERR is represented by a second order polynomial fitting. The trend expresses the adhesive failure by quality of interface, which increases

and crosses the cohesive failure threshold where the fracture would occur in the hydrogel. Indeed, depending on the hydrogel-tissue design, the limiting factor of failure can either be the interface or the bulk properties.
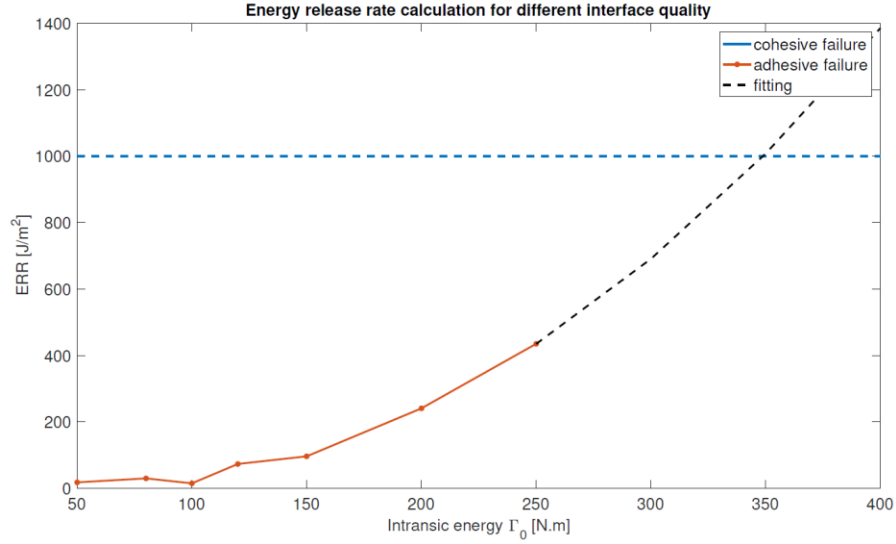
Figure 7.11. Energy release rate in function of the intrinsic work of adhesion. Note that the cohesive failure threshold is set as an example and does not necessarily correspond to the actual fracture toughness of hydrogel used in the simulation.

7.5.3 FE model with dissipation capability employment

From the experimental data obtained for Mullins effect and tensile tests of the four different hydrogels used in this study, we defined the material properties of each hydrogel in the developed FE model. Therefore, we are able to estimate the intrinsic work of adhesion in hydrogel-cartilage interface for each hydrogel, using the experimental data obtained from the developed hydrogel-tissue fracture tests. Thereafter, the role of various parameters such as hydrogel dissipation around the interface, and formation and size of the affected zone can be analyzed for the adhesive systems.

Figure 7.12 reports the affected zone around the interface of different hydrogels adhered to cartilage.
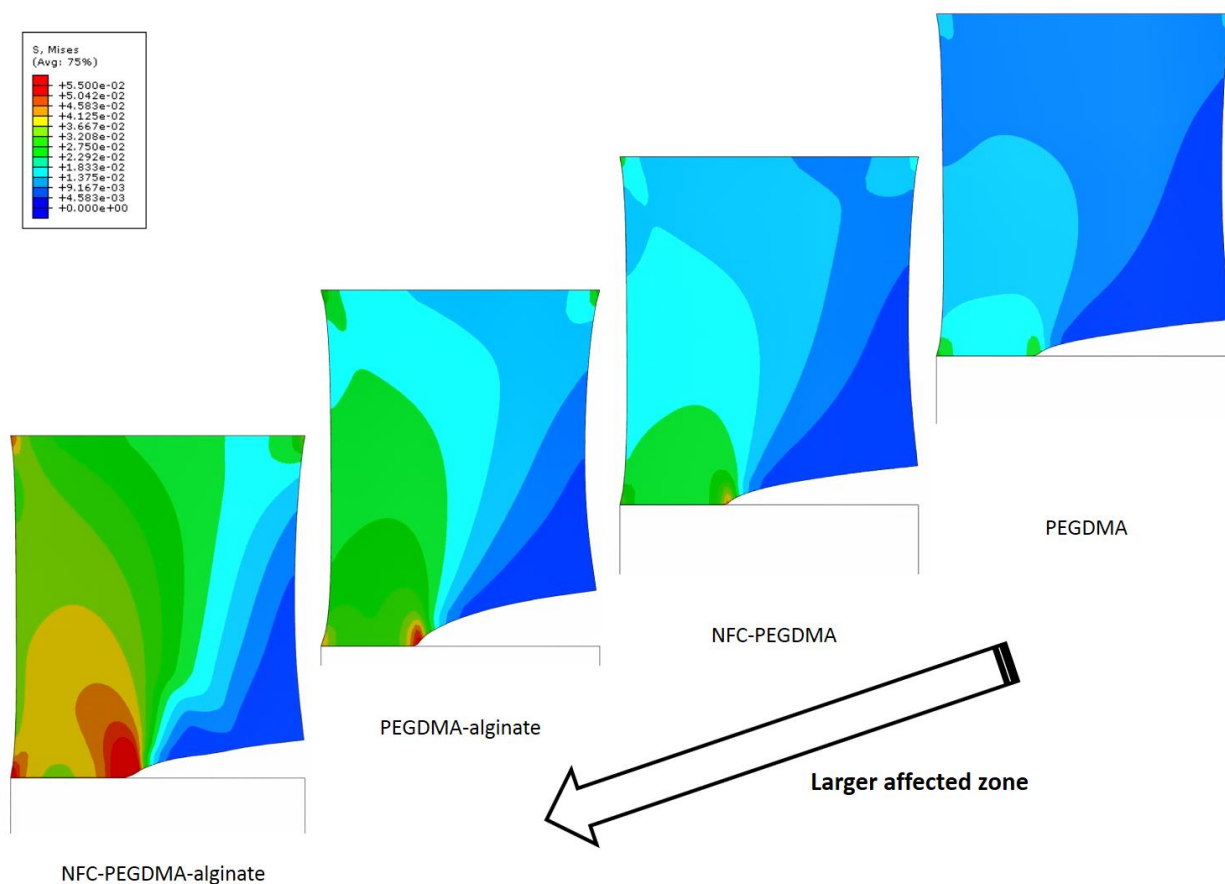
Figure 7.12. Formation of the affected zone around the interface during the crack advancing, for SN, DN, fiber-reinforced and fiber-reinforced DN hydrogels.

Figure 7.13 reports the energy dissipation per unit area during hydrogels detachment. It is clearly seen that the composite double-network hydrogel dissipates much energy around the crack opening as a result of the capability for high dissipation and stress transfer. This is in line with our experimental observations, as employing various toughening mechanisms in hydrogel design can provide protection for interfacial interactions though the energy transfer over a larger region. The larger affected zone of the composite DN hydrogel in Figure 7.12 also indicates a better interfacial toughness through higher stress values around the crack.
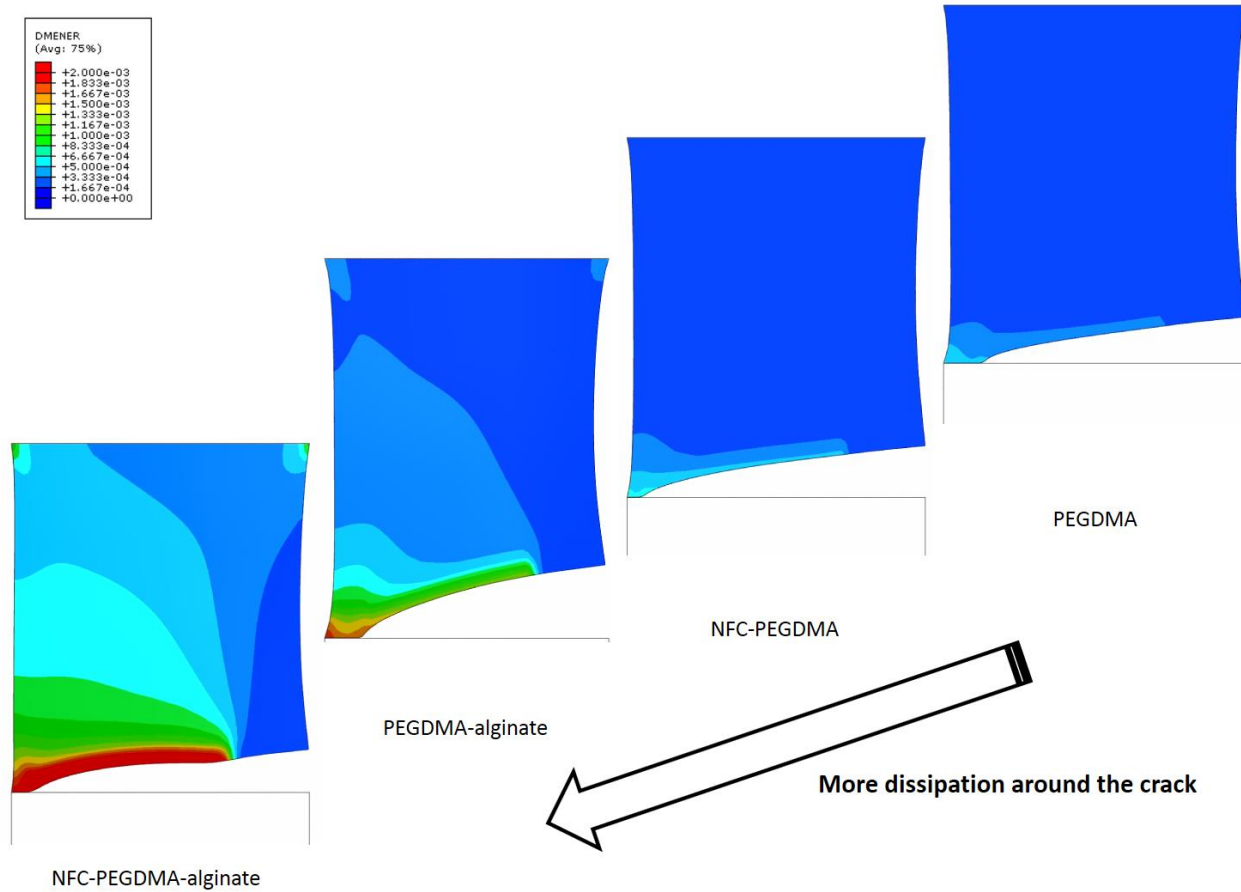
Figure 7.13. Energy dissipation per unit area during hydrogel detachment, for SN, DN, fiber-reinforced and fiber-reinforced DN hydrogels.

Comparison between the obtained pattern for the affected zone from the experimental fracture test and the simulation shows a good agreement (Figure 7.14). Due to the presence of the crack notch in both experiment and FE model, the diagonal going from the crack tip to the opposite clamped corner of the hydrogel shows the direction of the affected zone which is around 45 ˚.
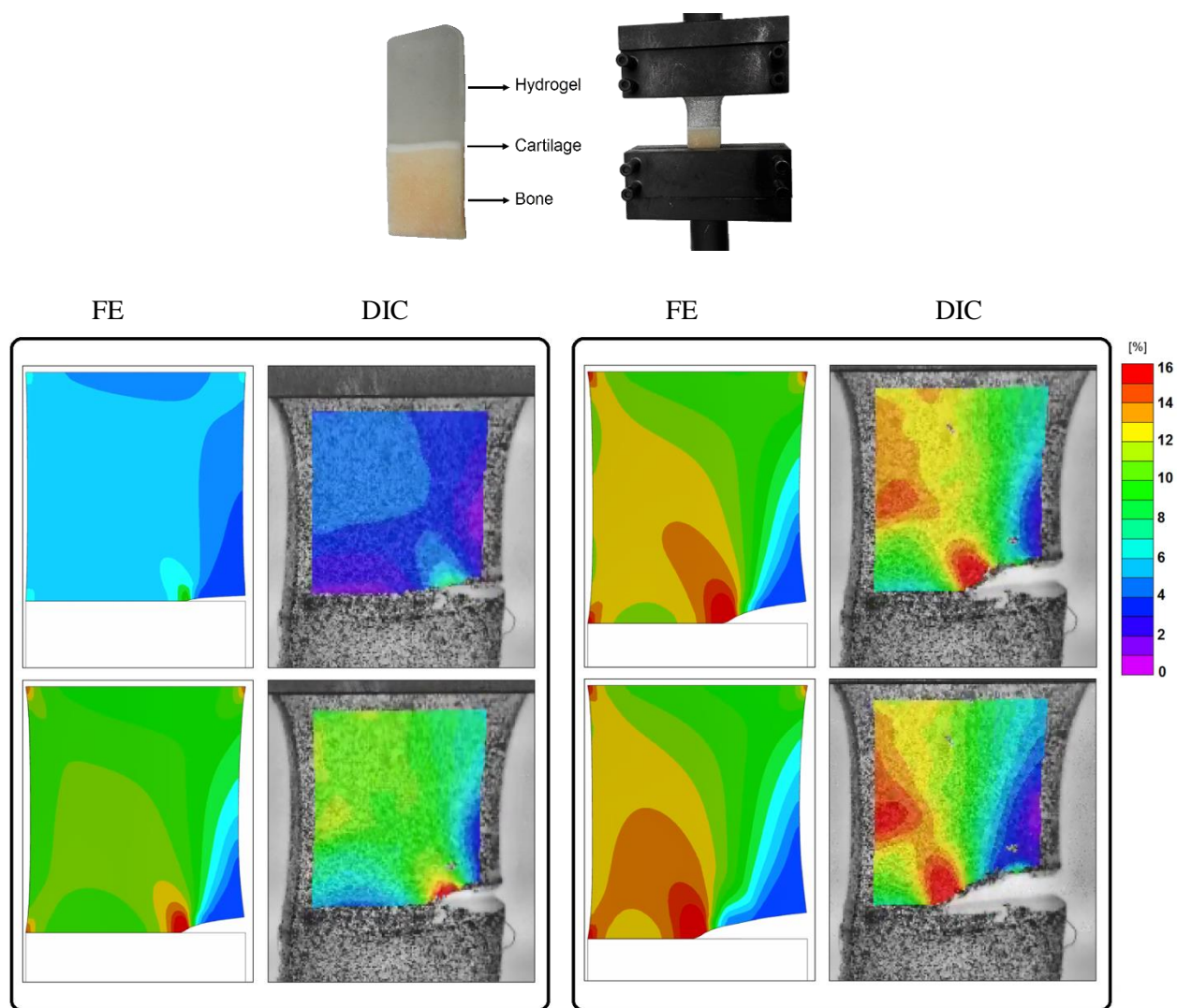
Figure 7.14. Strain distribution during crack advancing numerical simulation (FE) and Digital Image Correlation (DIC), for the dissipative hydrogels.

7.6 Conclusions

The objective of this work is to propose hydrogels with tunable adhesive and mechanical properties for biomedical applications. Therefore, understanding of adhesion phenomenon, the contributory parameters for highly adhesive systems, characterization and proposing a material design strategy need to be studied. With the experimental observations, numerical analysis can be used to provide new insights on adhesion performance of a hydrogel-tissue contact. We observed that the total interfacial toughness is not simply defined by the sum of the intrinsic work of adhesion and the

mechanical energy dissipated in the hydrogel but rather by a synergetic combination of the contributory parameters. The simulation during the study was limited by convergence errors when large deformations were applied. By optimizing the mesh for larger strains, the scope of results could be augmented and therefore we could obtain a larger range of data for higher intrinsic work of adhesion.

Appendix 2 -   **Observations for AFM analysis**

Figure 8.1-4 show a typical Force-Separation curve during the analysis, maximum pull-off force, total pull-off energy of hydrogel-cartilage detachment, and total pull-off length during cantilever retraction for four different hydrogels, respectively.
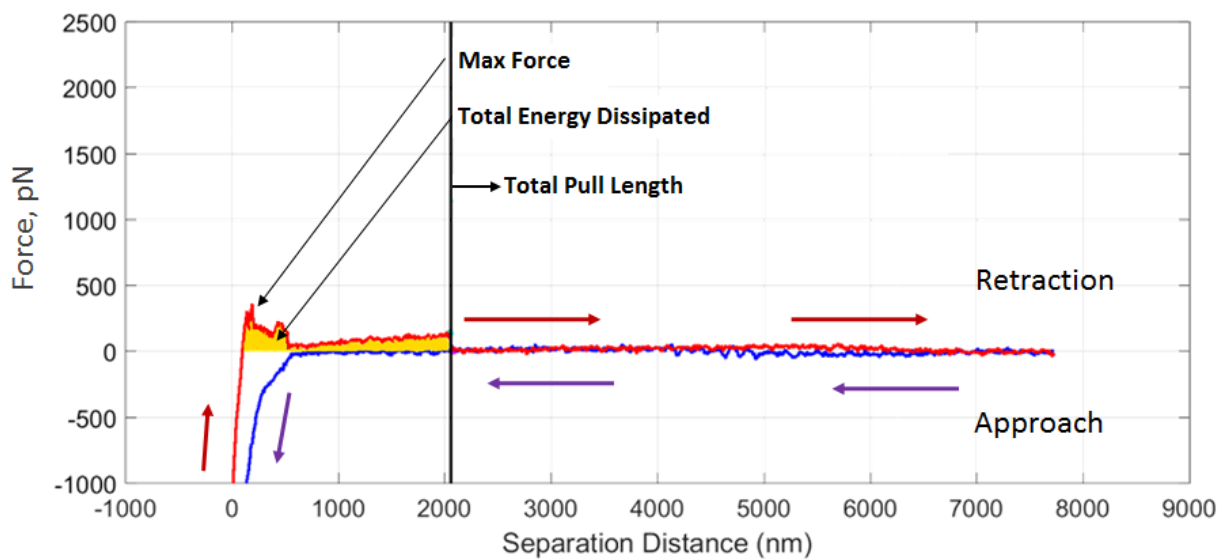
Figure 8.1. A typical Force-Separation curve during cantilever approach to and retraction from hydrogel surface. For each single measurement, maximum force, total energy and total pull length are measured.
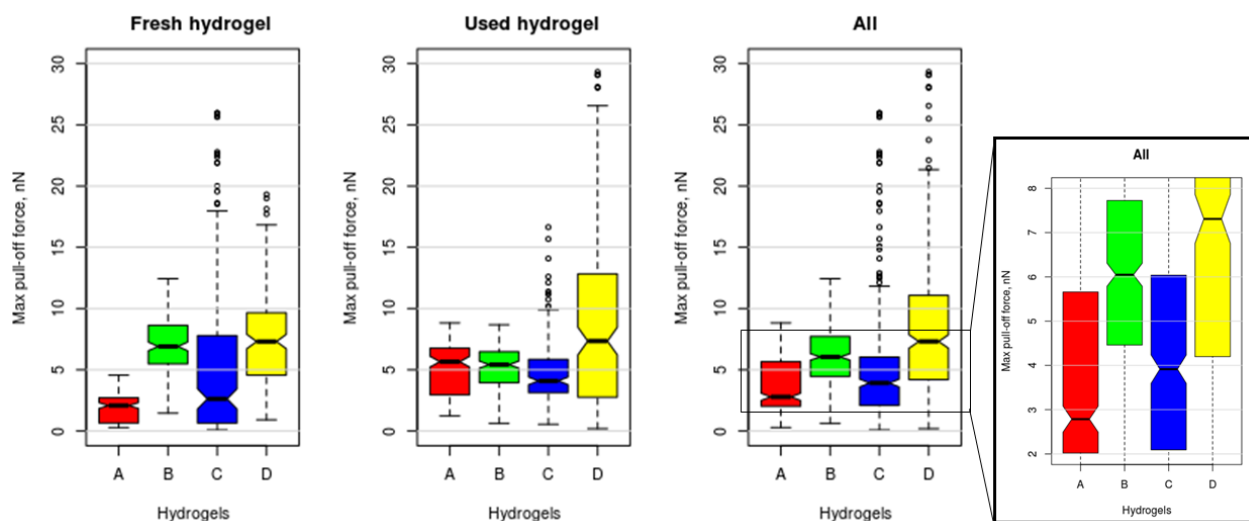
Figure 8.2. Maximum pull-off force during cantilever retraction for four different hydrogels: single-network PEGDMA (red), DN PEGDMA-alginate hydrogel (green), NFC-reinforced PEGDMA (blue) and NFC-reinforced PEGDMA-alginate (yellow).
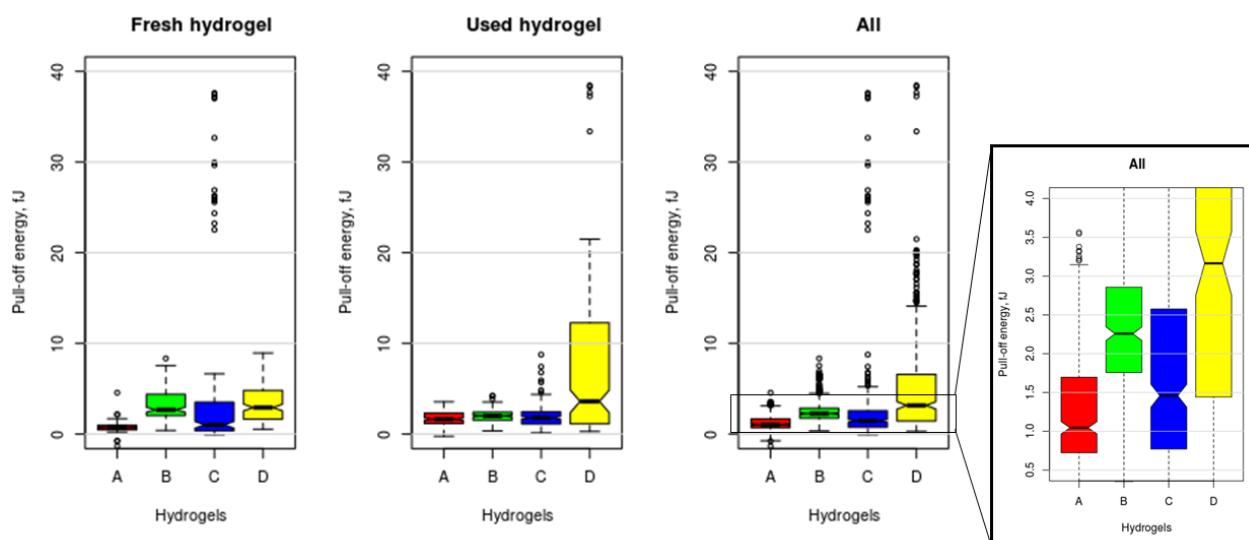
Figure 8.3. Total pull-off energy of hydrogel-cartilage detachment for four different hydrogels: single-network (red), DN (green), fiber-reinforced (blue) and fiber-reinforced DN hydrogel (yellow).
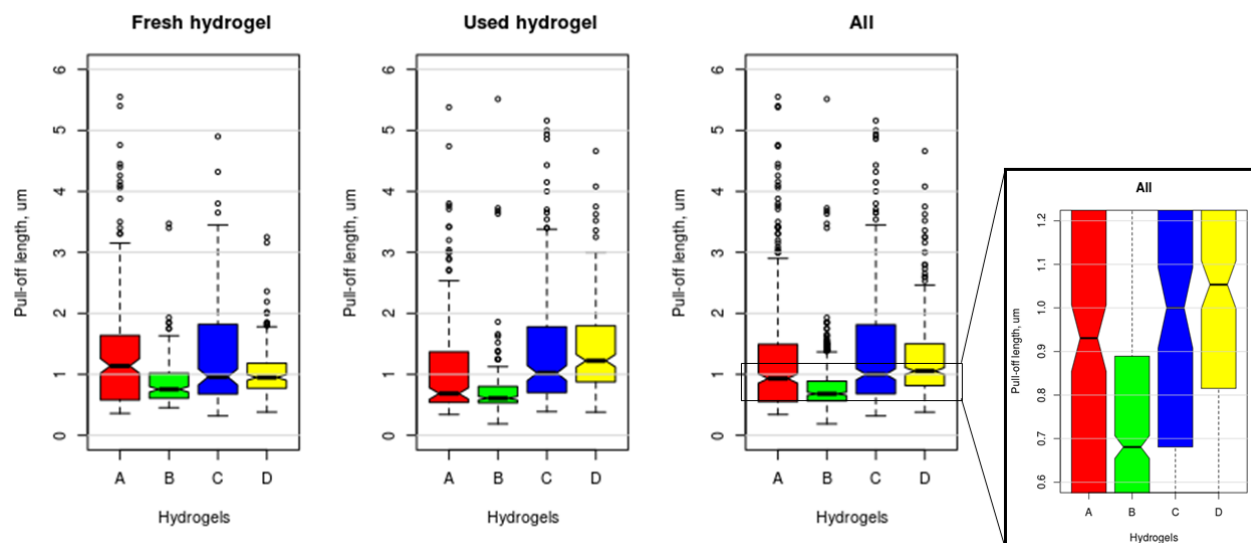
Figure 8.4. Total pull-off length during cantilever retraction for four different hydrogels: single-network (red), DN (green), fiber-reinforced (blue) and fiber-reinforced DN hydrogel (yellow).

References

1. Han, L., et al., *Tough, self-healable and tissue-adhesive hydrogel with tunable multifunctionality.* NPG Asia Materials, 2017. **9**(4): p. e372.
2. Ahsan, T. and R.L. Sah, *Biomechanics of integrative cartilage repair.* Osteoarthritis and cartilage, 1999. **7**(1): p. 29-40.
3. Prausnitz, M.R. and R. Langer, *Transdermal drug delivery.* Nature biotechnology, 2008. **26**(11): p. 1261.
4. Feiner, R., et al., *Engineered hybrid cardiac patches with multifunctional electronics for online monitoring and regulation of tissue function.* Nature materials, 2016. **15**(6): p. 679.
5. Annabi, N., et al., *Elastic sealants for surgical applications.* European Journal of Pharmaceutics and Biopharmaceutics, 2015. **95**: p. 27-39.
6. Sierra, D.H., *Fibrin sealant adhesive systems: a review of their chemistry, material properties and clinical applications.* Journal of Biomaterials Applications, 1993. **7**(4): p. 309-352.
7. Vinters, H., et al, *The histotoxicity of cyanoacrylates. A selective review.* Neuroradiology, 1985. **27**: p. 279-91.
8. Rose, S., et al., *Nanoparticle solutions as adhesives for gels and biological tissues.* Nature, 2014. **505**(7483): p. 382.
9. Roy, C.K., et al., *Self-Adjustable Adhesion of Polyampholyte Hydrogels.* Advanced materials, 2015. **27**(45): p. 7344-7348.
10. Sudre, G., et al., *Reversible adhesion between a hydrogel and a polymer brush.* Soft Matter, 2012. **8**(31): p. 8184-8193.
11. Okada, M., et al., *Biocompatible nanostructured solid adhesives for biological soft tissues.* Acta biomaterialia, 2017. **57**: p. 404-413.
12. Cui, X., et al., *Direct human cartilage repair using three-dimensional bioprinting technology.* Tissue Engineering Part A, 2012. **18**(11-12): p. 1304-1312.
13. Rey-Rico, A., M. Cucchiarini, and H. Madry, *Hydrogels for precision meniscus tissue engineering: a comprehensive review.* Connective tissue research, 2017. **58**(3-4): p. 317-328.
14. Narkar, A.R., et al., *pH responsive and oxidation resistant wet adhesive based on reversible catechol–boronate complexation.* Chemistry of Materials, 2016. **28**(15): p. 5432-5439.
15. Xu, J., et al., *Mollusk glue inspired mucoadhesives for biomedical applications.* Langmuir, 2012. **28**(39): p. 14010-14017.
16. Liu, Y., et al., *Injectable dopamine-modified poly (ethylene glycol) nanocomposite hydrogel with enhanced adhesive property and bioactivity.* ACS applied materials & interfaces, 2014. **6**(19): p. 16982-16992.
17. Strehin, I., et al., *A versatile pH sensitive chondroitin sulfate–PEG tissue adhesive and hydrogel.* Biomaterials, 2010. **31**(10): p. 2788-2797.
18. Barrett, D.G., G.G. Bushnell, and P.B. Messersmith, *Mechanically robust, negative-swelling, mussel-inspired tissue adhesives.* Advanced healthcare materials, 2013. **2**(5): p. 745-755.
19. Guvendiren, M., P.B. Messersmith, and K.R. Shull, *Self-assembly and adhesion of DOPA-modified methacrylic triblock hydrogels.* Biomacromolecules, 2007. **9**(1): p. 122-128.
20. Ye, M., et al., *In situ formation of adhesive hydrogels based on PL with laterally grafted catechol groups and their bonding efficacy to wet organic substrates.* Journal of Materials Science: Materials in Medicine, 2015. **26**(12): p. 273.
21. Tamesue, S., et al., *Highly Tolerant and Durable Adhesion between Hydrogels Utilizing Intercalation of Cationic Substituents into Layered Inorganic Compounds.* ACS Macro Letters, 2016. **5**(6): p. 704-708.
22. Abbott, S., *Adhesion science: principles and practice*. 2015: DEStech Publications, Inc.
23. Ahn, B.K., *Perspectives on mussel-inspired wet adhesion.* Journal of the American Chemical Society, 2017. **139**(30): p. 10166-10171.
24. Yuk, H., et al., *Tough bonding of hydrogels to diverse non-porous surfaces.* Nature materials, 2016. **15**(2): p. 190.

25. Kurokawa, T., et al., *Formation of a strong hydrogel–porous solid interface via the double-network principle.* Acta biomaterialia, 2010. **6**(4): p. 1353-1359.

26. Derail, C., et al., *Relationship between viscoelastic and peeling properties of model adhesives. Part 2. The interfacial fracture domains.* The Journal of Adhesion, 1998. **68**(3-4): p. 203-228.

27. Li, J., et al., *Tough adhesives for diverse wet surfaces.* Science, 2017. **357**(6349): p. 378-381.

28. Vakalopoulos, K.A., et al., *Mechanical strength and rheological properties of tissue adhesives with regard to colorectal anastomosis: an ex vivo study.* Annals of surgery, 2015. **261**(2): p. 323-331.

29. Wallace, D., et al., *A tissue sealant based on reactive multifunctional polyethylene glycol.* Journal of Biomedical Materials Research Part A, 2001. **58**(5): p. 545-555.

30. Dastjerdi, A.K., et al., *Cohesive behavior of soft biological adhesives: experiments and modeling.* Acta Biomaterialia, 2012. **8**(9): p. 3349-3359.

31. Wang, D.-A., et al., *Multifunctional chondroitin sulphate for cartilage tissue–biomaterial integration.* Nature materials, 2007. **6**(5): p. 385.

32. Guo, J., et al., *Development of tannin-inspired antimicrobial bioadhesives.* Acta biomaterialia, 2018. **72**: p. 35-44.

33. Yuk, H., et al., *Dry double-sided tape for adhesion of wet tissues and devices.* Nature, 2019. **575**(7781): p. 169-174.

34. Caló, E. and V.V. Khutoryanskiy, *Biomedical applications of hydrogels: A review of patents and commercial products.* European Polymer Journal, 2015. **65**: p. 252-267.

35. Gaharwar, A.K., N.A. Peppas, and A. Khademhosseini, *Nanocomposite hydrogels for biomedical applications.* Biotechnology and bioengineering, 2014. **111**(3): p. 441-453.

36. Hoffman, A.S., *Hydrogels for biomedical applications.* Advanced drug delivery reviews, 2012. **64**: p. 18-23.

37. Li, Y., et al., *Magnetic hydrogels and their potential biomedical applications.* Advanced Functional Materials, 2013. **23**(6): p. 660-672.

38. Seliktar, D., *Designing cell-compatible hydrogels for biomedical applications.* Science, 2012. **336**(6085): p. 1124-1128.

39. Peak, C.W., J.J. Wilker, and G. Schmidt, *A review on tough and sticky hydrogels.* Colloid and Polymer Science, 2013. **291**(9): p. 2031-2047.

40. Mizrahi, B., et al., *Elasticity and safety of alkoxyethyl cyanoacrylate tissue adhesives.* Acta biomaterialia, 2011. **7**(8): p. 3150-3157.

41. Duarte, A., et al., *Surgical adhesives: systematic review of the main types and development forecast.* Progress in Polymer Science, 2012. **37**(8): p. 1031-1050.

42. Artzi, N., et al., *Aldehyde-Amine Chemistry Enables Modulated Biosealants with Tissue-Specific Adhesion.* Advanced materials, 2009. **21**(32-33): p. 3399-3403.

43. Lang, N., et al., *A blood-resistant surgical glue for minimally invasive repair of vessels and heart defects.* Science translational medicine, 2014. **6**(218): p. 218ra6-218ra6.

44. Buckwalter, J. and H. Mankin, *Articular cartilage: Part II Degeneration and osteoarthrosis, repair, regeneration, and transplantation.* JBJS, 1997. **79**(4): p. 612-632.

45. Hunziker, E., *Articular cartilage repair: basic science and clinical progress. A review of the current status and prospects.* Osteoarthritis and cartilage, 2002. **10**(6): p. 432-463.

46. Hangody, L., et al., *Autologous osteochondral grafting—technique and long-term results.* Injury, 2008. **39**(1): p. 32-39.

47. Shinya, N., et al., *Improvement of the tissue-adhesive and sealing effect of fibrin sealant using polyglycolic acid felt.* Journal of Investigative Surgery, 2009. **22**(5): p. 383-389.

48. Krych, A.J., et al., *Arthroscopic repair of isolated meniscal tears in patients 18 years and younger.* The American journal of sports medicine, 2008. **36**(7): p. 1283-1289.

49. Henning, C.E., et al., *Arthroscopic meniscal repair using an exogenous fibrin clot.* Clinical orthopaedics and related research, 1990(252): p. 64-72.

50. Englund, M., *Meniscal tear—a feature of osteoarthritis.* Acta Orthopaedica Scandinavica, 2004. **75**(sup312): p. 1-45.

51. Mehta, V.M. and M.A. Terry, *Cyclic testing of 3 all-inside meniscal repair devices: a biomechanical analysis.* The American journal of sports medicine, 2009. **37**(12): p. 2435-2439.

52.   Gelber, A.C., et al., *Joint injury in young adults and risk for subsequent knee and hip osteoarthritis.* Annals of internal medicine, 2000. **133**(5): p. 321-328.

53.   Bochyńska, A., et al., *Tissue adhesives for meniscus tear repair: an overview of current advances and prospects for future clinical solutions.* Journal of Materials Science: Materials in Medicine, 2016. **27**(5): p. 85.

54.   Simson, J.A., et al., *Bonding and fusion of meniscus fibrocartilage using a novel chondroitin sulfate bone marrow tissue adhesive.* Tissue Engineering Part A, 2013. **19**(15-16): p. 1843-1851.

55.   Kim, T. and B.V. Kharod, *Tissue adhesives in corneal cataract incisions.* Current opinion in ophthalmology, 2007. **18**(1): p. 39-43.

56.   Khademhosseini, A., et al., *Bioadhesive for corneal repair* 2017.

57.   Grinstaff, M.W., *Designing hydrogel adhesives for corneal wound repair.* Biomaterials, 2007. **28**(35): p. 5205-5214.

58.   O'Sullivan, F., R. Dalton, and C. Rostron, *Fibrin glue: an alternative method of wound closure in glaucoma surgery.* Journal of glaucoma, 1996. **5**(6): p. 367-370.

59.   Pourshahrestani, S., et al., *Polymeric Hydrogel Systems as Emerging Biomaterial Platforms to Enable Hemostasis and Wound Healing.* Advanced Healthcare Materials, 2020. **9**(20): p. 2000905.

60.   Li, J., et al., *Advances of injectable hydrogel-based scaffolds for cartilage regeneration.* Regenerative Biomaterials, 2019. **6**(3): p. 129-140.

61.   Palacio, M.L. and B. Bhushan, *Bioadhesion: a review of concepts and applications.* Phil. Trans. R. Soc. A, 2012. **370**(1967): p. 2321-2347.

62.   von Fraunhofer, J.A., *Adhesion and cohesion.* International journal of dentistry, 2012. **2012**.

63.   Lin, Q., et al., *Adhesion mechanisms of the mussel foot proteins mfp-1 and mfp-3.* Proceedings of the National Academy of Sciences, 2007. **104**(10): p. 3782-3786.

64.   Kendall, K., *Molecular adhesion and its applications: the sticky universe*. 2007: Springer Science & Business Media.

65.   Chen, B., et al., *Crack path selection in adhesively bonded joints: the roles of external loads and speciment geometry.* International journal of fracture, 2002. **114**(2): p. 167-190.

66.   Adams, R.D., *Adhesive bonding: science, technology and applications*. 2005: Elsevier.

67.   Johnson, K.L., K. Kendall, and A. Roberts, *Surface energy and the contact of elastic solids.* Proc. R. Soc. Lond. A, 1971. **324**(1558): p. 301-313.

68.   Gordon, J.E., *Structures: or why things don't fall down*. 2009: Da Capo Press.

69.   Lee, H., N.F. Scherer, and P.B. Messersmith, *Single-molecule mechanics of mussel adhesion.* Proceedings of the National Academy of Sciences, 2006. **103**(35): p. 12999-13003.

70.   Wang, R., et al., *Cartilage adhesive and mechanical properties of enzymatically crosslinked polysaccharide tyramine conjugate hydrogels.* Polymers for advanced technologies, 2014. **25**(5): p. 568-574.

71.   Yu, F., et al., *Multifunctional hydrogel with good structure integrity, self-healing, and tissue-adhesive property formed by combining Diels–Alder click reaction and acylhydrazone bond.* ACS applied materials & interfaces, 2015. **7**(43): p. 24023-24031.

72.   Tan, Y., et al., *Designing starch-based nanospheres to make hydrogels with high mechanical strength.* Macromolecular Materials and Engineering, 2009. **294**(12): p. 855-859.

73.   Myung, D., et al., *Biomimetic strain hardening in interpenetrating polymer network hydrogels.* Polymer, 2007. **48**(18): p. 5376-5387.

74.   Gong, J.P., et al., *Double-network hydrogels with extremely high mechanical strength.* Advanced materials, 2003. **15**(14): p. 1155-1158.

75.   Shin, H., B.D. Olsen, and A. Khademhosseini, *The mechanical properties and cytotoxicity of cell-laden double-network hydrogels based on photocrosslinkable gelatin and gellan gum biomacromolecules.* Biomaterials, 2012. **33**(11): p. 3143-3152.

76.   Tan, Y., et al., *High mechanical strength and rapid response rate of poly (N-isopropyl acrylamide) hydrogel crosslinked by starch-based nanospheres.* Soft Matter, 2010. **6**(7): p. 1467-1471.

77.   Hu, J., et al., *Microgel-reinforced hydrogel films with high mechanical strength and their visible mesoscale fracture structure.* Macromolecules, 2011. **44**(19): p. 7775-7781.

78.   Dai, T., et al., *Conducting hydrogels with enhanced mechanical strength.* Polymer, 2009. **50**(22): p. 5236-5241.

79.   Wang, X., H. Wang, and H.R. Brown, *Jellyfish gel and its hybrid hydrogels with high mechanical strength.* Soft Matter, 2011. **7**(1): p. 211-219.

80.   Hu, J., et al., *High fracture efficiency and stress concentration phenomenon for microgel-reinforced hydrogels based on double-network principle.* Macromolecules, 2012. **45**(23): p. 9445-9451.

81.   Jeong, J.W., et al., *High-resolution nanotransfer printing applicable to diverse surfaces via interface-targeted adhesion switching.* Nature communications, 2014. **5**: p. 5387.

82.   Mark, H.F., *Encyclopedia of polymer science and technology, concise.* 2013: John Wiley & Sons.

83.   Jabbari, E. and N.A. Peppas, *Polymer-polymer interdiffusion and adhesion.* Journal of Macromolecular Science, Part C: Polymer Reviews, 1994. **34**(2): p. 205-241.

84.   Sun, J.-Y., et al., *Highly stretchable and tough hydrogels.* Nature, 2012. **489**(7414): p. 133.

85.   Harrass, K., et al., *Mechanically strong hydrogels with reversible behaviour under cyclic compression with MPa loading.* Soft Matter, 2013. **9**(10): p. 2869-2877.

86.   Yang, W., H. Furukawa, and J.P. Gong, *Highly extensible double-network gels with self-assembling anisotropic structure.* Advanced Materials, 2008. **20**(23): p. 4499-4503.

87.   Henderson, K.J., et al., *Ionically cross-linked triblock copolymer hydrogels with high strength.* Macromolecules, 2010. **43**(14): p. 6193-6201.

88.   Wang, Q., et al., *High-water-content mouldable hydrogels by mixing clay and a dendritic molecular binder.* Nature, 2010. **463**(7279): p. 339.

89.   Carlsson, L., et al., *Nano-hybrid self-crosslinked PDMA/silica hydrogels.* Soft Matter, 2010. **6**(15): p. 3619-3631.

90.   Hao, J. and R. Weiss, *Mechanical behavior of hybrid hydrogels composed of a physical and a chemical network.* Polymer, 2013. **54**(8): p. 2174-2182.

91.   Baskan, T., D.C. Tuncaboylu, and O. Okay, *Tough interpenetrating Pluronic F127/polyacrylic acid hydrogels.* Polymer, 2013. **54**(12): p. 2979-2987.

92.   Rose, S.v., et al., *Time dependence of dissipative and recovery processes in nanohybrid hydrogels.* Macromolecules, 2013. **46**(10): p. 4095-4104.

93.   Zhu, A., G. Li, and J. Jiang, *Novel Poly (2-Hydroxyethyl Methacrylate-Acrylamid)/Clay Nanocomposite Gels with Enhanced Mechanical Strength.* Journal of Macromolecular Science, Part B, 2012. **51**(5): p. 1002-1010.

94.   Gaharwar, A.K., et al., *Photocrosslinked nanocomposite hydrogels from PEG and silica nanospheres: structural, mechanical and cell adhesion characteristics.* Materials Science and Engineering: C, 2013. **33**(3): p. 1800-1807.

95.   Zhao, J., et al., *Mechanically strong and thermosensitive macromolecular microsphere composite poly (N-isopropylacrylamide) hydrogels.* Polymer, 2013. **54**(6): p. 1596-1602.

96.   Bae, W.-G., D. Kim, and K.-Y. Suh, *Instantly switchable adhesion of bridged fibrillar adhesive via gecko-inspired detachment mechanism and its application to a transportation system.* Nanoscale, 2013. **5**(23): p. 11876-11884.

97.   Bhushan, B., *Adhesion and stiction: mechanisms, measurement techniques, and methods for reduction.* Journal of Vacuum Science & Technology B: Microelectronics and Nanometer Structures Processing, Measurement, and Phenomena, 2003. **21**(6): p. 2262-2296.

98.   Wang, M., et al., *Polymer nanocomposite hydrogels exhibiting both dynamic restructuring and unusual adhesive properties.* Langmuir, 2013. **29**(23): p. 7087-7095.

99.   Miserez, A. and P.A. Guerette, *Phase transition-induced elasticity of α-helical bioelastomeric fibres and networks.* Chemical Society Reviews, 2013. **42**(5): p. 1973-1995.

100.   Brown, A.E., et al., *Multiscale mechanics of fibrin polymer: gel stretching with protein unfolding and loss of water.* science, 2009. **325**(5941): p. 741-744.

101.   Bhushan, B., *Introduction to tribology.* 2013: John Wiley & Sons.

102.   Romito, L. and G.A. Ameer, *Mechanical interlocking of engineered cartilage to an underlying polymeric substrate: towards a biohybrid tissue equivalent.* Annals of biomedical engineering, 2006. **34**(5): p. 737.

103. Khoushabi, A., et al., *Photo-polymerization, swelling and mechanical properties of cellulose fibre reinforced poly (ethylene glycol) hydrogels.* Composites Science and Technology, 2015. **119**: p. 93-99.

104. Moutos, F.T., L.E. Freed, and F. Guilak, *A biomimetic three-dimensional woven composite scaffold for functional tissue engineering of cartilage.* Nature materials, 2007. **6**(2): p. 162.

105. Agrawal, A., N. Rahbar, and P.D. Calvert, *Strong fiber-reinforced hydrogel.* Acta biomaterialia, 2013. **9**(2): p. 5313-5318.

106. Coburn, J., et al., *Biomimetics of the extracellular matrix: an integrated three-dimensional fiber-hydrogel composite for cartilage tissue engineering.* Smart structures and systems, 2011. **7**(3): p. 213.

107. Jang, J., et al., *A cell-laden nanofiber/hydrogel composite structure with tough-soft mechanical property.* Applied Physics Letters, 2013. **102**(21): p. 211914.

108. Bacakova, L., et al., *Modulation of cell adhesion, proliferation and differentiation on materials designed for body implants.* Biotechnology advances, 2011. **29**(6): p. 739-767.

109. Hozbor, M.A., W.P. Hansen, and M. McPherson, *Plasma cleaning of metal surfaces.* Precis Cleaning, 1994. **2**: p. 46.

110. Švorčík, V., et al., *Cytocompatibility of Ar+ plasma treated and Au nanoparticle-grafted PE.* Nuclear Instruments and Methods in Physics Research Section B: Beam Interactions with Materials and Atoms, 2009. **267**(11): p. 1904-1910.

111. Toworfe, G.K., et al., *Fibronectin adsorption on surface-activated poly (dimethylsiloxane) and its effect on cellular function.* Journal of Biomedical Materials Research Part A: An Official Journal of The Society for Biomaterials, The Japanese Society for Biomaterials, and The Australian Society for Biomaterials and the Korean Society for Biomaterials, 2004. **71**(3): p. 449-461.

112. Legeay, G. and F. Poncin-Epaillard, *Surface engineering by coating of hydrophilic layers: bioadhesion and biocontamination.* Adhesion: Current Research and Applications, 2005: p. 175-188.

113. Noel, A.C., et al., *Frogs use a viscoelastic tongue and non-Newtonian saliva to catch prey.* Journal of The Royal Society Interface, 2017. **14**(127): p. 20160764.

114. *http://www.dailymail.co.uk/news/article-4178538/How-frogs-catch-flies-sticky-tongues.html*. Available from: http://www.dailymail.co.uk/news/article-4178538/How-frogs-catch-flies-sticky-tongues.html.

115. Graham, L.D., et al., *Characterization of a protein-based adhesive elastomer secreted by the Australian frog Notaden bennetti.* Biomacromolecules, 2005. **6**(6): p. 3300-3312.

116. *http://animal.memozee.com/view.php?tid=3&did=25526*. Available from: http://animal.memozee.com/view.php?tid=3&did=25526.

117. *https://en.wikipedia.org/wiki/Crucifix_toad*.

118. Cui, M., et al., *Natural and bio-inspired underwater adhesives: Current progress and new perspectives.* APL Materials, 2017. **5**(11): p. 116102.

119. Stewart, R.J., C.S. Wang, and H. Shao, *Complex coacervates as a foundation for synthetic underwater adhesives.* Advances in colloid and interface science, 2011. **167**(1-2): p. 85-93.

120. Lee, B.P., et al., *Mussel-inspired adhesives and coatings.* Annual review of materials research, 2011. **41**: p. 99-132.

121. Wainwright, D.K., et al., *Stick tight: suction adhesion on irregular surfaces in the northern clingfish.* Biology letters, 2013. **9**(3): p. 20130234.

122. *https://www.popsci.com/suction-cups-have-nothing-northern-clingfish*. Available from: https://www.popsci.com/suction-cups-have-nothing-northern-clingfish.

123. Favi, P.M., et al., *Inspiration from the natural world: from bio-adhesives to bio-inspired adhesives.* Journal of Adhesion Science and Technology, 2014. **28**(3-4): p. 290-319.

124. *https://commons.wikimedia.org/wiki/File:Gecko_Palm.jpg*. Available from: https://commons.wikimedia.org/wiki/File:Gecko_Palm.jpg.

125. Arzt, E., S. Gorb, and R. Spolenak, *From micro to nano contacts in biological attachment devices.* Proceedings of the National Academy of Sciences, 2003. **100**(19): p. 10603-10606.

126. Melzer, B., et al., *The attachment strategy of English ivy: a complex mechanism acting on several hierarchical levels.* Journal of the Royal Society Interface, 2010. **7**(50): p. 1383-1389.

127. Zhang, M., et al., *Nanofibers and nanoparticles from the insect-capturing adhesive of the Sundew (Drosera) for cell attachment.* Journal of nanobiotechnology, 2010. **8**(1): p. 20.

128. Mostaert, A.S., et al., *Nanoscale mechanical characterisation of amyloid fibrils discovered in a natural adhesive.* Journal of biological physics, 2006. **32**(5): p. 393-401.

129. *Ivy image*. Available from: https://asknature.org/strategy/roots-attach-firmly/.

130. *Sundew*. Available from: http://animals.sandiegozoo.org/plants/sundew.

131. Tibbitt, M.W. and K.S. Anseth, *Hydrogels as extracellular matrix mimics for 3D cell culture.* Biotechnology and bioengineering, 2009. **103**(4): p. 655-663.

132. Strange, D.G. and M.L. Oyen, *Composite hydrogels for nucleus pulposus tissue engineering.* Journal of the mechanical behavior of biomedical materials, 2012. **11**: p. 16-26.

133. Ullah, F., et al., *Classification, processing and application of hydrogels: A review.* Materials Science and Engineering: C, 2015. **57**: p. 414-433.

134. Lee, J.H. and D.G. Bucknall, *Swelling behavior and network structure of hydrogels synthesized using controlled UV-initiated free radical polymerization.* Journal of Polymer Science Part B: Polymer Physics, 2008. **46**(14): p. 1450-1462.

135. Nguyen, K.T. and J.L. West, *Photopolymerizable hydrogels for tissue engineering applications.* Biomaterials, 2002. **23**(22): p. 4307-4314.

136. Colombani, D., *Chain-growth control in free radical polymerization.* Progress in polymer science, 1997. **22**(8): p. 1649-1720.

137. Zavada, S.R., T. Battsengel, and T.F. Scott, *Radical-mediated enzymatic polymerizations.* International journal of molecular sciences, 2016. **17**(2): p. 195.

138. Bryant, S.J., C.R. Nuttelman, and K.S. Anseth, *Cytocompatibility of UV and visible light photoinitiating systems on cultured NIH/3T3 fibroblasts in vitro.* Journal of Biomaterials Science, Polymer Edition, 2000. **11**(5): p. 439-457.

139. Odian, G., *Radical chain polymerization.* Principles of polymerization, 2004. **3**: p. 198-349.

140. Zhao, X., *Multi-scale multi-mechanism design of tough hydrogels: building dissipation into stretchy networks.* Soft Matter, 2014. **10**(5): p. 672-687.

141. Zhong, M., Y.-T. Liu, and X.-M. Xie, *Self-healable, super tough graphene oxide–poly (acrylic acid) nanocomposite hydrogels facilitated by dual cross-linking effects through dynamic ionic interactions.* Journal of Materials Chemistry B, 2015. **3**(19): p. 4001-4008.

142. Lin, P., et al., *Molecularly Engineered Dual-Crosslinked Hydrogel with Ultrahigh Mechanical Strength, Toughness, and Good Self-Recovery.* Advanced Materials, 2015. **27**(12): p. 2054-2059.

143. Bakarich, S.E., et al., *Recovery from applied strain in interpenetrating polymer network hydrogels with ionic and covalent cross-links.* Soft Matter, 2012. **8**(39): p. 9985-9988.

144. Gong, J.P., *Why are double network hydrogels so tough?* Soft Matter, 2010. **6**(12): p. 2583-2590.

145. Wirthl, D., et al., *Instant tough bonding of hydrogels for soft machines and electronics.* Science advances, 2017. **3**(6): p. e1700053.

146. Patel, N.R., et al., *Poly (ethylene glycol) hydrogels with tailorable surface and mechanical properties for tissue engineering applications.* ACS Biomaterials Science & Engineering, 2016. **3**(8): p. 1494-1498.

147. Killion, J.A., et al., *Mechanical properties and thermal behaviour of PEGDMA hydrogels for potential bone regeneration application.* Journal of the mechanical behavior of biomedical materials, 2011. **4**(7): p. 1219-1227.

148. Einchhorn, S., et al., *Review: current international research into cellulose nanofibres and composites.* J. Mater. Sci, 2010. **45**: p. 1-33.

149. Borges, A.C., et al., *Nanofibrillated cellulose composite hydrogel for the replacement of the nucleus pulposus.* Acta biomaterialia, 2011. **7**(9): p. 3412-3421.

150. Lee, K.Y. and D.J. Mooney, *Alginate: properties and biomedical applications.* Progress in polymer science, 2012. **37**(1): p. 106-126.

151. Yang, S.Y., et al., *A bio-inspired swellable microneedle adhesive for mechanical interlocking with tissue.* Nature communications, 2013. **4**: p. 1702.

152. Lin-Gibson, S., et al., *Synthesis and characterization of PEG dimethacrylates and their hydrogels.* Biomacromolecules, 2004. **5**(4): p. 1280-1287.

153. Josset, S., et al., *Energy consumption of the nanofibrillation of bleached pulp, wheat straw and recycled newspaper through a grinding process.* Nord Pulp Pap Res J, 2014. **29**(1): p. 167-175.

154. Broguiere, N., et al., *Factor XIII cross-linked hyaluronan hydrogels for cartilage tissue engineering.* ACS Biomaterials Science & Engineering, 2016. **2**(12): p. 2176-2184.

155. Dehne, T., et al., *A method to screen and evaluate tissue adhesives for joint repair applications.* BMC musculoskeletal disorders, 2012. **13**(1): p. 175.

156. Hong, S., et al., *3D printing of highly stretchable and tough hydrogels into complex, cellularized structures.* Advanced materials, 2015. **27**(27): p. 4035-4040.

157. Yang, J. and C. Han, *Mechanically viscoelastic properties of cellulose nanocrystals skeleton reinforced hierarchical composite hydrogels.* ACS applied materials & interfaces, 2016. **8**(38): p. 25621-25630.

158. Yang, J. and F. Xu, *Synergistic Reinforcing Mechanisms in Cellulose Nanofibrils Composite Hydrogels: Interfacial Dynamics, Energy Dissipation, and Damage Resistance.* Biomacromolecules, 2017. **18**(8): p. 2623-2632.

159. Vilatela, J.J., J.A. Elliott, and A.H. Windle, *A model for the strength of yarn-like carbon nanotube fibers.* Acs Nano, 2011. **5**(3): p. 1921-1927.

160. Sun, L., et al., *A bio-inspired approach for in situ synthesis of tunable adhesive.* Bioinspiration & biomimetics, 2013. **9**(1): p. 016005.

161. Lacombe, R., *Adhesion measurement methods: theory and practice*. 2005: CRC Press.

162. Josse, G., et al., *Measuring interfacial adhesion between a soft viscoelastic layer and a rigid surface using a probe method.* The Journal of Adhesion, 2004. **80**(1-2): p. 87-118.

163. Tessmer, I., et al., *Investigating bioconjugation by atomic force microscopy.* Journal of nanobiotechnology, 2013. **11**(1): p. 25.

164. F2255-05, A.I.A., *Standard Test Method for Strength Properties of Tissue Adhesives in Lap-Shear by Tension Loading.* West Conshohocken, PA; ASTM International, 2015. DOI: 10.1520/F2255-05R15, 2015.

165. Chai, Q., Y. Jiao, and X. Yu, *Hydrogels for biomedical applications: their characteristics and the mechanisms behind them.* Gels, 2017. **3**(1): p. 6.

166. Zhang, W., et al., *Catechol-functionalized hydrogels: biomimetic design, adhesion mechanism, and biomedical applications.* Chemical Society Reviews, 2020. **49**(2): p. 433-464.

167. Karami, P., et al., *Composite double-network hydrogels to improve adhesion on biological surfaces.* ACS applied materials & interfaces, 2018. **10**(45): p. 38692-38699.

168. Li, X., et al., *Functional hydrogels with tunable structures and properties for tissue engineering applications.* Frontiers in chemistry, 2018. **6**: p. 499.

169. Nasrollahzadeh, N., P. Karami, and D.P. Pioletti, *Control of dissipation sources: a central aspect for enhancing the mechanical and mechanobiological performances of hydrogels.* ACS applied materials & interfaces, 2019. **11**(43): p. 39662-39671.

170. Kamata, H., et al., *Design of hydrogels for biomedical applications.* Advanced healthcare materials, 2015. **4**(16): p. 2360-2374.

171. Assmann, A., et al., *A highly adhesive and naturally derived sealant.* Biomaterials, 2017. **140**: p. 115-127.

172. Zhao, Q., et al., *Underwater contact adhesion and microarchitecture in polyelectrolyte complexes actuated by solvent exchange.* Nature materials, 2016. **15**(4): p. 407-412.

173. Desmond, K.W., et al., *Dynamics of mussel plaque detachment.* Soft matter, 2015. **11**(34): p. 6832-6839.

174. Ghareeb, A. and A. Elbanna, *On the role of the plaque porous structure in mussel adhesion: implications for adhesion control using bulk patterning.* Journal of Applied Mechanics, 2018. **85**(12).

175. Wyss, C.S., et al., *Cyclic loading of a cellulose/hydrogel composite increases its fracture strength.* Extreme Mechanics Letters, 2018. **24**: p. 66-74.

176.   Liu, J., et al., *Fatigue-resistant adhesion of hydrogels.* Nature communications, 2020. **11**(1): p. 1-9.

177.   Chen, Z., et al., *Biomaterials for corneal bioengineering.* Biomedical Materials, 2018. **13**(3): p. 032002.

178.   Han, W.T., et al., *Improved cell viability for large-scale biofabrication with photo-crosslinkable hydrogel systems through a dual-photoinitiator approach.* Biomaterials science, 2020. **8**(1): p. 450-461.

179.   Wang, C.S. and R.J. Stewart, *Localization of the bioadhesive precursors of the sandcastle worm, Phragmatopoma californica (Fewkes).* Journal of Experimental Biology, 2012. **215**(2): p. 351-361.

180.   Pujari-Palmer, M., et al., *A novel class of injectable bioceramics that glue tissues and biomaterials.* Materials, 2018. **11**(12): p. 2492.

181.   Gu, Z., et al., *Understanding surface adhesion in nature: a peeling model.* Advanced Science, 2016. **3**(7): p. 1500327.

182.   Kord Forooshani, P. and B.P. Lee, *Recent approaches in designing bioadhesive materials inspired by mussel adhesive protein.* Journal of Polymer Science Part A: Polymer Chemistry, 2017. **55**(1): p. 9-33.

183.   Walker, B.W., et al., *Engineering a naturally-derived adhesive and conductive cardiopatch.* Biomaterials, 2019. **207**: p. 89-101.

184.   Wyss, C.S., et al., *Hybrid granular hydrogels: combining composites and microgels for extended ranges of material properties.* Soft Matter, 2020. **16**(15): p. 3769-3778.

185.   Li, J. and D.J. Mooney, *Designing hydrogels for controlled drug delivery.* Nature Reviews Materials, 2016. **1**(12): p. 1-17.

186.   Lee, K., et al., *Measuring water contents in animal organ tissues using terahertz spectroscopic imaging.* Biomedical optics express, 2018. **9**(4): p. 1582-1589.

187.   Levental, I., P.C. Georges, and P.A. Janmey, *Soft biological materials and their impact on cell function.* Soft Matter, 2007. **3**(3): p. 299-306.

188.   Ranneva, E., *The Use of Hyaluronidase to Treat the Excess of Cross-Linked Hyaluronic Acid Following Aesthetic Medicine Procedures: A Practical Point of View.* Emergency Medicine: Open Access, 2017(07. 10.4172/2165-7548.1000357).

189.   Sani, E.S., et al., *Sutureless repair of corneal injuries using naturally derived bioadhesive hydrogels.* Science advances, 2019. **5**(3): p. eaav1281.

190.   Rienks, M., J. Barallobre-Barreiro, and M. Mayr, *The emerging role of the ADAMTS family in vascular diseases.* Circulation Research, 2018. **123**(12): p. 1279-1281.

Peyman KARAMI

Chemin de Chandieu 24
1006 Lausanne
Tel: +41 78 895 77 34

Education

2016-2020	PhD student. in Material Science and Engineering École Polytechnique Fédérale de Lausanne (EPFL), Lausanne
2012-2015	Master of Science in Mechanical Engineering University of Tehran (UT), Tehran
2008-2012	Bachelor of Science in Mechanical Engineering Iran University of Science and Technology (IUST), Tehran

Professional Experience

2016-2020	PhD Assistant, Laboratory of Biomechanical Orthopedics (LBO), Laboratory of Applied Photonics Devices (LAPD), EPFL Objective: Design and development of advanced adhesive and tough hydrogels for human tissue repair, such as cartilage regeneration and corneal treatment *Main Activities:* Teaching assistant and project mentoring Research and laboratory experimentations Researcher in collaborative projects with Polymers Laboratory (LP), Laboratory for Bio and Nano Instrumentation (LBNI), and University of Uppsala Responsible for laboratory testing equipment and staff training
2014-2016	Laboratory of Composites, University of Tehran Research Assistant: Experimental and numerical analysis of progressive damage in nanoparticle-reinforced composites Teaching Assistant in Mechanics of Materials Laboratory
2012 & 2015 (10 months)	Kushavaran Co. and Wagon Pars Co INTERN Material selection (Metals, Composites, Polymers) Mechanical testing

Technical Skills

Materials characterization: Mechanical testing, Rheology, Adhesion testing, , Spectrophotometry, Confocal Microscopy, Atomic Force Microscopy
Chemical synthesis and characterization: NMR, FTIR, Polymer synthesis, Photopolymerization
Biological assays: Cell Culture, Cell viability assays, Biochemical analysis
Numerical analysis: Abaqus, SolidWorks, Matlab

Research Interests

Biomaterials, Hydrogels, Bioadhesion, Tissue engineering, Polymer synthesis, Mechanical/ Chemical/ Biological Characterization

Recent Publications, 2018-2020

Karami, P., Nasrollahzadeh, N., Wyss, C.S., O'Sullivan, A., Broome, M., Procter, P., Bourban, P.E., Moser, C., and Pioletti, D.P., 2020. An intrinsically-adhesive family of injectable hydrogels with functional physicochemical performance for regenerative medicine. Submitted, 2020.

Karami, P., Wyss, C.S., Khoushabi, A., Schmocker, A., Broome, M., Moser, C., Bourban, P.E. and Pioletti, D.P., 2018. Composite double-network hydrogels to improve adhesion on biological surfaces. ACS applied materials & interfaces, 10(45), pp.38692-38699.

Wang, J., Karami, P., Ataman, N.C., Pioletti, D.P., Steele, T.W. and Klok, H.A., 2019. Light-Activated, Bioadhesive, Poly (2-hydroxyethyl methacrylate) Brush Coatings. Biomacromolecules, 21(1), pp.240-249.

Nasrollahzadeh, N., Karami, P. and Pioletti, D.P., 2019. Control of Dissipation Sources: A Central Aspect for Enhancing the Mechanical and Mechanobiological Performances of Hydrogels. ACS Applied Materials & Interfaces, 11(43), pp.39662-39671.

Wyss, C.S., Karami, P., Bourban, P.E. and Pioletti, D.P., 2020. Hybrid granular hydrogels: combining composites and microgels for extended ranges of material properties. Soft Matter, 16(15), pp.3769-3778. (Collaboration)

Wyss, C.S., Karami, P., Bourban, P.E. and Pioletti, D.P., 2018. Cyclic loading of a cellulose/hydrogel composite increases its fracture strength. Extreme Mechanics Letters, 24, pp.66-74.

Karami, P., Wyss, C.S., P., Bourban, P.E., Moser, C., and Pioletti, D.P. PCT filed patent. International Patent Application no. PCT/EP2019/076874, CROSS-LINKABLE POLYMER, HYDROGEL, AND METHOD OF PREPARATION THEREOF

Stampoultzis T, Karami P, Pioletti, P, review on: Thoughts on cartilage tissue engineering: A 21st century perspective, submitted.

Selected Conferences & Seminars 2018-2020

2020   Orthopaedic Research Society (ORS) - 2020 Annual Meeting, Phoenix, Arizona, USA

2019   Tissue Engineering Therapies: From Concept to Clinical Translation & Commercialisation, TERMIS EU 2019, Rhodes, Greece

2019,   6th International Conference on Multifunctional, Hybrid and Nanomaterials - HYBRID 2019, Sitges, Spain

2018   Annual Conference of the European Society for Biomaterials - ESB 2018, Maastricht, Netherlands

2018   World Congress of Biomechanics - WCB 2018, Dublin, Ireland

2018   Swiss Society for Biomaterials and Regenerative Medicine - SSBRM 2018, Fribourg, Switzerland